T.R.
BOLU ABANT İZZET BAYSAL UNIVERSITY
INSTITUTE OF GRADUATE STUDIES
Department of Chemistry

FABRICATION OF NANO-CRYSTALLINE UNDOPED AND SOME LANTHANIDE IONS (Eu^{3+} and Sm^{3+}) DOPED CALCIUM PYROBORATE CERAMIC POWDERS

MASTER OF SCIENCE

SEDA AYTEN KEMER

ACADEMIC SUPERVISOR
Prof.Dr. Ayşe MORKAN

BOLU, JANUARY 2024

APPROVAL OF THE THESIS

FABRICATION OF NANO-CRYSTALLINE UNDOPED AND SOME LANTHANIDE IONS (Eu^{3+} and Sm^{3+}) DOPED CALCIUM PYROBORATE CERAMIC POWDERS submitted by **Seda AYTEN KEMER** and defended before the Examining Committe Members listed below in partial fulfillment of the requirements for the degree of **Master of Science** in **Department of Chemistry, Institute of Graduate Studies of Bolu Abant Izzet Baysal University in 3.01.2024** by

Examining Committee Members	**Signature**
Supervisor Prof. Dr. Ayşe MORKAN Bolu Abant Izzet Baysal University	.....
Member Prof. Dr. F. Devrim ÖZDEMİRHAN Bolu Abant Izzet Baysal University	.....
Member Prof. Dr. Mecit AKSU Düzce University	.....

Prof. Dr. İbrahim KÜRTÜL

Director of Institute of Graduate Studies

ETHICAL DECLARATION

In this thesis dissertation that was properly prepared according to the Thesis Writing Rules of Bolu Abant İzzet Baysal University of the Institute of Graduates Studies, I hereby declare that:

- All data, information, and documents presented in the thesis were obtained in accordance with the academic and ethical rules,
- All data, documents, assessments, and results were presented in accordance with the scientific ethical and moral rules,
- All works that were benefitted in the thesis were appropriately cited,
- No alteration was made in the data used,
- Study presented in this thesis is original,

Otherwise, I declare that I accept the loss of all my rights in case any contradiction that may arise against me.

The similarity rate obtained by using the Turnitin program, a plagiarism detection software, is within the limits approved by the University Senate.

_____

Seda AYTEN KEMER

ABSTRACT

FABRICATION OF NANO-CRYSTALLINE UNDOPED AND SOME LANTHANIDE IONS (Eu^{3+} and Sm^{3+}) DOPED CALCIUM PYROBORATE CERAMIC POWDERS
MSC THESIS
SEDA AYTEN KEMER
BOLU ABANT IZZET BAYSAL UNIVERSITY
INSTITUTE OF GRADUATE STUDIES
DEPARTMENT OF CHEMISTRY
(SUPERVISOR: PROF. DR. AYŞE MORKAN))
BOLU, JANUARY 2024
xiii + 70

In this study, nano-crystalline undoped and some lanthanide ion (Eu^{+} and Sm^{3+}) doped calcium pyroborate ceramic powders production were successfully synthesized by solution combustion synthesis (SCS) method using calcium nitrate, boric acid, rare earth metals, and several fuels (urea, tartaric acid, glycine, citric acid and HMTA) as starting materials. Different concentrations of rare earth metals were applied such as Eu^{3+} (0.005, 0.01, 0.02, 0.05) and Sm^{3+} (0.005, 0.01, 0.015). The characterization processes of products were analyzed using X-Ray Diffraction (XRD) and Infrared spectroscopy (FTIR). The impact of several fuel resources and annealing temperatures (400-900 °C) on the structural features of the synthesized products was examined by the XRD technique. Based on the XRD data, it was found that the single-phase alpha forms of undoped and lanthanide ion doped calcium pyroborates were fabricated at 900 °C with monoclinic crystal structure. Examining the FT-IR spectra, the bond variation of calcium pyroborates were observed at >1000 cm^{-1} assigned to the B–O stretching modes of the triangular $[BO_3]^{3-}$. It was also determined that the bands betweeen 600 to 820 cm^{-1} originated from the bending vibrational motions of B-O bond of BO_3 groups.

KEYWORDS: Solution combustion synthesis (SCS), Calcium pyroborate, Nano-crystalline, Eu^{3+} - Sm^{3+} doped, XRD, FTIR.

ÖZET

BAZI LANTANİT İYONU (Eu^{3+} ve Sm^{3+}) KATKILI VE KATKISIZ NANO-KRİSTAL KALSİYUM PİROBORAT SERAMİK TOZLARIN ÜRETİMİ
YÜKSEK LİSANS TEZİ
SEDA AYTEN KEMER
BOLU ABANT İZZET BAYSAL ÜNİVERSİTESİ
LİSANSÜSTÜ EĞİTİM ENSTİTÜSÜ
KİMYA ANABİLİM DALI
(TEZ DANIŞMANI: PROF. DR. AYŞE MORKAN
BOLU, OCAK - 2024
xiii + 70

Bu çalışmada, nano-kristalin katkısız ve bazı lantanit iyonu (Eu^{3+} ve Sm^{3+}) katkılı kalsiyum piroborat seramik tozların üretimi, başlangıç malzemeleri, kalsiyum nitrat ve borik asit, nadir toprak metalleri ve çeşitli yakıtlar (üre, tartarik asit, glisin, sitrik asit, HMTA) kullanılarak çözeltide yanma sentezi (SCS) yöntemiyle başarıyla sentezlendi. Nadir toprak metallerinin farklı konsantrasyonları olarak; Eu^{3+} (0.005, 0.01, 0.02, 0,05) ve Sm^{3+} (0.005, 0.01, 0.015) uygulandı. Ürünler, X-Işını Kırınımı (XRD) ve Kızılötesi spektroskopisi (FTIR) kullanılarak karakterize edildi. Çeşitli yakıt kaynaklarının ve değişen sıcaklık aralıklarının (400-900C°) sentezlenen ürünlerin yapısal özelliklerine etkisi XRD tekniği kullanılarak analiz edilmiş ve bor-oksijen bağının etkisini belirlemek için FT-IR analizi yapılmıştır.
Verilere dayanarak, 900°C'de tek fazlı alfa formunda katkısız ve bazı lantanit iyonu (Eu^{3+} ve Sm^{3+}) katkılı kalsiyum piroboratların, monoklinik kristal yapısıyla oluştuğu belirlendi. FT-IR verilerinin belirlenmesiyle, kalsiyum piroboratların bağ değişikliği, üçgen $[BO_3]^{3-}$ yapısının B–O germe modlarına atfedilen >1000 cm^{-1} civarında gözlendi. Ayrıca 600 ila 820 cm^{-1} arasındaki bantların, BO_3 gruplarının B-O bağının bükülme titreşiminden kaynaklandığı saptandı.

ANAHTAR KELİMELER: Çözelti Yanma Sentezi (SCS), kalsiyum piroborat, nano-kristal, , Eu^{3+}- Sm^{3+} katkısı, XRD, FTIR.

TABLE OF CONTENTS

LIST OF FIGURES

Page

LIST OF TABLES

Page

LIST OF PICTURES

Page

LIST OF ABBREVIATIONS AND SYMBOLS

CA	**:** Citric Acid
TA	**:** Tartaric Acid
HMTA	**:** Hexamethylenetetramine
GLY	**:** Glycine
U	**:** Urea
FT-IR	**:** Fourier Transform Infrared
XRD	**:** X-Ray Diffraction
TL	**:** Thermoluminescence
SCS	**:** Solution Combustion Synthesis

ACKNOWLEDGEMENTS

I would like to thank my advisor, Prof. Dr. Ayşe MORKAN, for her great guidance, valuable criticism, constant encouragement and tolerance throughout my graduate education. I would like to express my deepest gratitude to her.

I would like to express my profound gratitude to Liska FADLIYANI for her invaluable help and encouragement throughout my research.

I am very thankful to Gülden ÖZEN KAHVECİ for X-Ray studies.

I would also like to express my sincere gratitude to my husband İLKER CAN KEMER, my sister İNCİ AYTEN, my mother ŞENAY AYTEN, my father MURTAZA AYTEN for the affection, motivation, and backing they provided throughout my life.

I would like to express my sincere gratitude to my dear manager and dear friend BÜŞRA GÖKDEMİR, who provided me with the environment I needed throughout my thesis writing processes.

1. INTRODUCTION

Borax has been recognized since ancient times for its application in crafting glazes, hard glass, and glazes. Initial research efforts were made in the 18th century, with Davy, Gay Lussac, and Thenard leading the way in purifying impure boron in 1808. H. Moisson achieved samples with 95-98% purity through magnesium reduction. A notable development of the last century is the production of high-purity boron. Over the past few decades, it has been observed that various crystal structures react with most metals, oxygen, and nitrogen at elevated temperatures, and their elemental nature is not easily compromised. The term "boron" was proposed by Davy to describe the element's origin. (1)

It is noteworthy that volcanic gases and hot spring waters exhibit elevated levels of boron, reaching economic concentrations in specific locations. The boron concentration in hot spring waters in regions hosting boron deposits, such as Turkey and America, exceeds 100 ppm. Most researchers attribute the source of boron to magma. Analyzing the distribution of boron in different rocks reveals that the boron content in marine sediments surpasses that in igneous rocks. The quantity of boron that marine sediments absorb from seawater exceeds the amount of boron present in the sea. (2)

1.1 BORON ELEMENT

Boron, positioned as the 5^{th} element on the periodic table, possesses a relative atomic mass of 10.81 amu and an atomic number of 5. Classified in group IIIA, Boron serves as both a semiconductor and semi-metal. It holds a place in the 13^{th} group of the periodic table. Boron exhibits higher ionization energies when compared (Table 1.1) to the other elements in the III-A group (3)

Boron is composed of two stable isotopes: 19.78% B10, which renders it an effective and its pure elemental form with 80.22% B11. boron has two distinct forms which are amorphous and crystalline boron appearing as brown powder and black shiny solid, respectively. The atoms in boron crystals organize into a intricate three-dimensional structure, known for their extreme hardness yet susceptibility to easy breakage. (4-5)

Furthermore, boron demonstrates high stability at low temperatures and reacts with other chemicals under elevated temperatures Differing from

neighboring elements like carbon and silicon, boron exhibits one fewer valence orbitals, a characteristic referred to as electron deficiency. (4-5)

Crystal boron, also known as elemental boron exhibits notable characteristics like elevated sturdiness, a significant melting threshold, remarkable durability, strong substance stabilility, and semiconductor properties. (8)

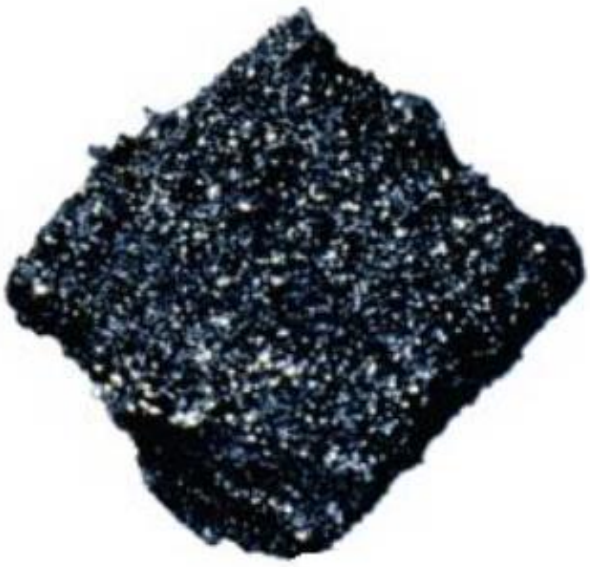

Figure 1.1. Crystalline boron element

The amorphous powder state of the boron element is dark brown, while its hard monolinic crystal form is a yellowish-brown color. It has a melting point of approximately 2300 °C. In the periodic table, it exhibits similarities to carbon and silicon elements in Group IIIA, and it has a high affinity for oxygen. (9)

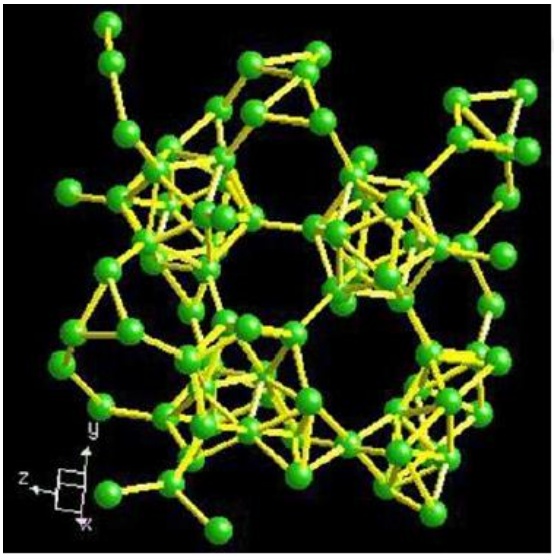

Figure 1.2. Crystal structure of boron (6)

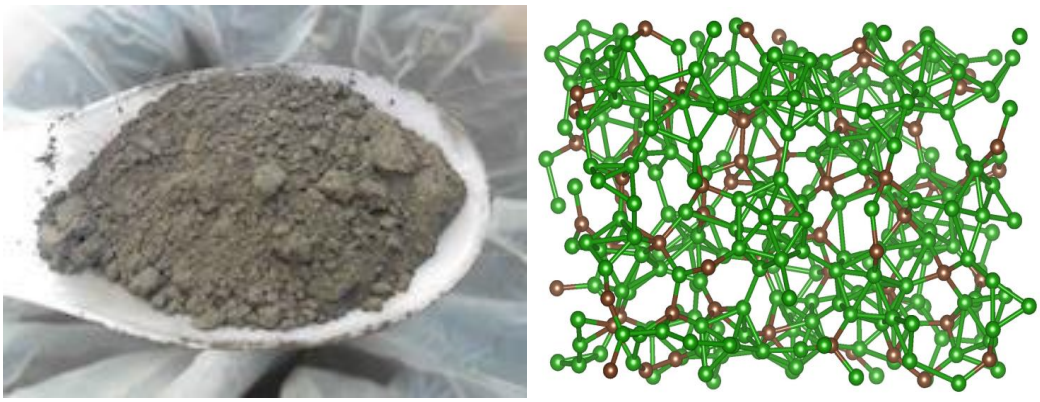

Figure 1.3. Amorphous boron and structure of boron element (7)

Table 1.1. Chemical, atomic features of boron element

Atomic size	4,6 cm^3/mol
Atomic radius	1.17 Å
Ionic scale	0.23 Å
(E-) configuration	1s2 2s2p1
Crystal structure	Rhombohedral
Valence electrons	2s2p1
Number of uncharged particles	6
Number of positive particles	5
Number of negative particles	5
Heat of fusion	50.2 kJ/mol
Electronegativity (Pauling)	2.04
Valence electron potential (-eV)	190
Equivalent electrohemical quantity	0.1344 g/amp.hr
Ionization threshold	Initial:8,298 Subsequent:25,154 Final: 37.93

Table 1.2. Physical features of boron element (10)

Physical state (20 °C, 1 atm)	Solid
Appearance	Yellow-Brown nonmetallic crystal
Fusion temperature	2300 °C
Evaporation point	4002 °C
Heat of vaporization	489 kJ/mol
Heat retention	11,087 J/mol.K
Thermal capacity	1.027 J/g.K.
Density	2.34 g/cm3
Thermal conductivity	0.274 W/cm.K
Electrical conductivity	1.0 E-12 106/cm.Ω
Coefficient of expansion due to temperature	0.0000083 1/ °C
Hardness	9.3 Mohs
Atom dissosiation enthalpy	573 kJ/mol (25 °C)
Evaporation enthalpy	480 kJ/mol
Molar volume	4.69 cm3/mol
Vapor pressure	0.348 Pa
Fusion enthalpy	22.18 kJ/mol
Elastic modulus	320/GPa

Boron possesses a remarkably high melting point, around 2300 °C, showcasing its capacity to withstand elevated temperatures with a robust structure. Furthermore, the intricate crystal formation of boron renders it exceptionally hard, yet prone to easy fracture. (10)

In summary, the various physical attributes of boron make it widely applicable in both industrial and scientific settings, without altering its intended meaning. (10)

1.1.1 Boron: Mineral Resources

There are 250 types of boron compounds exist ın the world reserved which are mainly discovered in the form of boron minerals. These boron minerals are primarily formed in the Earth's crust within senozoic-aged sedimentary layers and are also present in volcanic roks, particularly andesite and dacite. Typically, these minerals consist of hydrous borates combined with alkaline cations such as Na^{+}, Ca^{++}, and Mg^{++}. Despite the shared composition among the extensive range of boron minerals in nature, distinctions arise due to variations in the quantity of crystal water present in their structures. (11)

Boron minerals vary in the proportions of boron oxide ($B_2 O_3$) they contain in their structures. (12) Boron minerals exhibit varying levels of boron oxide ($B_2 O_3$) in their compositions. Notably, among those with significant commercial importance are ($Na_2 B_4 O_7 \cdot 4H_2 O$) kernite, hydroboracite, ($NaCaB_5 O_9 \cdot 8H_2 O$) ulexite, ($Na_4 B_4 O_2 \cdot 10H_2 O$) tincal (borax), probertite, boracite, pandermite, and syzabelite (Table 1.3). (2)

Bor minerals are types of minerals that vary in terms of the boron oxide ($B_2 O_3$) ratios they contain. Among the boron minerals commonly found in Turkey are tincal, ulexite, and colemanite. A substantial part of the world's colemanite reserves is located in Turkey. Presented in Table 1.4, the distribution of various boron minerals around the world. (14)

The majority of boron reserves known as boron deposits are located in Turkey. According to the data obtained in 2017 (Table 1.5), the majority of our boron reserve deposits are composed of colemanite in Kestelek, Colemanite-Ulexite in Bigadiç, Tincal in Kırka, and Colemanite-Ulexite-Probertite in Emet. (13)

Table 1.3. Commercially significant boron minerals (13)

Minerals Formula	**Formula**
Inyoite	$Ca_2 B_6 O_{11} \cdot 13H_2 O$
Datolite	$Ca_2 B_2 Si_2 O_9 \cdot H_2 O$
Ascharite	$Mg_2 B_2 O_5 \cdot H_2 O$
Inderite	$Mg_2 B_6 O_{11} \cdot 15H_2 O$
Boracite	$Mg_3 B_7 O_{13} Cl$
Kernite	$Na_2 B_4 O_7 \cdot 4H_2 O$
Pandermite	$Ca_4 B_{10} O_{19} \cdot 7H_2 O$

Hydroboracite	$CaMgB_6O_{11} \cdot 6H_2O$
Meyerhofferite	$Ca_2B_6O_{11} \cdot 7H_2O$
Probertite	$NaCaB_5O_9 \cdot 5H_2O$
Tincal	$Na_2B_4O_7 \cdot 10H_2O$
Tincalconite	$Na_2B_4O_7 \cdot 5H_2O$
Colemanite	$Ca_2B_6O_{11} \cdot 5H_2O$
Sassolite (natural boric acid)	H_3BO_3
Ulexite	$NaCaB_5O_9 \cdot 8H_2O$

Table 1.4. Distribution of boron compound minerals at all the world (14)

Type	Mineral	Compound	B_2O_3 %	Location of minerals
Hydrogen Borates	SASSOLIT	H_3BO_3	56,3	Italy
Sodium Borates	TINKAL (BORAX)	$Na_2B_4O_7 \cdot 10H_2O$	36,5	USA, India, Argentina, Bolivia, Turkey
	TINTALCONITE	$Na_2B_4O_7 \cdot 5H_2O$	48,8	It is generally used as an accessory.
	KERNITE RASORITE	$Na_2B_4O_7 \cdot 4H_2O$	51	Turkey, Argentina, USA, China
Sodium-Calcium Borates	ULEXITE (BORONATRCALCITE)	$NaCaB_5O_9 \cdot 8H_2O$	43	Turkey, USA, Serbia, Peru, Bolivia, China, Chile
	PROBERTITIS (CRAMERITE)	$NaCaB_3O_9 \cdot 5H_2O$	49,6	USA (California/Death Valley)
Sodium-Calcium Borates	ULEXITE (BORONATRCALCITE)	$NaCaB_5O_9 \cdot 8H_2O$ (Tekrar)	43	Turkey, USA, Serbia, Peru, Bolivia, China, Chile
Calcium Borates	PROBERTITIS (CRAMERITE)	$NaCaB_3O_9 \cdot 5H_2O$ (Tekrar)	49,6	USA (California/Death Valley)
	COLEMANITE	$Ca_2B_6O_{11} \cdot 5H_2O$	50,8	Turkey (largest reserve)
	PANDERMITI (PRISEIT)	$Ca_4B_{10}O_{19} \cdot 7H_2O$	49,8	Turkey (Kırka, Bigadiç), Peru

Calcium Borosilicates	NOBLEIT	$CaB_6O_{10} \cdot 4H_2O$	62	USA (California/Death Valley)
	INYOITE	$Ca_2B_6O_{11} \cdot 13H_2O$	37,6	
	MEYERHOFFERITE	$Ca_2B_6O_{11} \cdot 7H_2O$	46,7	
	DATOLITE	$CaBSiO_4OH$	24,9	Russia, Kazakhstan
	DANBURITE	$CaB_2Si_2O_8$	28,3	USA (Danbury and Connecticut)
	HAVLIT	$Ca_4Si_2B_{10}O_{23} \cdot 5H_2O$	44,5	Turkey (Bigadic, Susurluk)
Magnesium Borates	HYDROBORASITE	$CaMgB_6O_{11} \cdot 6H_2O$	50,5	Turkey, Kazakhstan, Argentina
	INDERBORIT	$CaMgB_6O_{11} \cdot 11H_2O$	41,5	Kazakhstan (Lake Inder)
	ASHART(SZAYBELT)	$MgBO_2OH$	41,4	Kazakhstan, China
	BORASITE	$Mg_3B_7O_{13}Cl$	62,2	Turkey (Kırka, Emet, Bigadiç)
	KURNAKOVIT	$Mg_2B_6O_{11} \cdot 15H_2O$	37,3	Kazakhstan (Lake Inder)
	INDERIT	$MgB_3O_3(OH)_5 \cdot 5H_2O$	37,3	Kazakhstan (Lake Inder)
	SUANIT	$Mg_2B_2O_5$	46,3	North Korea (Suan)
	KOTOIT	$Mg_3B_2O_6$	36,5	Bundjiro Koto (1856-1935)
	PINNOITE	$MgB_2O_4 \cdot 3H_2O$	42,5	Germany, USA (California/Death Valley)
Other Borates	KAHNIT	$CaAsBO_6 \cdot 2H_2O$	11,7	Turkey (Emet)
	VONSENITIS	$(Fe,Mg)_2FeBO_5$	10,3	USA (California/Riverside)

	LUDVIGIT	$(Fe,Mg)_4\ Fe_2\ B_2\ O_7$	17,8	Ernst Ludwig (1842-1915)
	TUNELITE	$SrB_6\ O_{10}\cdot 4H_2O$	52,9	George Tunnel (1900-1996)
	BAKERITE	$Ca_4\ B_4\ (BO_4)(SiO_4)_3\ (OH)_3\cdot(H_2O)$	27,9	USA (California/Death Valley)
	SEARLESITE	$NaBSi_2\ O_5\ (OH)_2$	17	USA (California / Searles Lake)
	TEEPLEIT	$Na_2\ B(OH)_4\ Cl$	21,7	USA (California / Searles Lake)

Although boron is one of the less common and unevenly spread elements in the Earth's crust, there exist remarkable concentrations of boron at an industrial scale in specific localized regions. The most significant economic deposits are in Turkey, the United States, South America. (Figure 1.4).

Figure 1.4. World major borate mines

Table 1.5. The reserves of boron the distribution in Turkey (13)

REGION	**ORE TYPE**	**TOTAL(TON)**
KESTELEK	Colemanite	5,254,920
BİGADİÇ	Colemanite-Ulexite	628,350,480
KIRKA	Tincal	824,720,950
EMET	Colemanite-Ulexite Probertite	1,811,072,520
	TOTAL	**3,269,398.87**

1.1.2 History of the Boron Element

The presence of boron salts has captivated human interest since ancient times. The initial indications of utilizing boron salts, employed across various domains in antiquity, trace back to Tibet nearly 4 thousand years ago. During this era, Babylonians utilized boron salts diversely melting valuable items, Egyptians applied them in mummification (as an antiseptic), and Ancient Greeks and Romans used them for arena cleaning. In 875, Arabs embarked on the early stages of medicinal applications of boron salts:

The historical journey involving boron unfolds as follows:

- In the 13th century, Marco Polo introduced boron salts from Tibet to Europe.
- In 1771, Sassolite, a boron mineral, was uncovered in the hot springs of the Tuscany region, Italy.
- The ear 1808 marked the discovery by Louis Jacques Thernad and Joseph Louis Gay-Lussac, along with Sir Humphry Davy, who decomposed boric acid by heating it with potassium. The amorphous boron obtained through this method was deemed the purest known form for a considerable period.
- Boric acid production commenced in Italy in 1830, concurrent with the initiation of the first industrial borax mining in Chile in 1852.
- Subsequently, the USA rose to prominence as the primary contributor to the world's boron needs, discovering and operationalizing deposits in various regions.
- Turkey’s introduction to boron occurred in 1861 with the Mining Regulation, tracing its origins to the Sultançayırı region and Balıkesir – Susurluk district.
- In the contemporary era, Turkey, boasting the majority of boron reserves, has taken charge of production, marketing, and related activities through a state government decision, consolidating all its endeavors internally. (15,16)

1.1.3. Usage of Boron Element

Boron minerals find widespread applications in industries like glass, textile, insulation, and wood. Their versatile properties, including antiseptic and

water softening capabilities, make boron minerals valuable additives in detergents and soaps. Additionally, in the context of contemporary industrialization, boron minerals serve as effective flame retardants in textile materials. (17) It is observed to have applications as a plant micronutrient, semiconductor, optical fiber, and in the production of fiber-reinforced metal matrix composites for nuclear reactors. (18) To sum up, boron finds applications in the glass industry, soaps and detergents, textiles for its antiseptic properties, ceramics owing to its durability, and in insulating borosilicate glasses. (19)

Boron finds diverse applications, spanning from the glass industry to metallurgy and the aerospace sector to construction. In the glass industry, it contributes to the production of insulation and textile glass fibers, borosilicate glasses, optical fibers, and glass ceramics, while in the ceramic industry, it is utilized for enamel coatings and porcelain paints. In the nuclear industry, it plays a vital role in reactor control rods and waste storage, and in the aerospace sector, it is integral to spacecraft, aircraft, helicopters, and military armored vehicles. Widely employed in the electronics, electrical, and computer industries, boron is also a preferred additional additive in metallurgy. (37)

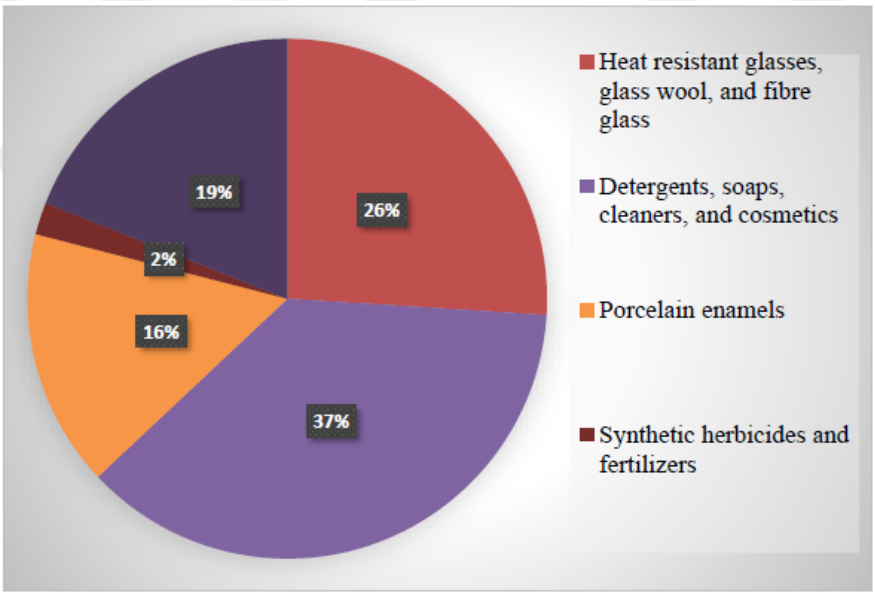

Figure 1.5. The reserves of boron the distribution in Turkey (19)

1.2 BORATES

Borates are the boric acid compound which composed of boron and oxygen known as boric acid. Boron is the only elements of non-metallic element with electron deficiency. Boron also forms a strong covalent bond

with oxygen, thanks to its high affinity for oxygen. In short, borates are expressed as $B_2\ O_3$ and are also defined as boric acid salt. (19)

Borates result from the combination of elemental boron atoms containing B-O or B-OH groups in their structures with oxygen. In uncomplicated borates, each boron atom bonds with three oxygen atoms. As a result, boron varieties such as $H_3\ BO_3$ contain only BO_3 units in their configuration. These aggregated BO_3 units give rise to various polymeric ring structures and chains. In addition to BO_3 units, many complex borate structures also contain BO_4 units. (20)

1.2.1. History of the Borates

The discovery of borates dates back thousands of years. It has been observed that borate minerals were first encountered in ancient times and have been used for gold and silver refining since the 8th century. Borates minerals have been used in many different areas such as ceramics, medicine, and wood preservatives (19). Figure 1.6 represents the list of countries where borate mineral resources have commonly occurred throughout. (24)

In the present era, borates find extensive applications across various fields owing to their distinctive features, including lightweight composition, heat resistance, effect, superb chemical durability, and remarkable mechanical strength. Borates are predominantly utilized in the production of fiber glass, enamel, textile. Furthermore, Borates are incorporated into daily and environmental applications. (24)

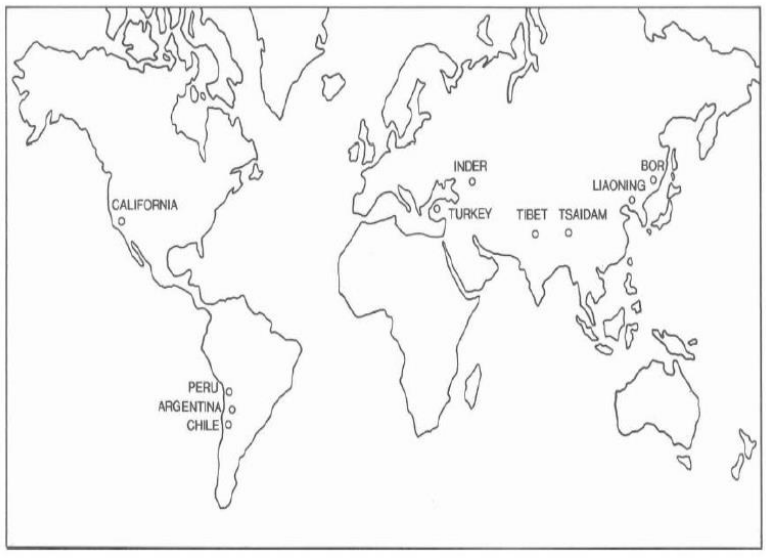

Figure 1.6. Source of Borate Minerals

1.2.2. Usage of Borates

Owing to their numorous properties, borates have found in the application of various chemistry domains. When used over extended periods under standard conditions, borates exhibit no adverse effects on humans, the environment, or other living organisms. With their diverse uses, borates are chosen as bactericides, fungicides, and insecticides in a broad of applications, spanning from cosmetics to wooden structures. Beyond playing a crucial role in the development and formation of plants, borates serve as fertilizers in agriculture, substantially enhancing product quality and yield. Leveraging their capacity to bind and consolidate dispersed particles in different compositions, borates function as adhesives in cosmetics and as viscosity agents in paints. (21)

1.2.3. Classifications of Borates

Borates are divided into two categories: non-hydrated and hydrated borates. In the structure of hydrated borates, H_2O crystalline water units and B-OH groups are present. Consequently, the primary borate units in fully hydrated forms are $B(OH)_3$ and $[B(OH)_4]^-$. (22) The trigonal-BO_3 (Δ) group results from the bonding of the boron atom with a three-coordinated oxygen atom, while the tetragonal-BO_4 (T) group forms when the four-coordinated boron atom bonds with oxygen. Hexa Borates, encompassing 3 BO_4 (T) and 3 BO_3 (Δ) groups in their structure, involve coordination of OH groups and H_2O molecules with the metal cation in the system.

The arrangement of the triangular planar BO_3 coordination can vary to produce oxyanions, containing boron, such as monomeric triangular or metaborate $[BO_3]^{3-}$, binuclear triangular planar or known as pyroborates $[B_2O_5]^{4-}$, triangular cyclic $[B_2O_3]^{3-}$ as orthoborates, and polynuclear infinite chains $[(BO_2)^-]$ (Figure 1.7 - 1.9).

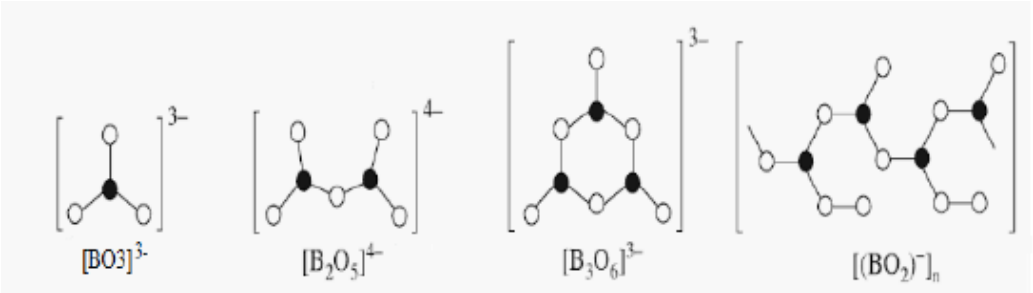

Figure 1.7. Structure of Borates (23)

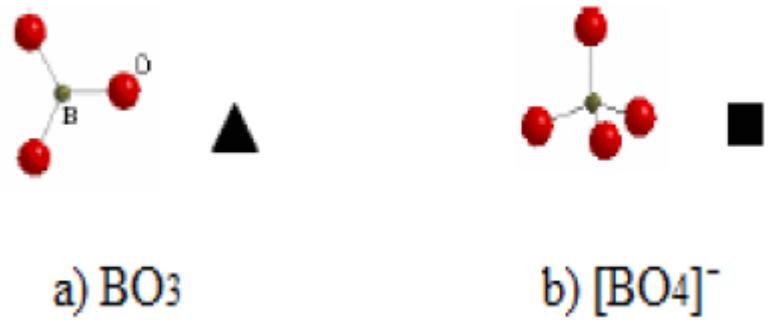

Figure 1.8. BO_4 tetrahedral and BO_3 triangular planar (23)

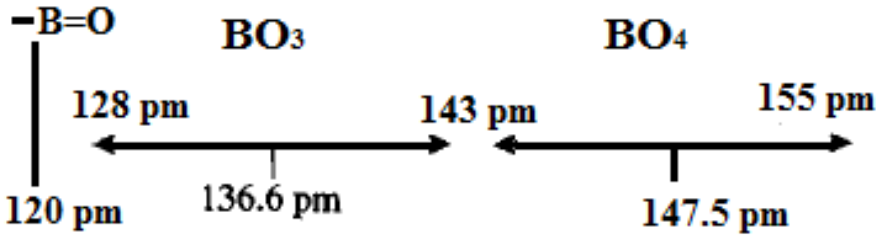

Figure 1.9. The change of bond distances of borates (22)

1.2.3.1. Pyroborates

In the borate crystal structure the interaction between BO_4 tetrahedral and BO_3 triangular planar units leads to the formation of the boric oxide group. Pyroborates, a subset of complex borates, exhibit a distinctive structure wherein two triangles of BO_3 are interconnected by sharing an oxygen atom, resulting in a non-planar arrangement of BO_3 units. (25)

1.2.3.2. Metal Pyroborates

Metal pyrobolates have attracted the attention of researchers because they have impressive properties such as resistance to decay, high thermal insulation, high heat-mechanical resistance, lightness and high elasticity coefficient, and numerous synthesis studies on metal borates have been employed by many research communities. (26,44)

Borate compounds have recognized by many researchers because of their potential in offering unique possibilities for uncovering novel compounds with intriguing characteristics, such as luminescent materials and materials for second harmonic generation materials (27,28). Calcium borates, specifically, exhibit remarkable stability even under elevated temperatures (flame retardancy),

remaining non-reactive and non-decomposable. Moreover, as of now, there is a lack of data regarding the toxic or carcinogenic nature of calcium borates. (29) Moreover, calcium borate are also known to be remains stable at high temperatures and no data on their toxic or carcinogenic nature, they also have flame retardant and antibacterial properties (Figure 1.10). (30)

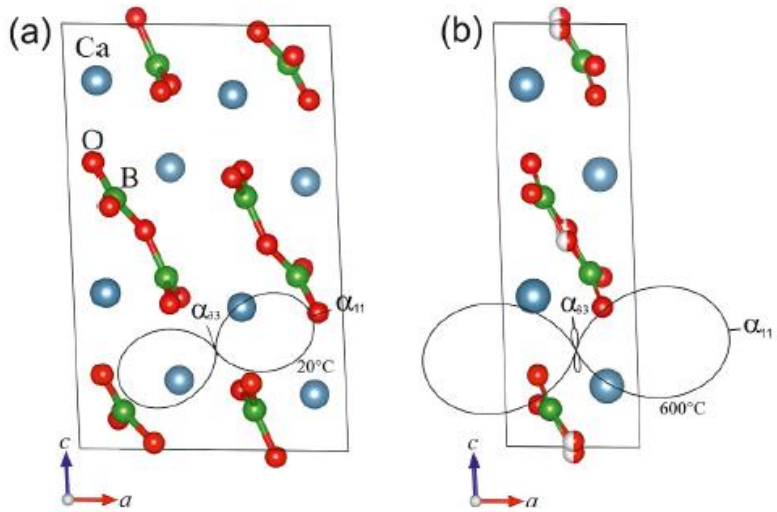

Figure 1.10. Crystal structures of low-temperature (a) γ-Ca_2 B_2 O_5 and high-temperature (b) α-Ca_2 B_2 O_5 polymorphs. (30)

Calcium borates offer promising optical properties when doped with various rare earth elements. Compounds such as $Ca3(BO_3)2:Eu^{3+}$ and Ca_2 B_2 O_5 :RE (RE = Eu^{3+}, Tb^{3+}, Dy^{3+}) exhibit high photoluminescence intensity, which is reflected in the thermoluminescence properties of lanthanide ions (Ce^{3+}, Sm^{3+}, Eu^{3+}, Dy^{3+} and Yb^{3+}). It has been determined that it provides more optical properties to the materials. (30)

A suggested sequence of phase transitions in Ca_2 B_2 O_5 is as follows:

γ-Ca_2 B_2 O_5 ↔ (at 511◦C) β′-Ca_2 B_2 O_5 ↔ (at 587◦C) α-Ca_2 B_2 O_5

Ca_2 B_2 O_5 polycrystals were obtained by solid state reaction from $CaCO_3$ and H_3 BO_3 compounds, which were pre-dried for 3 hours at high temperature (600 °C). A synthesis processes was carried out in air, in platinum crucibles, at 1250 °C for 10 hours. Due to volatility occurring at high temperatures (1250 °C / 10 hours), the Ca_2 B_2 O_5 sample contained a slight impurity of Ca_3 B_2 O_6 due to the loss of B_2 O_3 . To correct this situation, extra H_3 BO_3 was added at 5 wt%. According to the results observed in XRD, the crystal structure of monoclinic modification γ-Ca_2 B_2 O_5 at low temperature is completely ordered,

unlike the monoclinic α-Ca_2 B_2 O_5 at high temperature. The fundamental disparity among the structures of Ca_2 B_2 O_5 modifications arises from the specific arrangement of BO_3 triangles within pyroborate groups. (30)

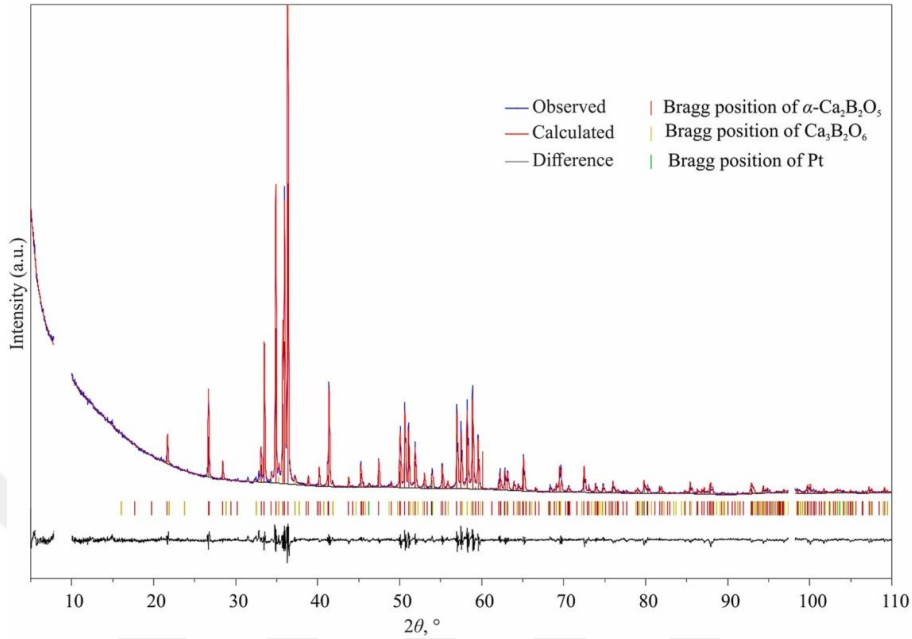

Figure 1.11. Intensity profiles for the powder X-ray Rietveld refinement of α-Ca_2 B_2 O_5

Figure 1.11 shows XRD patterns of α-Ca_2 B_2 O_5 at 600 °C, including impurities of Ca_3 B_2 O_6 . While borates replace acid radicals, these boron salts are alkali metal salts and are formed as a result of the reaction of Ca, Mg, Na and a boron acid with H_3 BO_3 radical. (31,32)

Calcium borate is involved and plays a role in many studies due to its various properties. Many literature studies have been done and discussed the properties of calcium pyroborate. One of them, the Ca_3 $(BO_3)_2$ compound, has a trigonal crystal structure with the space group R-3c (crystal lattice parameter information: a: 6.6377 Å, c: 11.849 Å and Z: 6 [6-7]). When Nd^{3+} , Dy^{3+} and Er3+ are added to this crystal structure, it is seen that the Ca_3 $(BO_3)_2$ compound can be used as a technological material in an important laser application.(33,34)

If we examine another literature study, we see that in a study initiated by Huang and Liu, they accepted the phosphorescent compound CaB_2 O_4 :Eu^{3+} and the substance Ca_4 B_{10} O_{19} ·$7H_2$ O:Eu^{3+} as precursors and characterized them by preparing them by the thermal conversion method. In this study, the effects of the preparation conditions of the above-mentioned precursor and the calcination

temperature on the luminescence property of the obtained compound were investigated. As a result, it was determined that the $CaB_2O_4:Eu^{3+}$ phosphorus maximum intensity of the luminescence was acquired by heating the products at 900 °C for 4 hours. Additionally, it has been recorded that the precursor was prepared by hydrothermal processes supported by 0.6 wt% PEG4000 at 120 °C for 24 hours. Huang and Liu also stated that the $CaB_2O_4:Eu^{3+}$ phosphorus prepared by this method had better dispersion and strong emission intensities than the $CaB_2O_4:Eu^{3+}$ synthesized by the traditional high-temperature solid-state method. (35)

In order to understand the emission colors of Eu^{2+} doped oxides, the frequent emission energies appearing in Eu^{2+} can be explained by looking at the coordination numbers and geometries of the oxygen atoms. Long wavelength emission of Eu^{2+} doped oxide was observed even in the UV red region. This emission energy was determined by doping Eu^{2+} in the host structures where atoms such as Ba and Sr are present with oxygen atoms. (36)

To examine the thermoluminescence effect of different doppler; the studies have been conducted on the production of $Ca_2B_2O_5$:Dy ceramics using the solid-state reaction method. It was stated that ceramics were prepared by doping $Ca_2B_2O_5$ with Dy and enriching it with 10B and 11B for neutron detection. The optimal Dy concentration, determined by comparing TL intensities at various Dy concentrations versus Ca, was found to be 4 mol%. The powders were subjected to stoichiometric mixing and heated for 8 hours at 1123 K. Then, the materials were crushed, homogenized and turned into tablets with a diameter of 13 mm. The materials was ground, homogenized and pressed into 13mm diameter tablet which then sintered for 6hours at 1123K. First, as a result of irradiation with basic neutrons, it was observed that the 10B-enriched Dy-doped sample was denser than the 11B-enriched Dy-doped sample. It has been shown that the TL of 10B ceramics increases with γ-rays, α-rays and 7Li produced from the reactions of 10B(n, α)7Li and 10B(n, α)7Li*. However, the lowest detected radiative flux (3.0 x 105 neutron cm−2) is lower than the detectable lower limits of $CaSO_4$:Dy + Dy_2O_3 + KCl and Dy^{3+} doped $CaO–Al_2O_3–B_2O_3$ TL materials. As a result of this study, the applicability of these materials as TL materials for neutron detection has been demonstrated. The main reasons for its suitability are the effective atomic numbers of calcium borates (CaB_4O_7 ; 12.5

26 and CaB_2O_4 ; 14.1 27), which are close to Zeff = 13.8 28 (human hard tissue). Additionally, the ionic radius of Ca^{2+} (1.00 Å at the six-coordination site) is rare, such as Ce^{3+} (1.01 Å), Sm^{3+} (0.95 Å), Tb^{3+} (0.92 Å) and Dy^{3+} (0.91 Å) (at the six-coordination site). It has been stated that it is similar to that of soil ions. (38)

It has been stated that Hajime Komiya and colleagues produced $Ca_2B_2O_5$ and Tb^{3+} -doped ceramics enriched with 10B (10B ceramics) and 11B (11B ceramics) to be used as thermoluminescence (TL) materials for neutron detection applications. The TL properties were examined after different irradiations (X-ray, particle beam, and neutron irradiation) of the ceramics. It was observed that the neutron-induced TL intensity was higher in the 10B ceramics. The neutron detection of the ceramics was identified to be below that of several TL materials reported before. Additionally, it was noted that the peak intensities at the lowest temperature of 375K were reached, and the density of 10B-enriched samples was higher than that of 11B-enriched Tb^{3+} -doped samples. Therefore, these ceramics demonstrate applicability as TL dosimeter materials for neutron detection. (39)

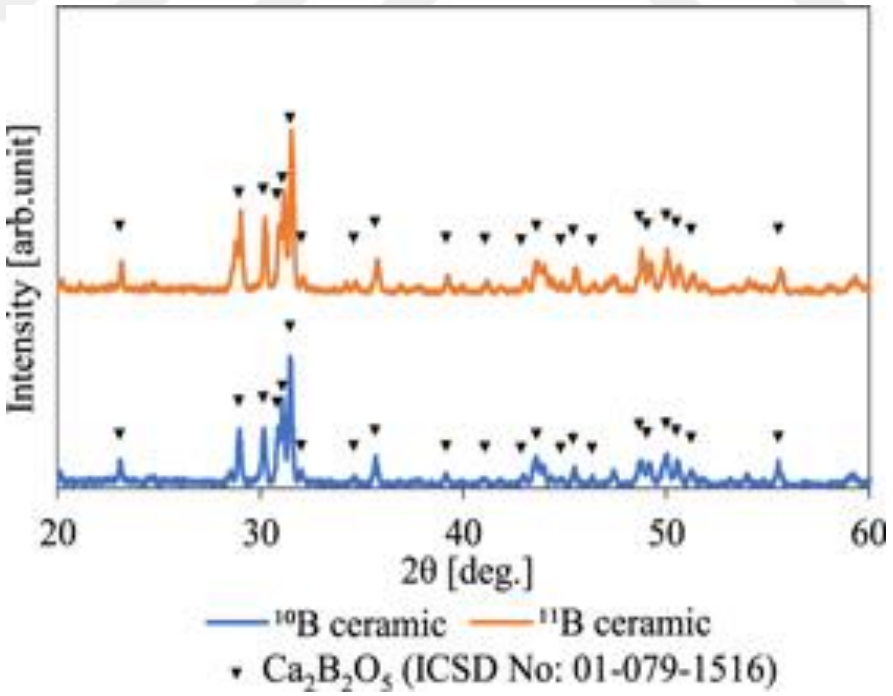

Figure 1.12. (Color online) X-ray diffraction patterns of 10B and 11B ceramics

In another study example, $Ca_2B_2O_5$ nanofibers are synthesized by the hydrothermal reaction method with the contributions of Eu^{3+}, Tb^{3+} and

Dy^{3+} ions. It was stated that the nanofibers in this synthesis were examined with TEM, EDS and SEM spectra. In the FTIR (Figure 1.13), it is seen that $Ca_2\ B_2\ O_5$ provides transparency with a wide band gap between 200 and 800 nm. It is observed that Eu^{3+} - and Tb^{3+} -doped $Ca_2\ B_2\ O_5$ nanofibers show intense transition of $^5D_4 \rightarrow {}^7F_5$ for Tb ions in red and green colors, respectively, with optical stimulation. Single phase $Ca_2\ B_2\ O_5$:Dy^{3+} white phosphor was obtained. The absolute quantum ratios for $Ca_2\ B_2\ O_5$ nanofibers are 65% Eu^{3+} -, 35% Tb^{3+} - and 37% Dy^{3+} doped, respectively. It is interpreted as $Ca_2\ B_2\ O_5$ doped with Eu^{3+} and Dy^3, which has good thermal stability and luminescence. (41)

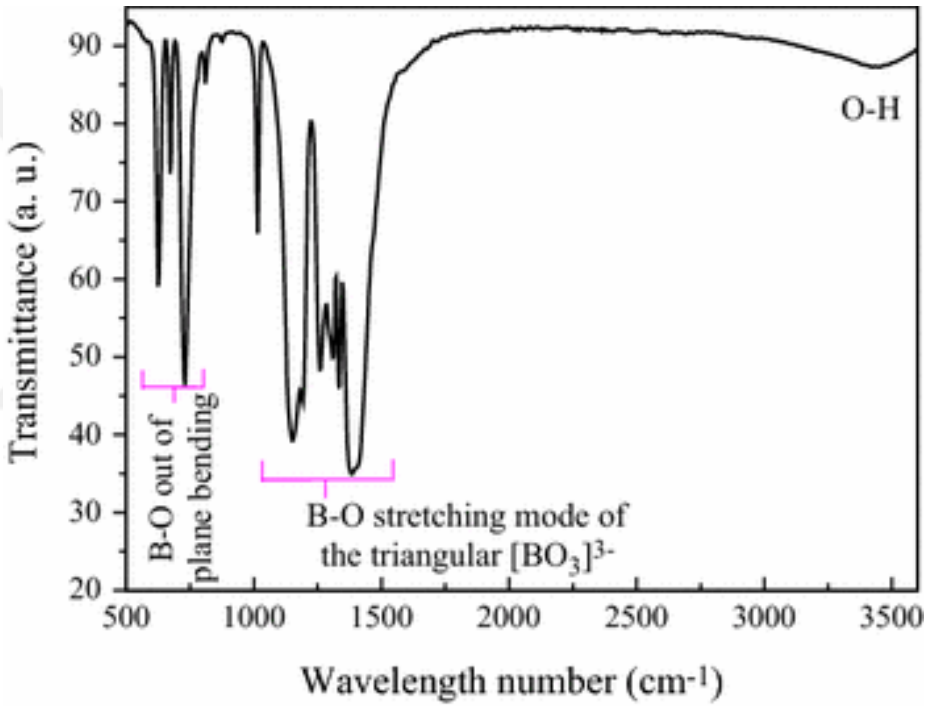

Figure 1.13. FT-IR spectrum of Eu^{3+} ion-doped $Ca_2\ B_2\ O_5$ nanofibers

1.2.4. Synthesis Methods of Borates

Various methods have been used to synthesize ceramic powders. Among these methods, a higher level of safe material is obtained with 3 collection methods: solid state method, solid gas method and solution method. (40)

1.2.4.1. Solid State Method

Solid-state methods offer various approaches for the synthesis of borates. In preparation of ceramic powders, many methods have been applied flux processes, ceramic method, metallurgical route, solid-state combustion method, mechano-chemical method, involve the use of finely ground powders derived

from oxides, oxalates, carbonates, nitrates, sulphides, phosphates, and others. metal-containing compounds. These precursor materials are exposed to high temperatures and long reaction times during the synthesis processes. The solid-state method provides a versatile platform for synthesizing borates, adding to the variety of techniques available for their production. (42)

1.2.4.2. Solid Gas Method

This method is recognized for the thermal decomposition of compounds containing boron. In these processes, especially at elevated temperatures like 900°C, diborane transforms into deca-borane, or boron chlorides undergo reduction with hydrogen. As a consequence of these reactions, elemental boron is produced with a crystalline structure and high purity. (43)

1.2.4.3. Solution Method

This approach is favored for producing high-purity fine particle powders and comprises three methods: the co-precipitation technique, solution combustion method, sol-gel processes. In the sol-gel processes, reactants like acetates, alkoxides, acetylacetones and formats undergo hydrolysis, polycondensation at carbon-based solvents. This is followed by the formation of polymeric gels at a specific temperature, ultimately resulting in the production of desired products. The co-precipitation method typically utilizes carbonates and nitrates as initial materials. (43)

1.2.4.3.1 Solution Combustion Synthesis (SCS)

The solution combustion method, whose foundations were laid by Merzhano and colleagues in 1967, is based on the main principle of the processes withstanding high temperatures. This method is exothermic and, over the years, evolved into the Solution Combustion Synthesis. It is characterized by its energy efficiency due to the self-sustained combustion reaction feature. (40)

We can examine this method in more detail by looking at the advantages it offers:

- When mass production is considered, it is preferred because it can be considered simple and cost-effective.
- It has the capacity to produce products with high active surface area in the field of photoatalysts.

- It facilitates the formation of metastable phases, providing new performance properties.
- During the synthesis, it enables the production of high purity ternary and quaternary oxides.
- It has the capacity to produce high quality products like metallic compounds, metal matrix composites, oxides, nitrides, carbides, ceramics.

2. AIM AND SCOPE OF THE STUDY

The main purpose of the first part of this study is to synthesize and characterize nano-crystalline calcium pyroborate ceramic powders by solution combustion synthesis, which is an easier and simpler method. The reaction conditions were changed using different organic fuels (citric acid, glycine, HMTA, tartaric acid and urea) and their effects on crystal structures were comparatively examined.

Secondly, some lanthanide ion (Eu^{3+} and Sm^{3+}) doped calcium pyroborate ceramic powders are also synthesized using similar procedure to determine the impact of type of dopant material (Eu^{3+} and Sm^{3+}) and their concentrations (0.005, 0.01, 0.02 and 0.05) on the structural properties of calcium pyroborates.

In the third stage, the crystal structures of calcium pyoborate ceramics fabricated in this work will be characterized by XRD technique and the crystallite sizes will be calculated with the Debye-Scherrer equation to estimate the nano-sized property of the resulting products. Additionally, the vibration movements of the bands in the BO_3 group will be examined by the FTIR spectroscopy method.

In the last stage, the optical properties of the products obtained throughout this thesis are studied by using UV-Visible spectroscopic technique.

3. MATERIALS AND METHODS

3.1 CHEMICALS

In this present work, the chemicals that were used are listed as follows;

Boric acid, $H_3\ BO_3$	: Merck, 99.00%
Calcium nitrate hexahydrate, $Ca(NO_3)_2 \cdot 4H_2O$	: Merck, 99.00%
Citric acid monohydrate, $C_6H_8O_7 \cdot H_2O$	: Merck, 99.50%
Carbohydrazide, CON_4H_6	: Aldrich, 98.00%
Hexamethylenetetramine (HMTA), $C_6H_{12}N_4$	: Merck, 99.90%
Glycine, $C_2H_5NO_2$	: Merck, 99.70%
Tartaric acid, $C_4H_6O_6$	: Merck, 99.00%
Potassium Bromide, KBr, for IR Spectroscopy	: Merck, 99.90%
Urea, CH_4N_2O	: Merck, 99.50%

3.2 INSTRUMENTS

3.2.1. **Fourier Transform Infrared Spectrophotometer**

To analyze the infrared spectra and bond variations of the final products, the Perkin Elmer Fourier Transform Infrared (FTIR) spectrophotometer was employed within the range of 4000-400 cm^{-1}. Infrared spectra were obtained by creating pellets with a KBr-to-product ratio of 0.1500:0.0010 (wt/wt).

3.2.2. **X-ray Powder Diffractometer**

The Rigaku miniflex and multiflex X-ray powder diffractometers were employed to analyze the structural properties of the products using CuKα radiation (30-40 kV, 10-20 mA, λ=1.54056 Å). The XRD patterns' data were acquired using Rigaku programs and verified against the ICDD data cards.

3.2.3. **Furnace**

The synthesis of metal pyroborates involved conducting reactions in the temperature range of 400-900°C using the Nuve MF 120 furnace.

3.2.4. **Hot plate**

A VELP brand heating device was employed in the synthesis of calcium pyroborates.

3.2.5. **UV-VIS Spectrometer**

The Perkin Elmer Lambda 35 UV-VIS Spectrophotometer, operating in the wavelength range of 200-900 nm, was utilized to record and determine the optical properties of the products. The acquired spectra were graphed using the Data Processesor WinLab program.

3.3 Experimental Procedure

The preparation of calcium pyroborates was successfully done by Solution Combustion Synthesis (SCS) method. The starting materials are calcium nitrate hexahydrate $Ca(NO_3)_2 \cdot 4H_2O$, H_3BO_3 and different types of fuels such as glycine, citric acid, HMTA, urea, tartaric acid. $Ca(NO_3)_2 \cdot 4H_2O$ and H_3BO_3 were used as Ca and B source, respectively with 1:1. of Ca:B mole ratio.

3.3.1. **Synthesis of Calcium Pyroborates**

In the calculation, the determined amount of $Ca(NO_3)_2 \cdot 4H_2O$, boric acid and each fuel source were dissolved separately in distilled water. The resulting homogeneous mixtures were mixed with a magnetic stirrer and allowed to evaporate at 370°C until a gel-like residue was formed. For the continuation of the experiment, a small portion of the gel was collected and the remaining gel was placed in an oven preheated to 400°C for 5 minutes (Figure 3.1). The resulting product was then ground and heated at temperatures ranging from 400°C to 1000°C for one hour each. All products heated at different temperatures were stored for characterization studies.

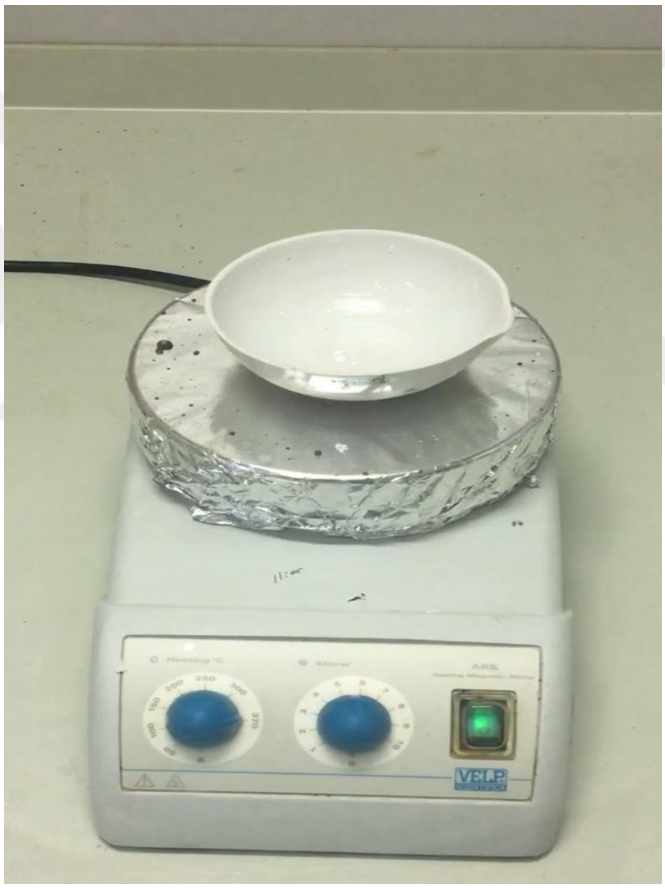

Figure 3.1. The experimental procedure section of the synthesis includes a image.

The same procedure mentioned above was conducted with different fuels, and the anticipated reactions are outlined below:

Glycine

$18Ca(NO_3)_2 \cdot 4H_2O_{(s)} + 2H_3BO_{3\,(s)} + 20C_2H_5NO_{2(s)} \rightarrow 9Ca_2B_2O_{5\,(s)} + 9N_{2(g)} + 20CO_{2(g)} + 72H_2O_{(g)}$

Urea

$6Ca(NO_3)_2 \cdot 4H_2O_{(s)} + 6H_3BO_{3\,(s)} + 10CH_4N_2O_{(s)} \rightarrow 3Ca_2B_2O_{5\,(s)} + 6N_{2(g)} + 10CO_{2(g)} + 24H_2O_{(g)}$

Tartaric Acid

$2Ca(NO_3)_2 \cdot 4H_2O_{(s)} + 2H_3BO_{3\,(s)} + 2C_4H_6O_{6(s)} \rightarrow Ca_2B_2O_{5\,(s)} + 2N_{2(g)} + 2CO_{2(g)} + 20H_2O_{(g)}$

HMTA

$18Ca(NO_3)_2 \cdot 4H_2O_{(s)} + 18H_3BO_{3\,(s)} + 5C_6H_{12}N_{4\,(s)} \rightarrow 9Ca_2B_2O_{5\,(s)} + 9N_{2(g)} + 20CO_{2(g)} + 72H_2O_{(g)}$

Citric Acid

$18Ca(NO_3)_2 \cdot 4H_2O_{(s)} + 18H_3BO_{3\,(s)} + 20C_6H_{10}O_{8(s)} \rightarrow 9Ca_2B_2O_{5\,(s)} + 9N_{2(g)} + 20CO_{2(g)} + 72H_2O_{(g)}$

3.3.2. **Synthesis of Rare Earth Metals (RE: Eu^{3+}, Sm^{3+}) doped $Ca_2B_2O_5$ using Glycine Fuels**

Calcium pyroborate ($Ca_2 B_2 O_5$) powders were synthesized with various quantities of Eu^{3+} and Sm^{3+} ion by solution combustion processes. Dopant concentrations were used as x = 0.005, 0.01, 0.02, 0.05 mol to obtain $Ca(2-x)RE(x)B_2 O_5$.

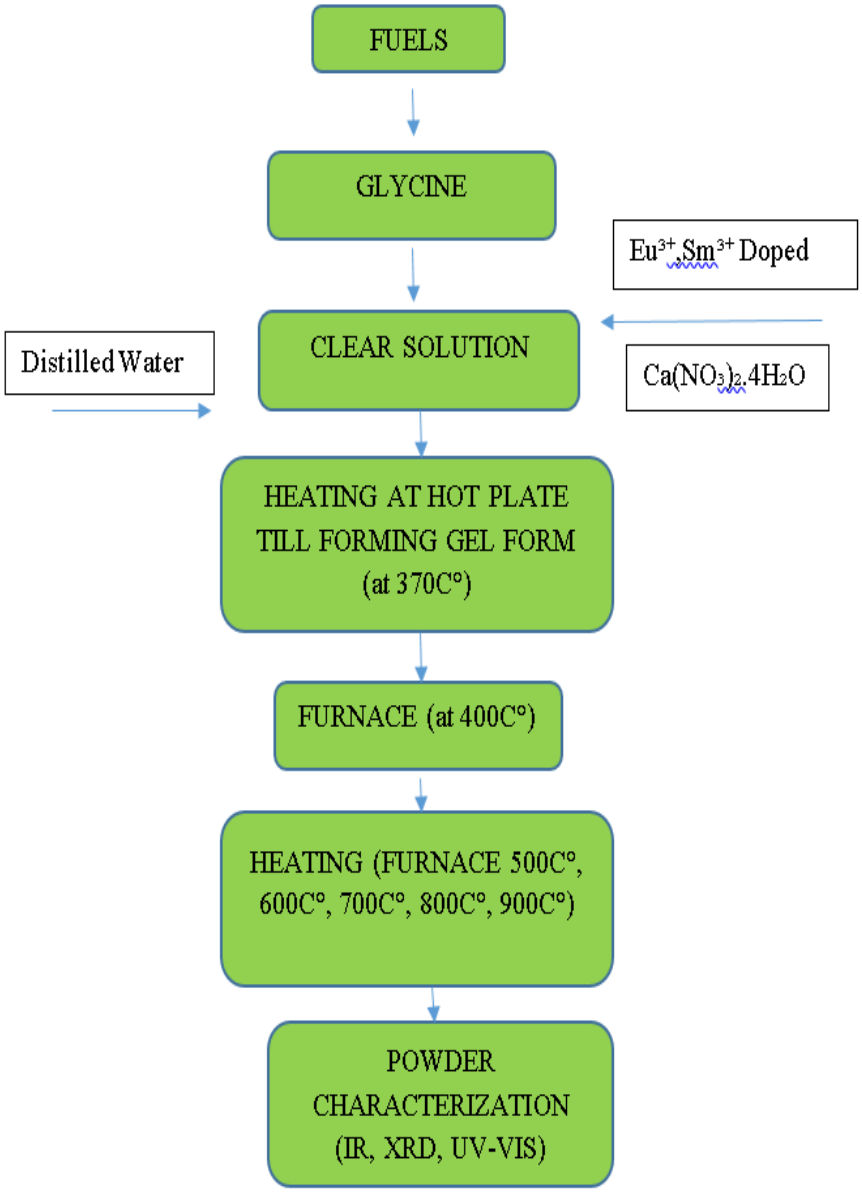

Figure 3.2. Procedure for RE metal ($Eu^{3+}$and Sm^{3+}) doped $Ca_2B_2O_5$ synthesis with SCS method.

4. RESULTS AND DISCUSSIONS

Calcium pyroborates, $Ca_2\ B_2\ O_5$ were synthesized by solution combustion synthesis (SCS) by adjusting the fuel types and temperatures. In order to examine its fuel effect glycine, citric acid, HMTA, urea, and tartaric acid were used. Furthermore, reaction temperatures were also varied from 400°C to 1000°C and the samples were heated for an hour. Fuel:oxidizer ratio and Ca:B ratio were applied in 1:1 mole ratio, respectively.

During the preparation of $Ca_2\ B_2\ O_5$, different behavior of solution was observed. In some fuels, more gas release was observed during the synthesis than in other fuels, while in some fuels, rapid dissolution in the solvent was observed.

Glycine:

Initially, the solution was homogeneous, colorless, and gel formation and gas evolution were observed at 370°C. The colorless gel produced a small amount of gas during the precursor gel was colorless and formed a soft, white product after preheating at 400°C for 5 min.

Picture 4.1. The pictures of $Ca_2\ B_2\ O_5$ samples for glycine fuel synthesis

Urea:

Colorless homogeneous solution, gel formation was observed at 370°C and gas evolution was observed. The colorless gel produced a small amount of gas

during. The gel was colorless and formed a light yellow-white product upon preheating at 400°C for 5 min.

Picture 4.2. The pictures of $Ca_2\ B_2\ O_5$ samples for urea fuel synthesis

HMTA:

The colorless precursor gel was obtained and formed a light brown product after heated for 5 minutes at 400°C and the light brown powder products were obtained.

Picture 4.3. The pictures of $Ca_2\ B_2\ O_5$ samples for HMTA fuel synthesis

Citric Acid:

The solution was homogeneous, colorless, and gel formation and gas evolution were observed at 370°C. The gel was colorless and formed a hard, black product after preheating at 400°C for 5 min.

Picture 4.4. The pictures of $Ca_2\ B_2\ O_5$ samples for citric acid fuel synthesis

Tartaric Acid:

The colorless homogeneous solution was turned into yellow-like gel after continuously stirred at 370°C. The amount of gas evaporated was normal. After preheating for 10 minutes at 400°C, a dark gray fluffy soft product was obtained.

Picture 4.5. The pictures of $Ca_2\ B_2\ O_5$ samples for tartaric acid fuel synthesis

Firstly, the heating process was done at 400°C 1 hour and followed by 500°C.1 hour. After the heating processes at 600°C for 1 hour, the doped $Ca_2\ B_2\ O_5$ product exhibited a white color when HMTA, gly, and urea were used as fuel. However, the product turned black when CA was used as fuel, and it appeared grey when TA was the fuel source. Subsequent processeses included heating at 700°C for 1 hour, followed by processeses at 800°C for 1 hour, 900°C for 1 hour, and 1000°C for 1 hour.

4.1 Rare Earth (RE: $Sm^{3+}$and Eu^{3+}) doped $Ca_2B_2O_5$ from Gly Fuel

$Ca_2\ B_2\ O_5$ doped with rare earth elements (RE: Sm^{3+} , Eu^{3+}) was synthesized at different temperatures (400C°-900C°) using the solution combustion method with calcium nitrate, boric acid.

- **Eu^{3+} doped $Ca_2\ B_2\ O_5$**

Initially, the concentration of rare earth metal ions was varied at 0.005, 0.010, 0.020, and 0.050 mol with utilizing a magnetic stirrer, the materials were thoroughly mixed in a porcelain evaporating dish and heated to 370°C until gel formation ocurred.

Subsequently, the mixture was placed in a preheated furnace set at 400°C. The entire combustion process for the production of $Ca_2\ B_2\ O_5$ material doped with rare earth metals (Eu^{3+}) took 10 minutes. The precursor gel was colorless, white product after preheating at 400°C for 10 min.

Secondly, each crushed samples were put into crucible and introduced to the preheated furnace at 400 - 900°C with 100°C interval for an hour to complete the combustion process and discard the organic compounds.

At first heating temperature (400°C 1h) processes and the heating processes of 500 °C 1h. was started. After the heating processes of 600°C 1h., the color of doped $Ca_2\ B_2\ O_5$ product was lighter white when glycerin were used as fuel. After 700°C 1h. processes, the heating processes of 800°C 1h. and 900°C 1 h. and 1000°C 1h. was completed.

At these temperatures, no detectable color difference or any other observable color change has been noted. A time difference of 10 to 30 seconds between concentrations during the combustion process has been observed.

- **Sm^{3+} doped $Ca_2\ B_2\ O_5$**

Initially, the concentration of rare earth metal ions was varied at 0.005, 0.010, 0.015 mol with utilizing a magnetic stirrer, the materials were thoroughly mixed in a porcelain evaporating dish and heated to 370°C until gel formation ocurred.

Subsequently, the mixture was placed in a preheated furnace set at 400°C. The entire combustion process for the production of $Ca_2\ B_2\ O_5$ material doped with rare earth metals (Sm^{3+}) took 10 minutes.

Secondly, each crushed samples were put into crucible and again gain put the preheated furnace at 400 - 900°C with 1000°C interval for an hour to complete the combustion process and discard the organic compounds.

At first heating temperature (400°C 1h) processes and the heating processes of 500 °C 1h. was started. After the heating processes of 600 °C 1h., the color of doped $Ca_2\ B_2\ O_5$ product was lighter white when glycin was used as fuel. After 700°C 1h. processes, the heating processes of 800 °C 1h. and 900 °C 1 h. and 1000°C 1h. was completed.

At these temperatures, no detectable color difference or any other observable color change has been noted. A time difference of 10 to 30 seconds between concentrations during the combustion process has been observed.

4.2 FT-IR Spectroscopy Studies

Strong IR absorption bands were observed above 1000 cm^{-1}. As for the IR spectroscopy, the modes selected by B–O from the $[BO_3]^{3-}$ groups can be examined. (41). The broad selection signals in O-H units between 3300-3500 cm^{-1} were assigned. (41) The IR spectra of the synthesis of the products obtained with glycine, tartaric ac1id, citric acid, HMTA, and urea as fuels at different temperatures are shown in the figures below**.**

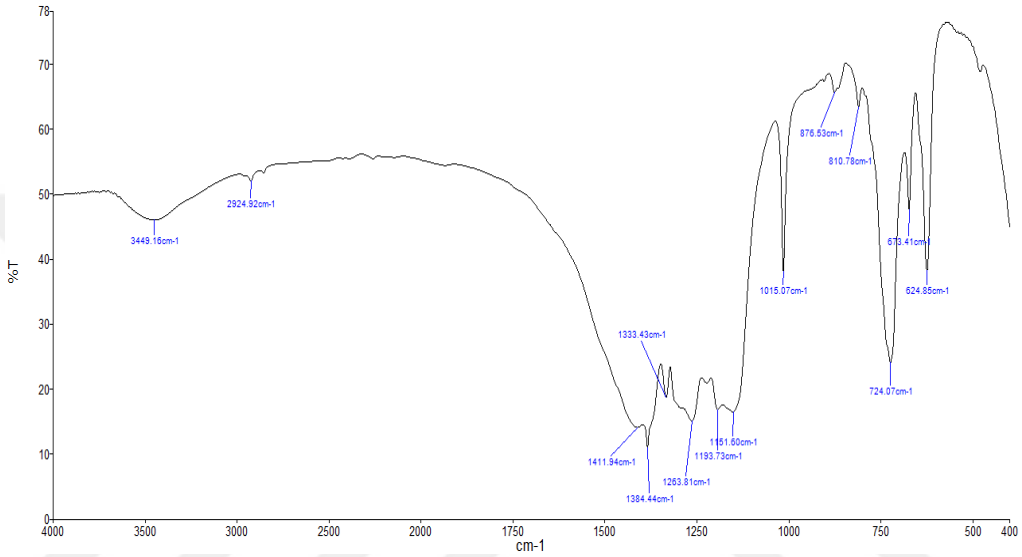

Figure 4.1. FT-IR Spectra of Synthesis $Ca_2\ B_2\ O_5$ Using Glycine (400C°.5mins)

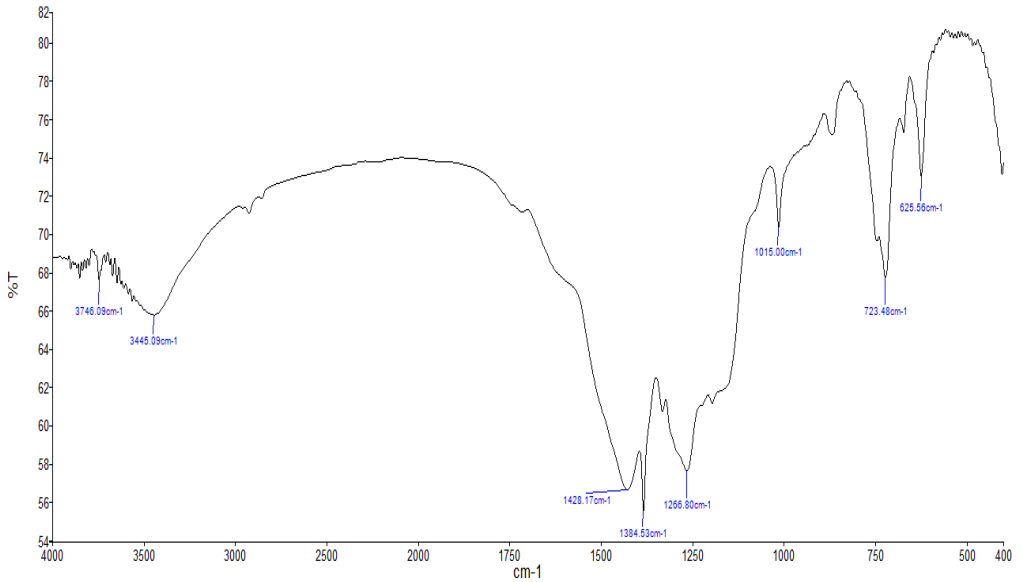

Figure 4.2. FT-IR Spectra of Synthesis $Ca_2\ B_2\ O_5$ Using TA (400C°.5mins)

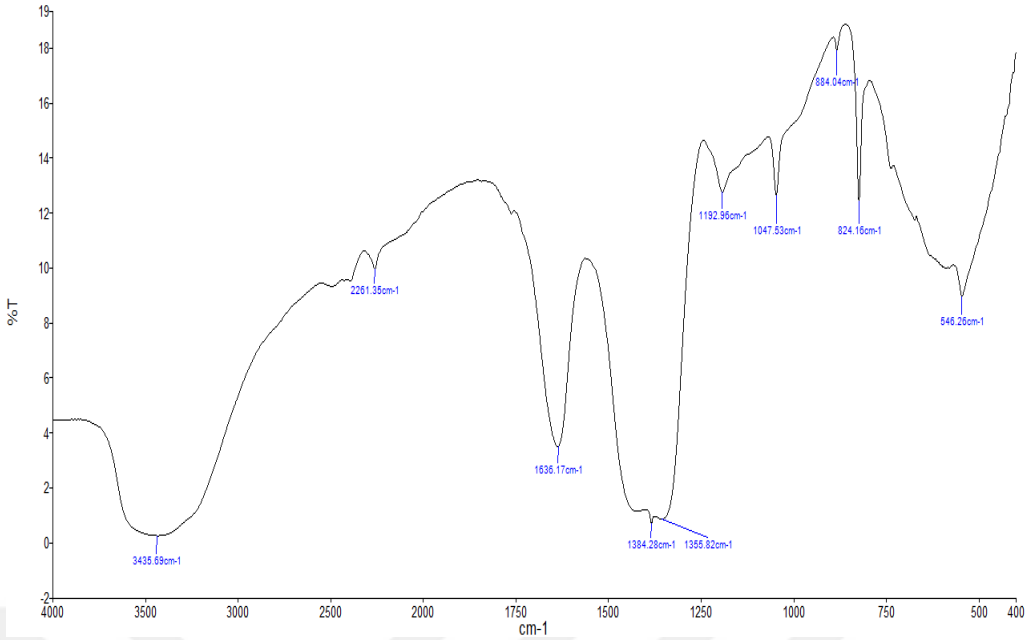

Figure 4.3. FT-IR Spectra of Synthesis Ca_2 B_2 O_5 Using Urea (400C°.5mins)

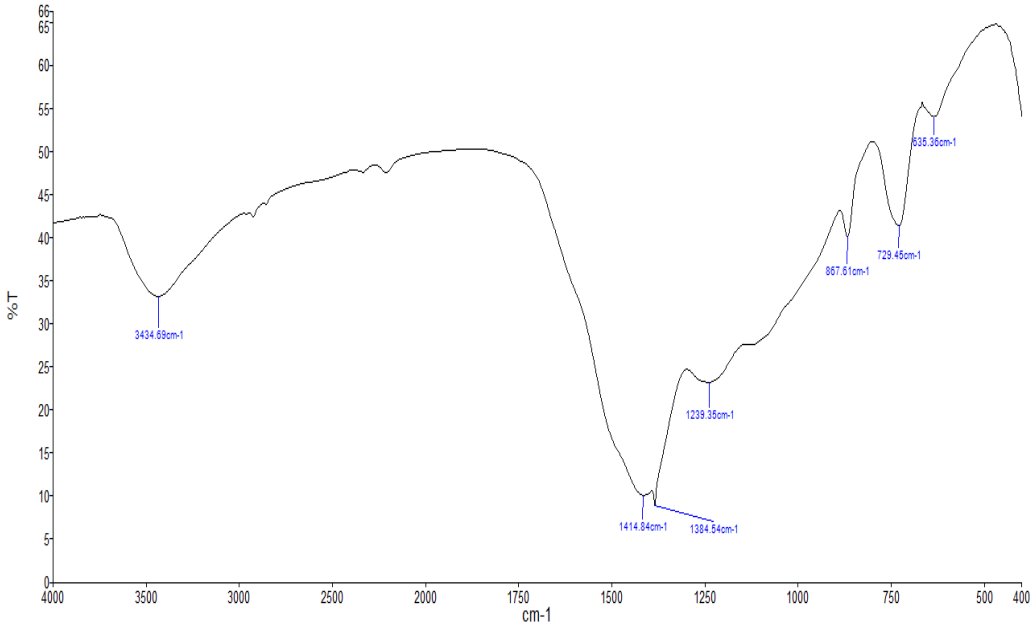

Figure 4.4. FT-IR Spectra of Synthesis Ca_2 B_2 O_5 Using CA (400C°.5mins)

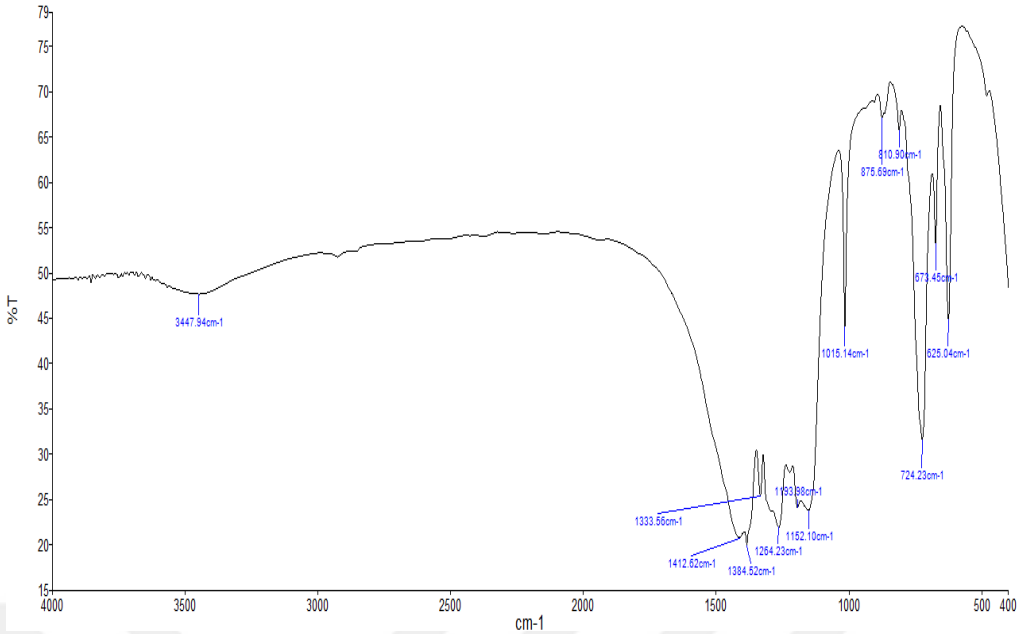

Figure 4.5. FT-IR Spectra of Synthesis Ca_2 B_2 O_5 Using Glycine (400C°.1h)

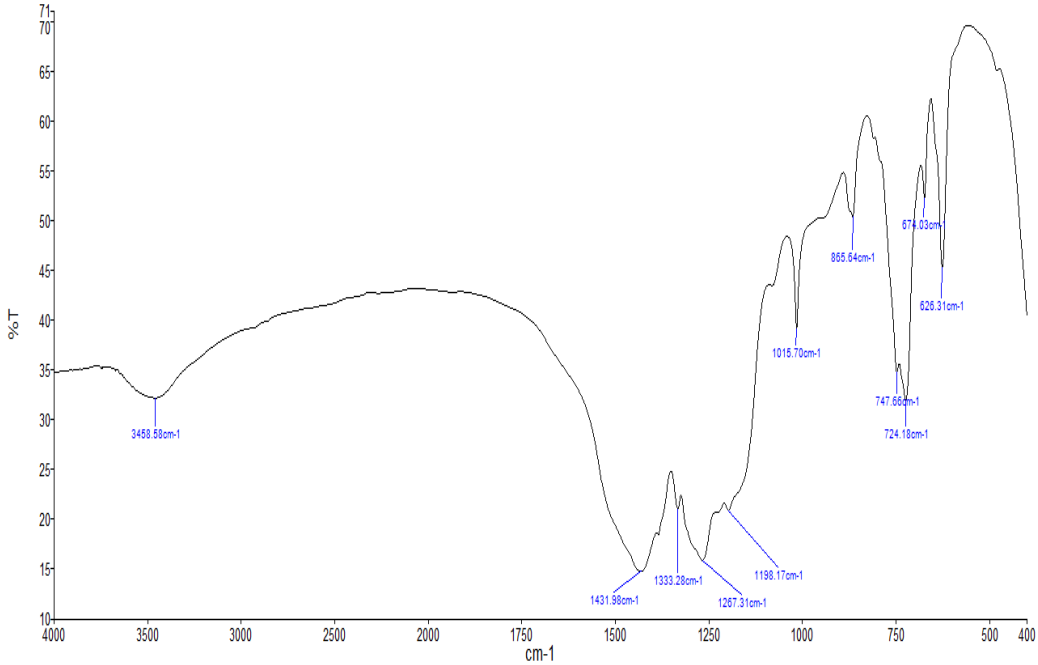

Figure 4.6. FT-IR Spectra of Synthesis Ca_2 B_2 O_5 Using TA (400C°.1h)

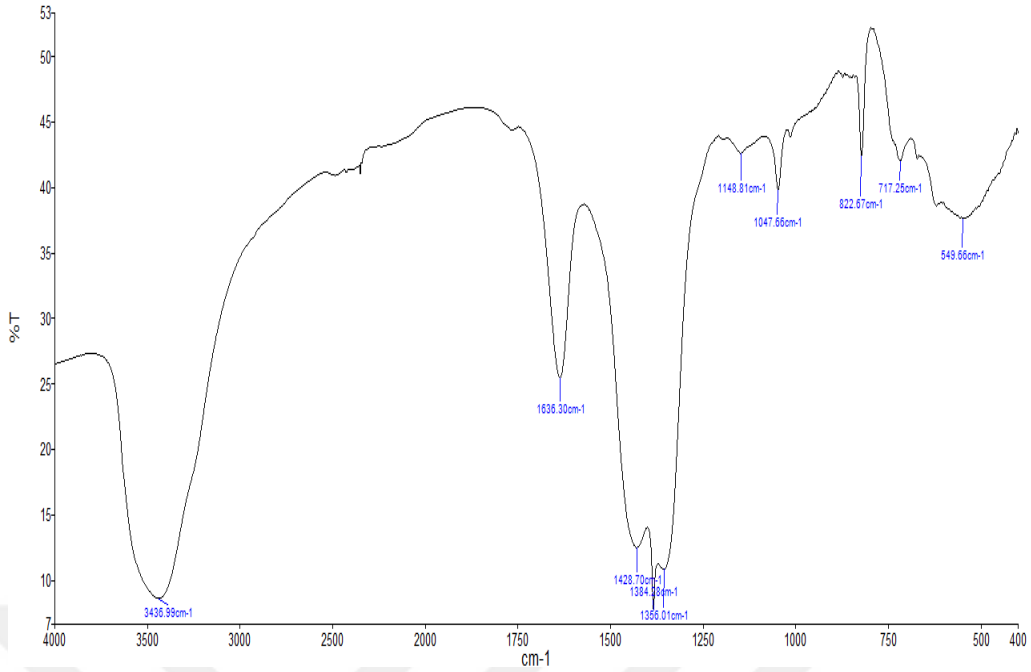

Figure 4.7. FT-IR Spectra of Synthesis $Ca_2\ B_2\ O_5$ Using HMTA (400C°.1h)

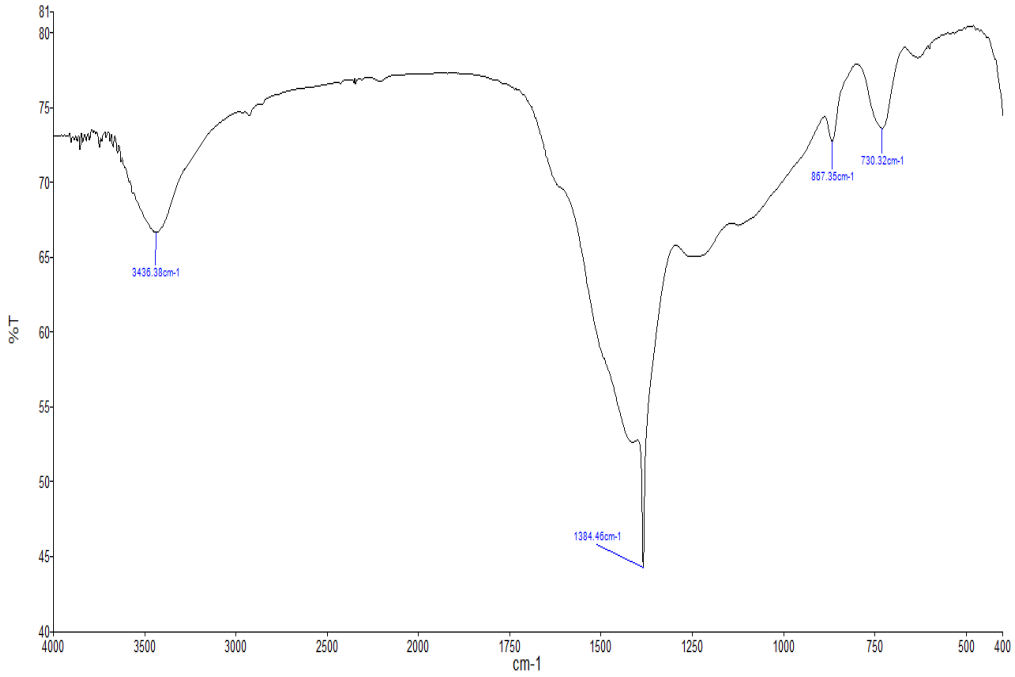

Figure 4.8. FT-IR Spectra of Synthesis $Ca_2\ B_2\ O_5$ Using CA (400C°.1h)

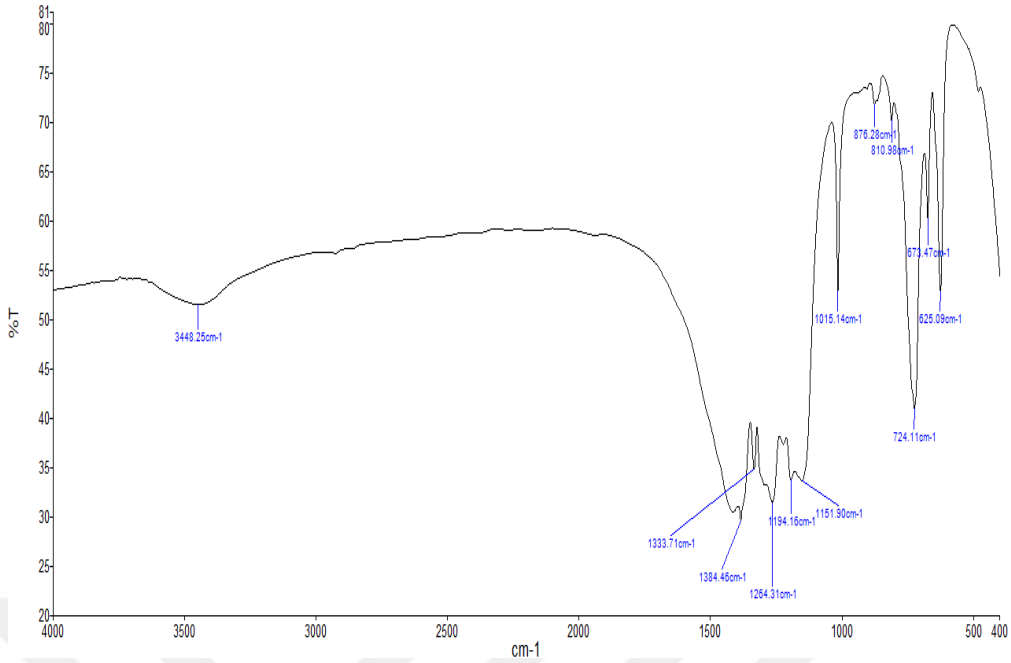

Figure 4.9. FT-IR Spectra of Synthesis $Ca_2\ B_2\ O_5$ Using Glycine (500C°. 1h)

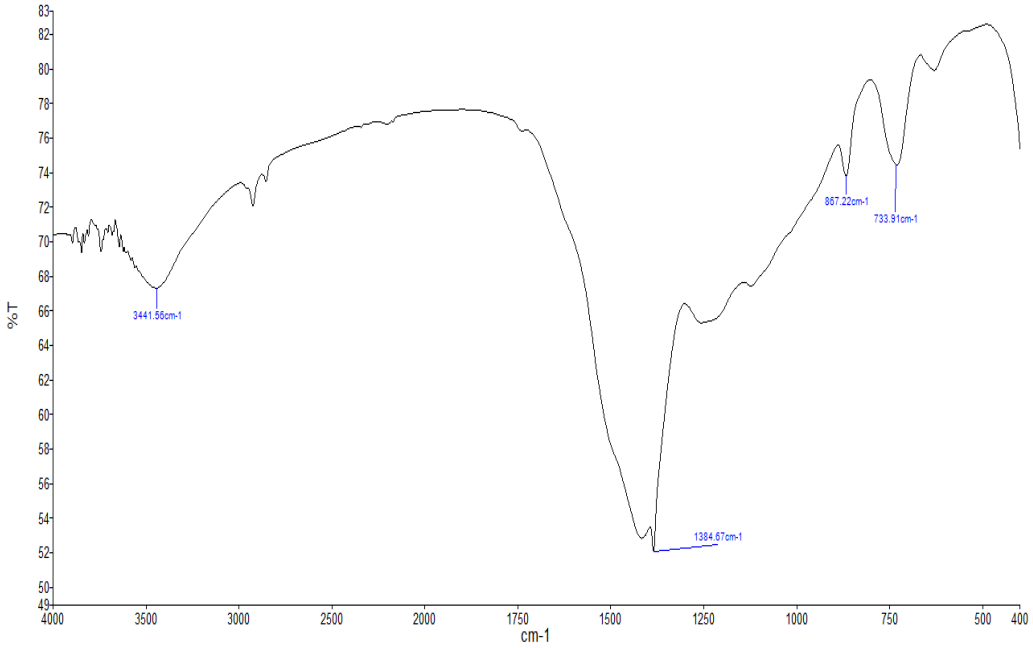

Figure 4.10. FT-IR Spectra of Synthesis $Ca_2\ B_2\ O_5$ Using CA (500C°. 1h)

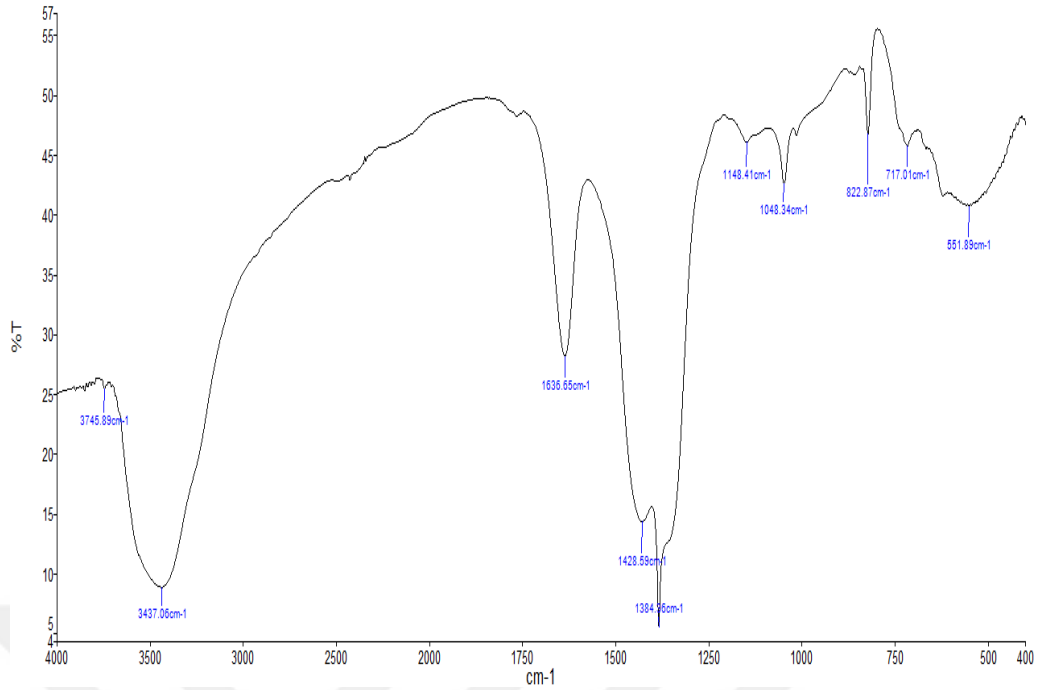

Figure 4.11. FT-IR Spectra of Synthesis $Ca_2\ B_2\ O_5$ Using HMTA (500C°. 1h)

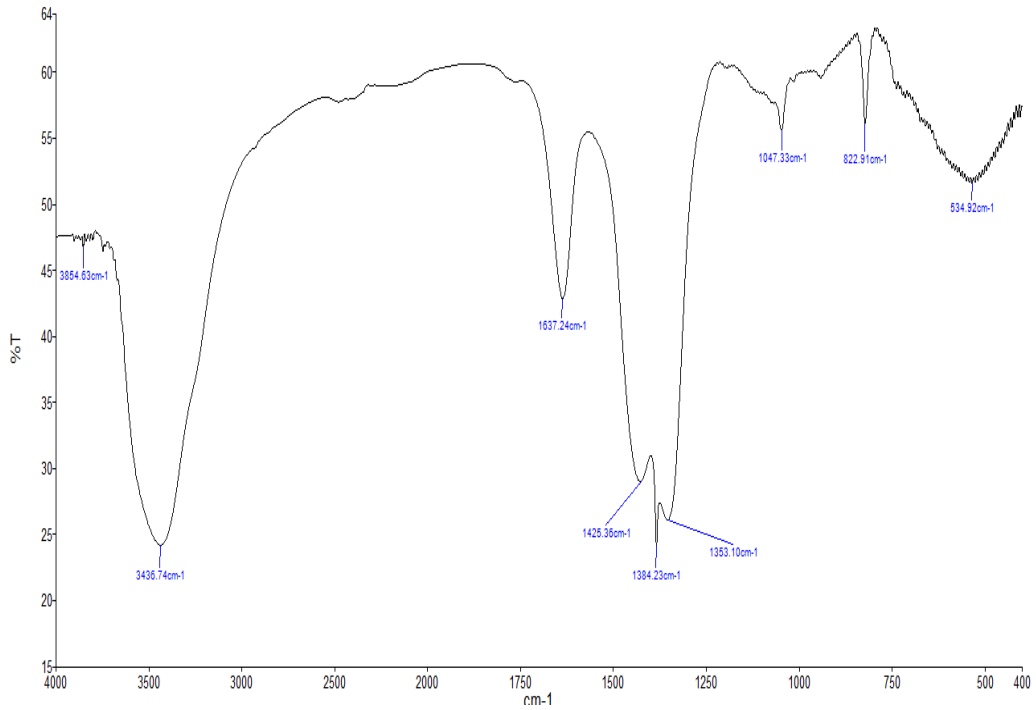

Figure 4.12. FT-IR Spectra of Synthesis $Ca_2\ B_2\ O_5$ Using Urea (500C°. 1h)

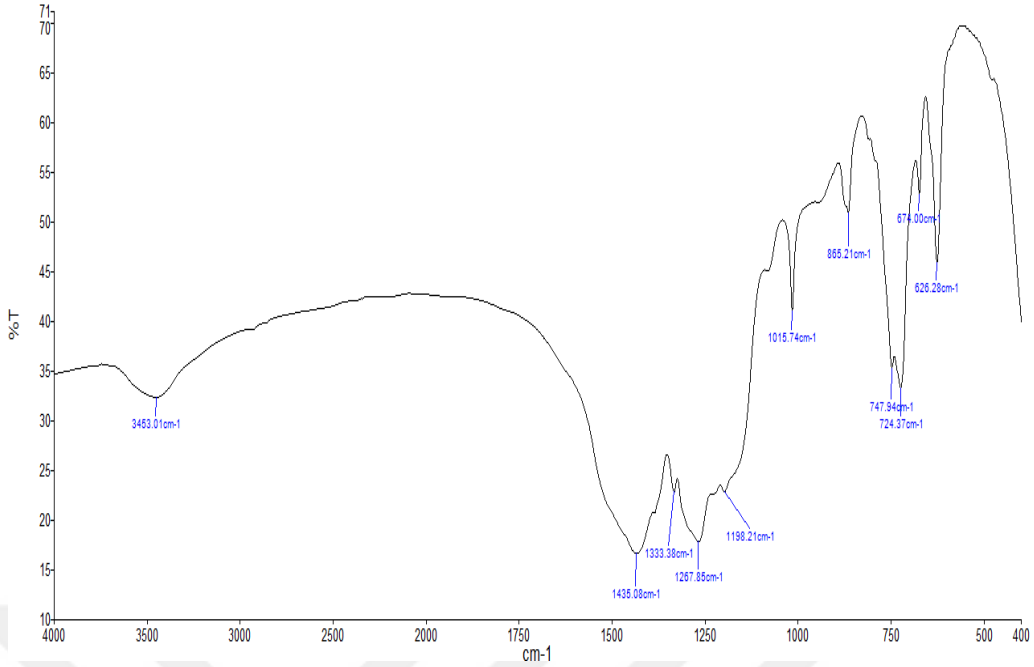

Figure 4.13. FT-IR Spectra of Synthesis $Ca_2\ B_2\ O_5$ Using TA (500C°. 1h)

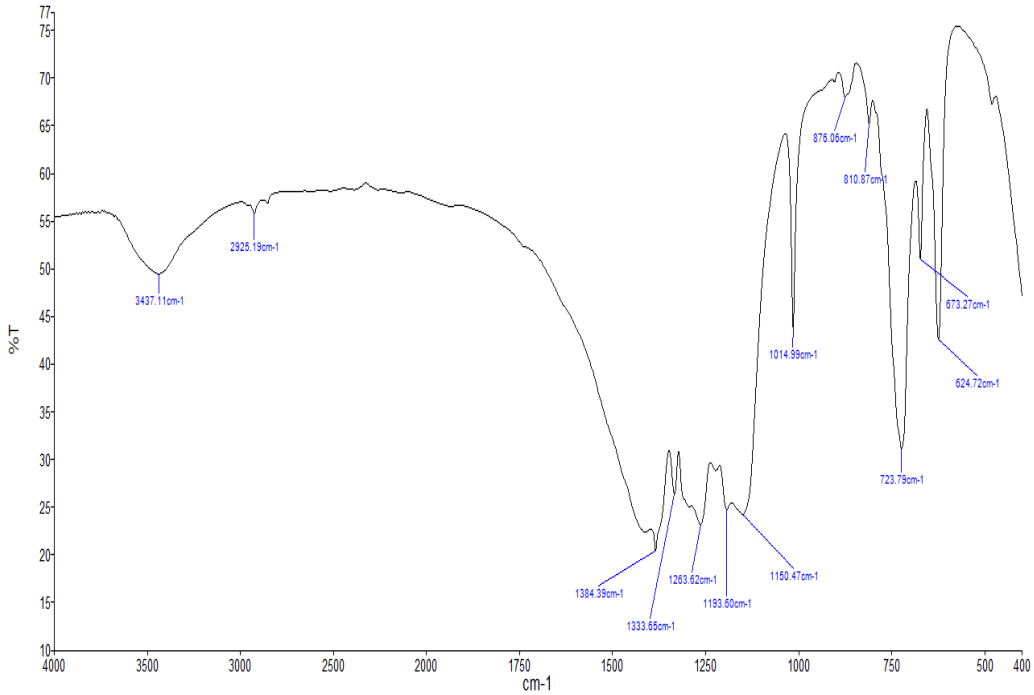

Figure 4.14. FT-IR Spectra of Synthesis $Ca_2\ B_2\ O_5$ Using Glycine (600C°. 1h)

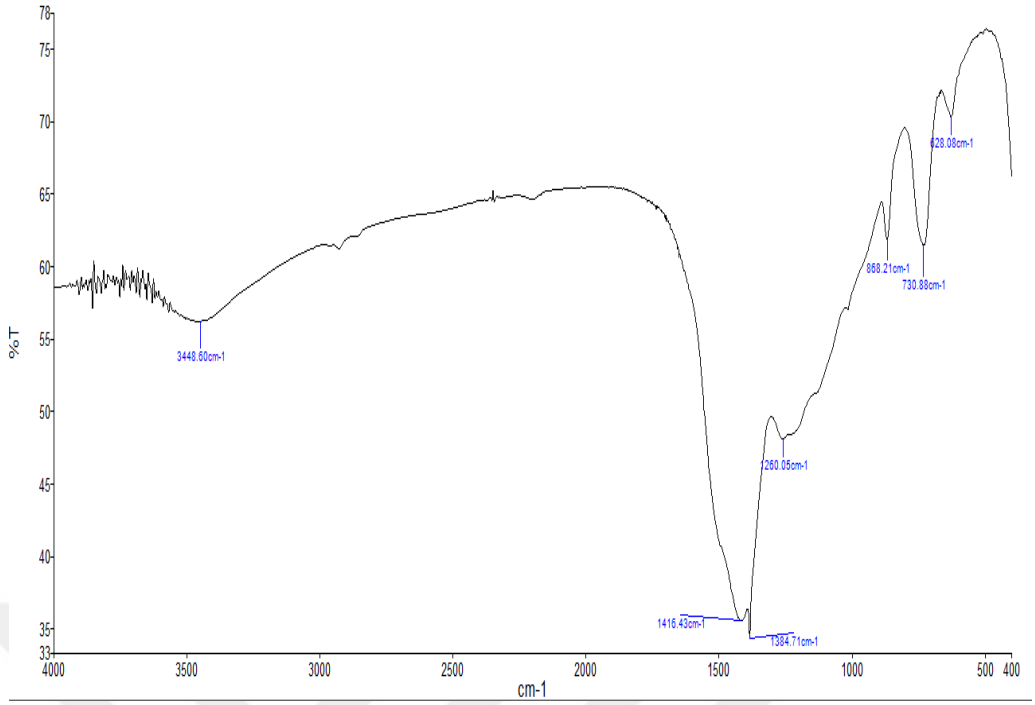

Figure 4.15. FT-IR Spectra of Synthesis $Ca_2\ B_2\ O_5$ Using CA (600C°. 1h)

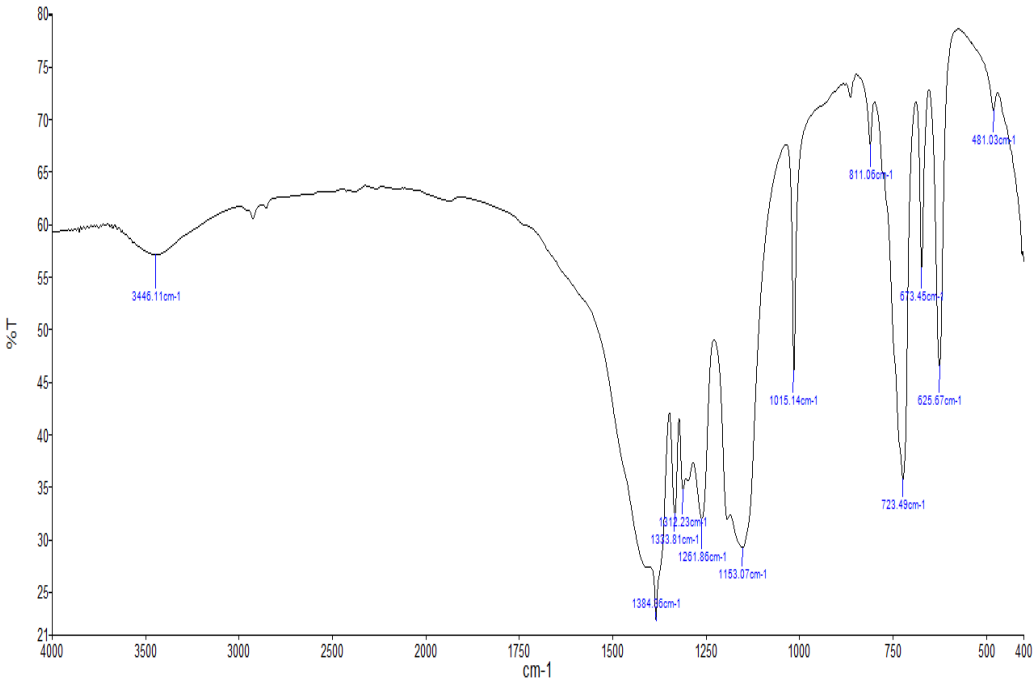

Figure 4.16. FT-IR Spectra of Synthesis $Ca_2\ B_2\ O_5$ Using HMTA (600C°. 1h)

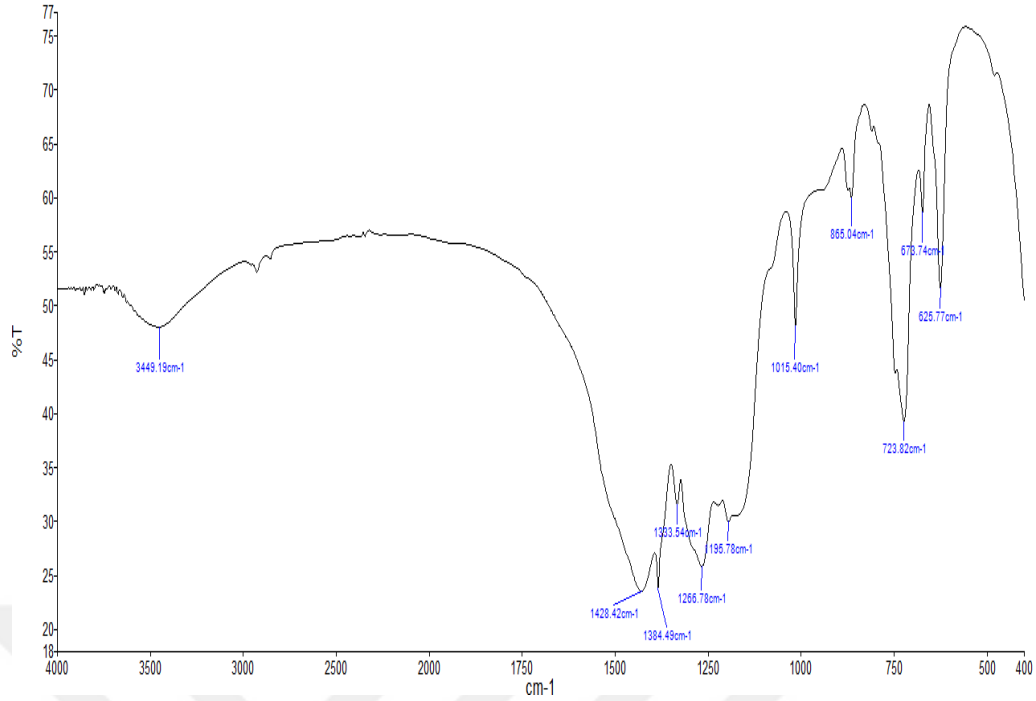

Figure 4.17. FT-IR Spectra of Synthesis $Ca_2\ B_2\ O_5$ Using TA (600C°. 1h)

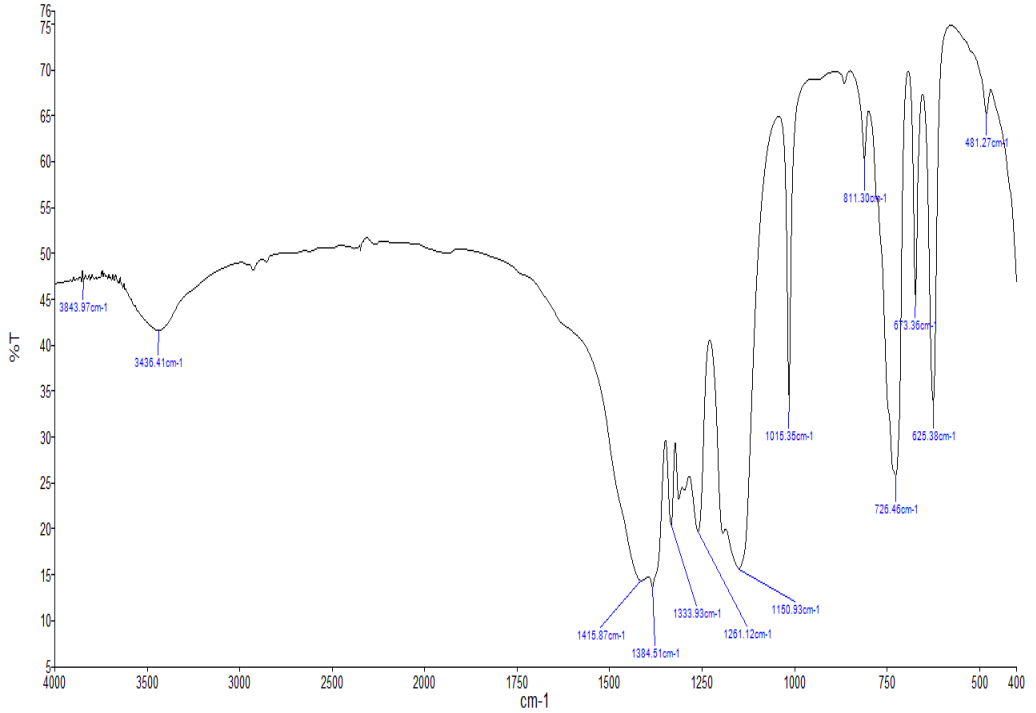

Figure 4.18. FT-IR Spectra of Synthesis $Ca_2\ B_2\ O_5$ Using Urea (600C°. 1h)

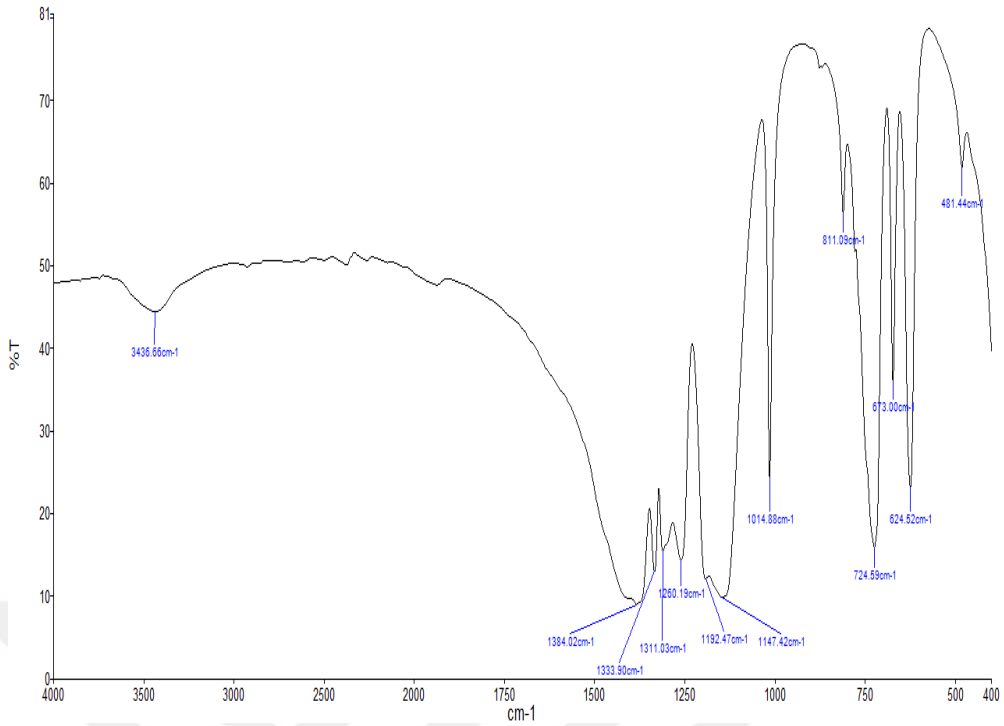

Figure 4.19. FT-IR Spectra of Synthesis $Ca_2\ B_2\ O_5$ Using Glycine (700C°. 1h)

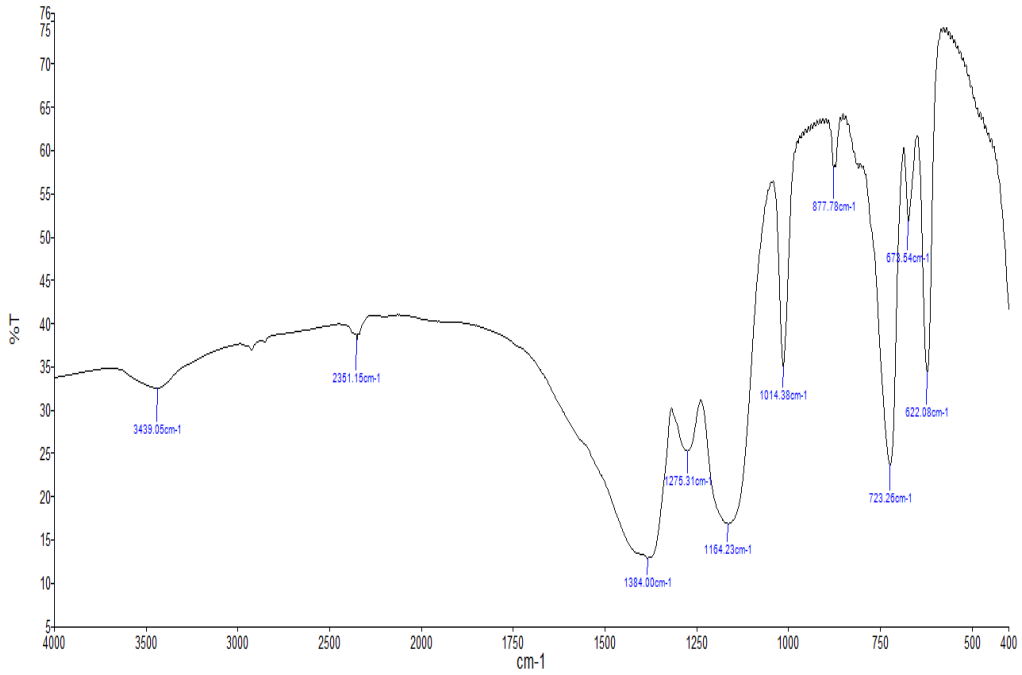

Figure 4.20. FT-IR Spectra of Synthesis $Ca_2\ B_2\ O_5$ Using HMTA (700C°. 1h)

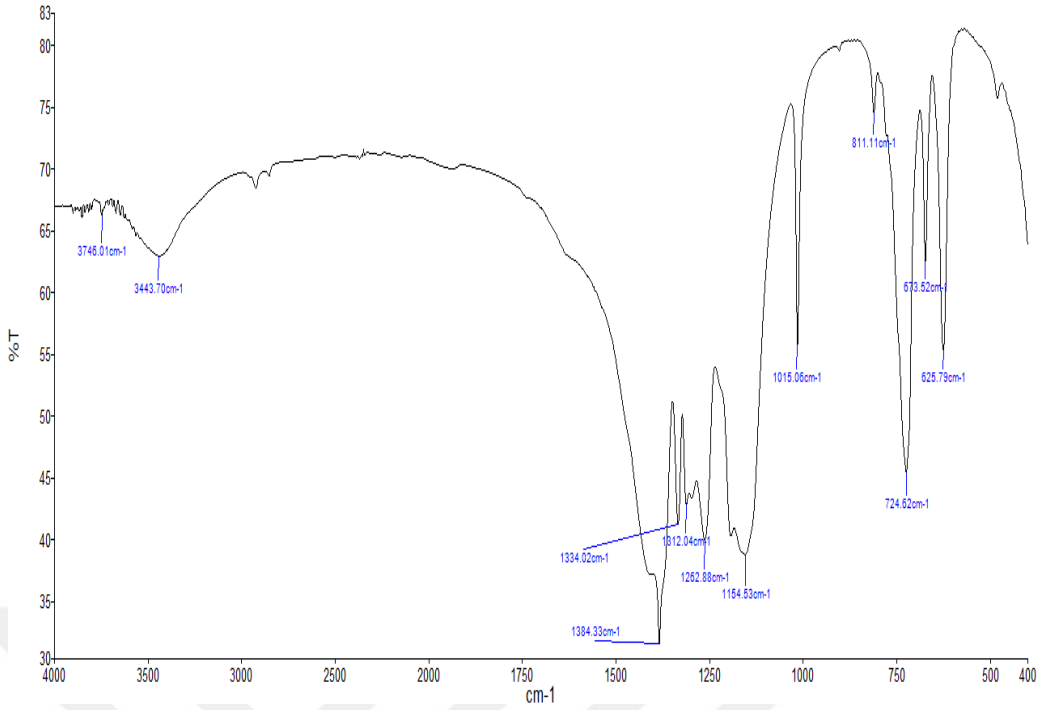

Figure 4.21. FT-IR Spectra of Synthesis $Ca_2\ B_2\ O_5$ Using Urea (700C°. 1h)

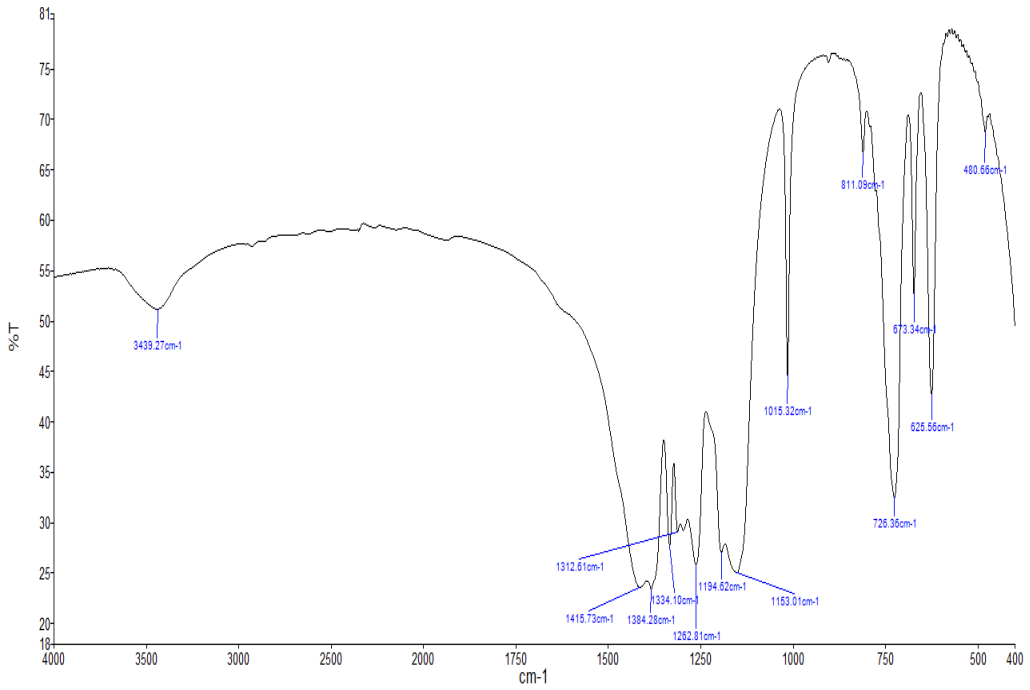

Figure 4.22. FT-IR Spectra of Synthesis $Ca_2\ B_2\ O_5$ Using TA (700C°. 1h)

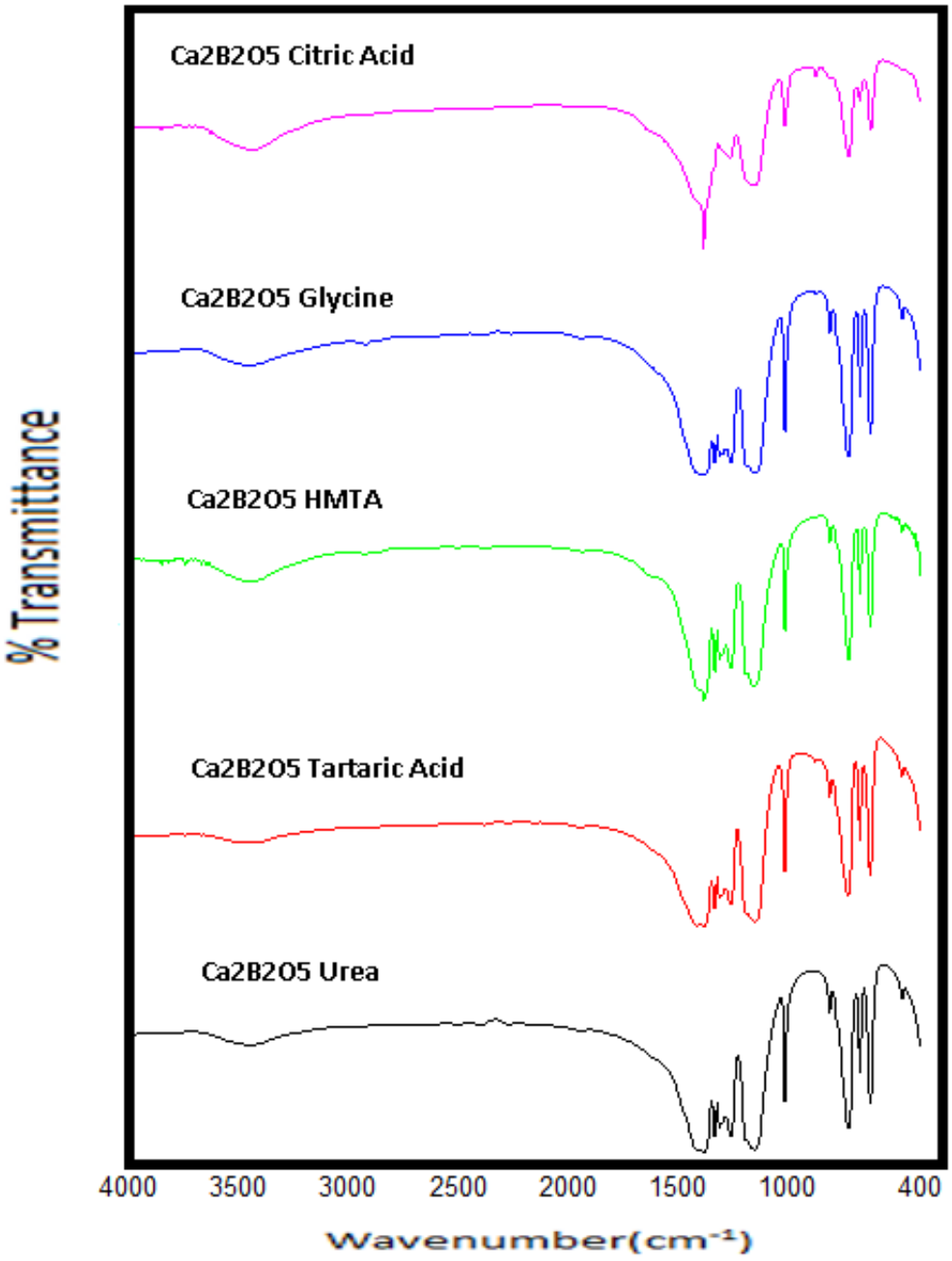

Figure 4.23. FT-IR Spectra of Synthesis Ca_2 B_2 O_5 Using All Fuels (800°C. 1h)

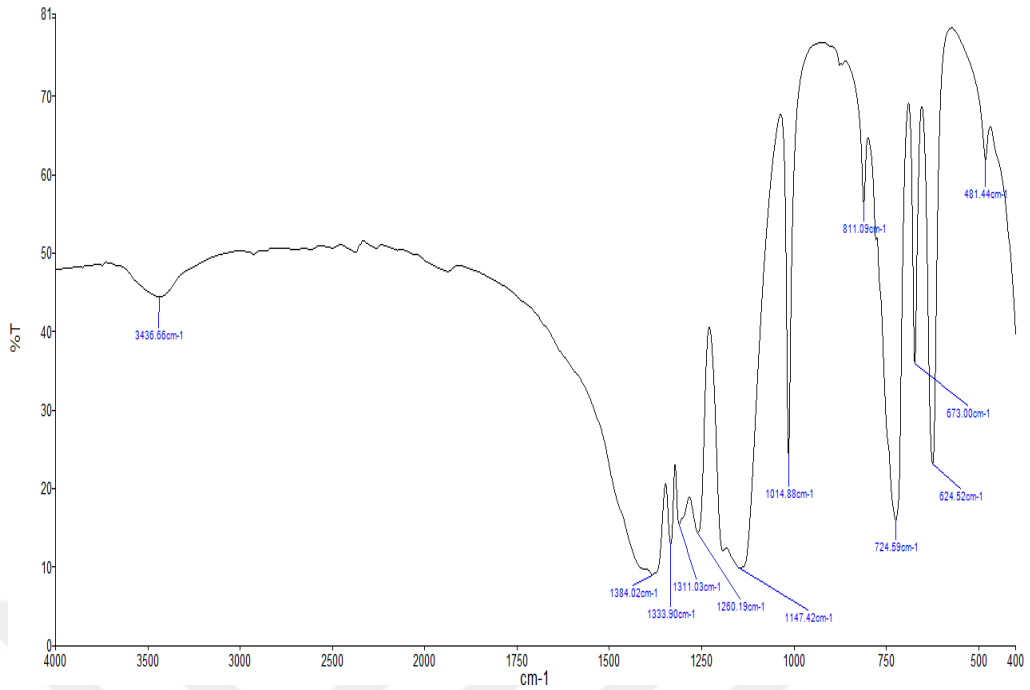

Figure 4.24. FT-IR Spectra of Synthesis $Ca_2\ B_2\ O_5$ Using Glycine (900C°. 1h)

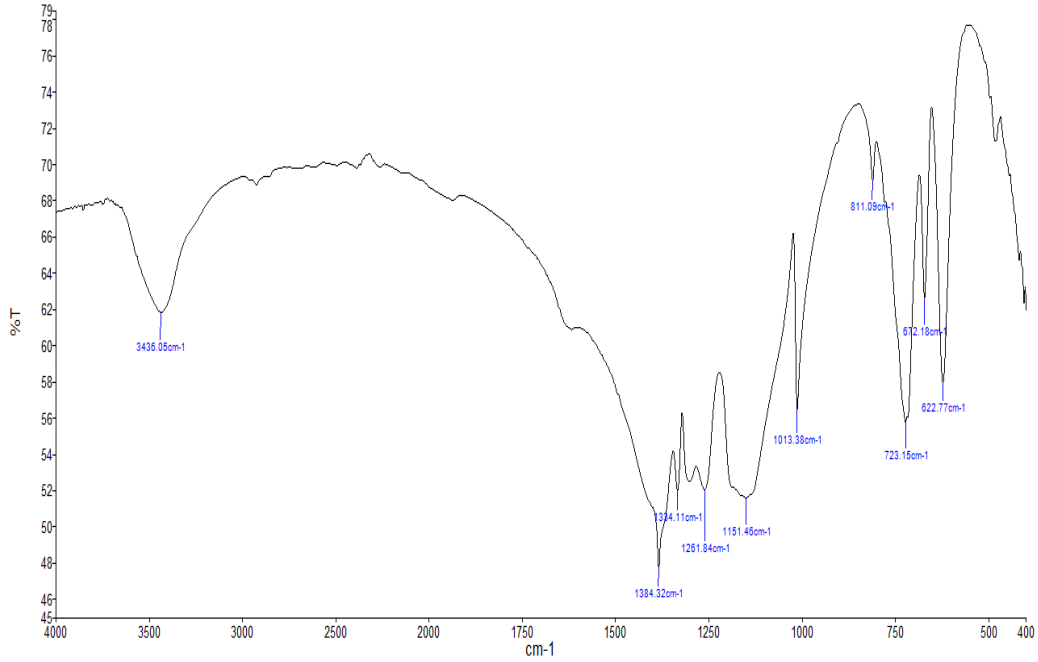

Figure 4.25. FT-IR Spectra of Synthesis $Ca_2\ B_2\ O_5$ Using Urea (900C°. 1h)

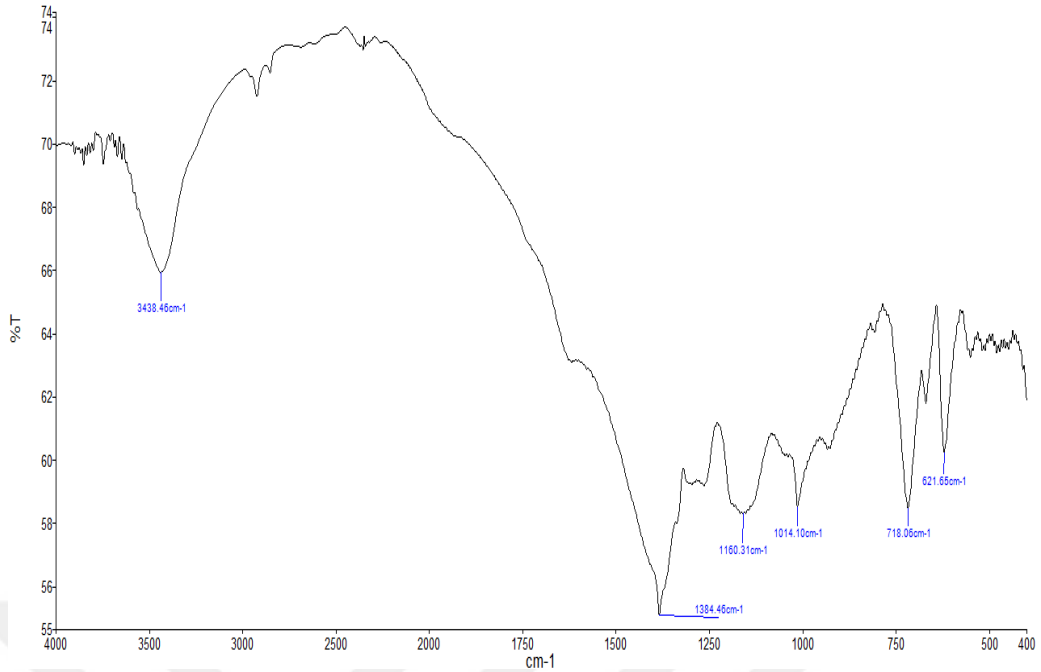

Figure 4.26. FT-IR Spectra of Synthesis $Ca_2\ B_2\ O_5$ Using Glycine (1000C°. 1h)

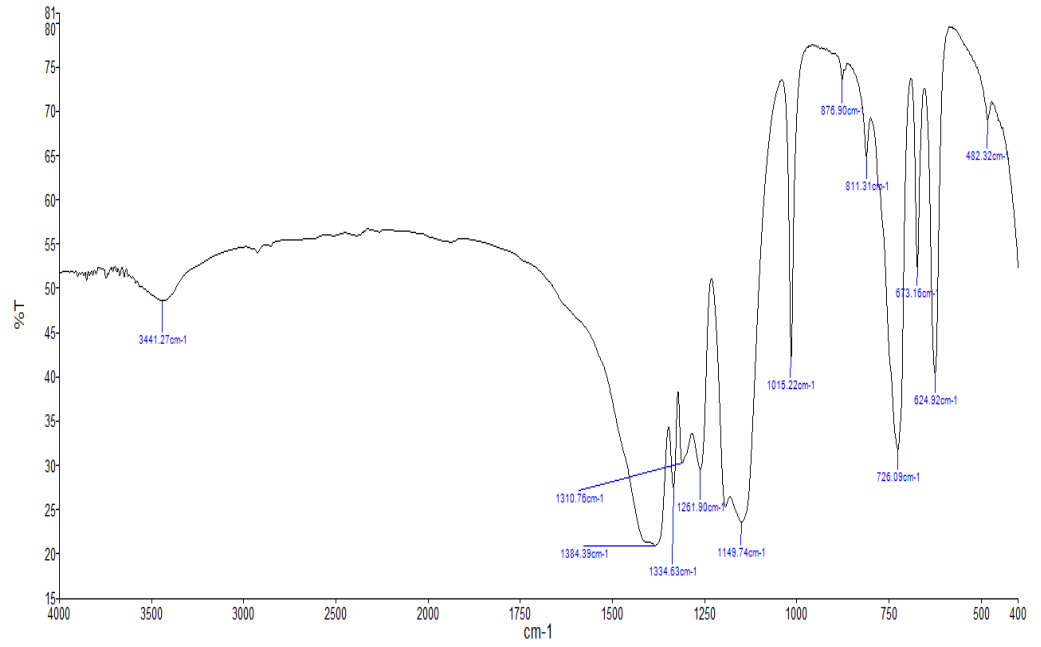

Figure 4.27. FT-IR Spectra of Synthesis $Ca_2\ B_2\ O_5$ Using CA (1000C°. 1h)

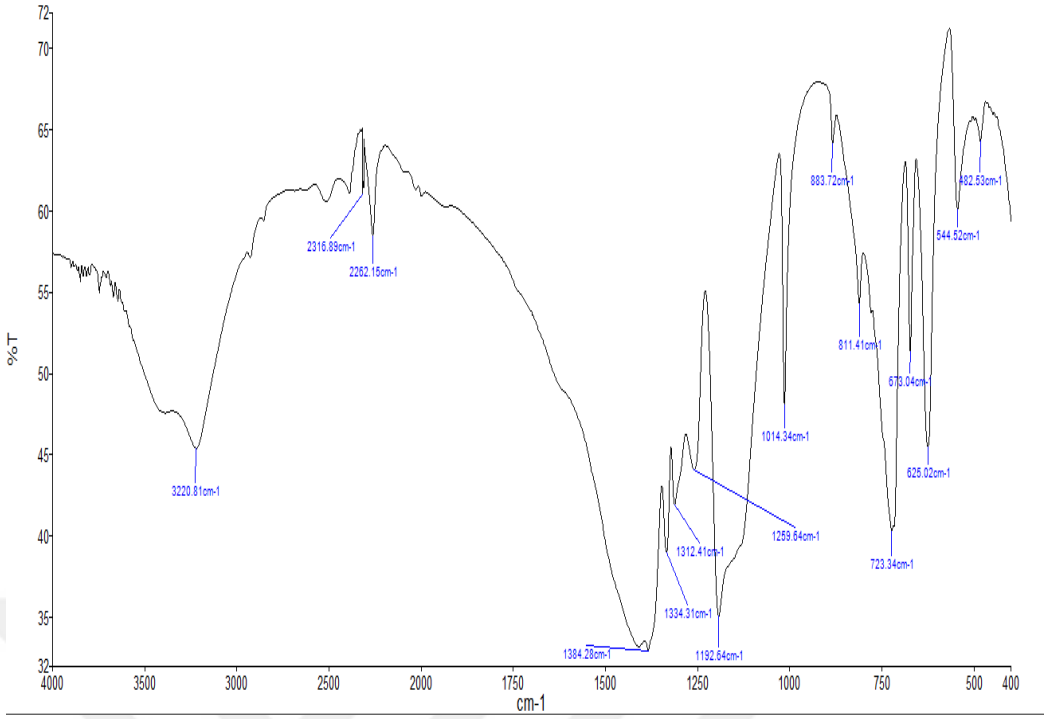

Figure 4.28. FT-IR Spectra of Synthesis $Ca_2\ B_2\ O_5$ Using HMTA (1000C°. 1h)

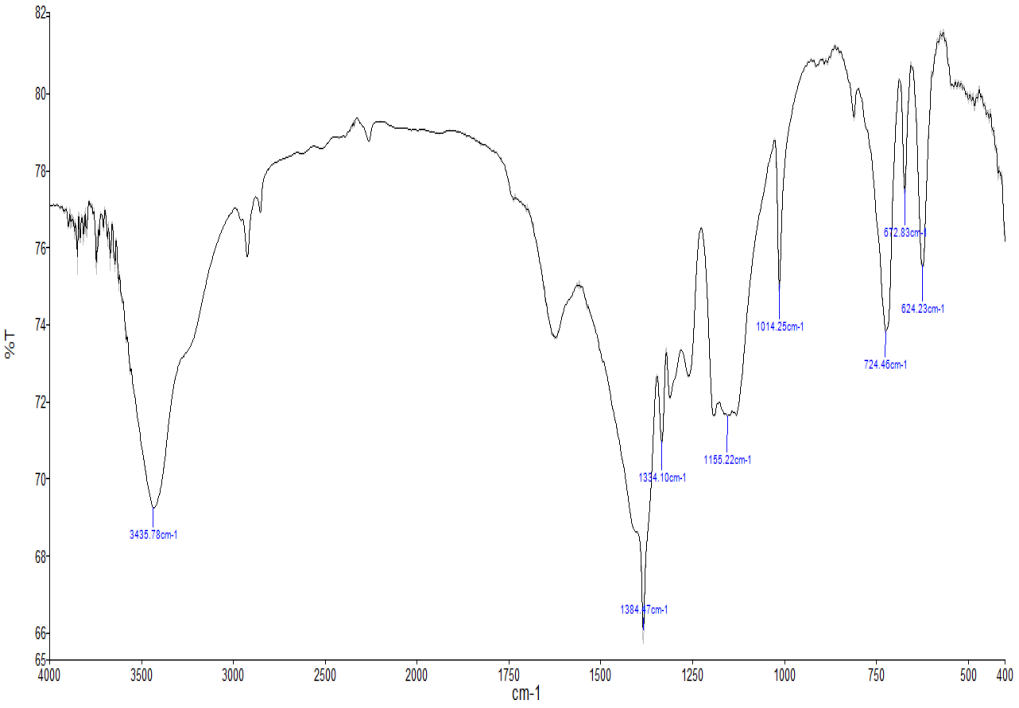

Figure 4.29. FT-IR Spectra of Synthesis $Ca_2\ B_2\ O_5$ Using Urea (1000C°. 1h)

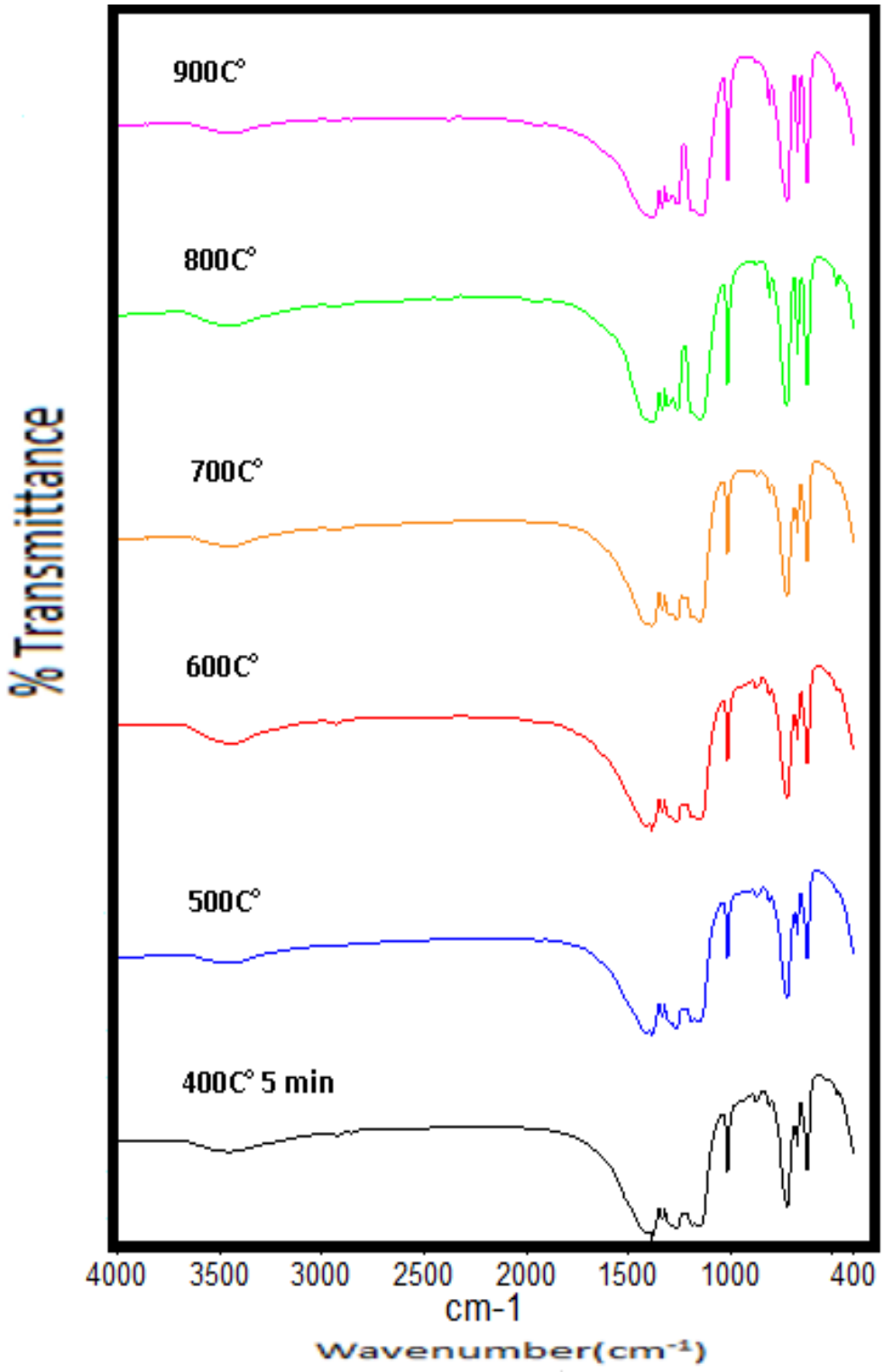

Figure 4.30. FT-IR Spectra of Synthesis Ca_2 B_2 O_5 Using Glycine (All Temperatures)

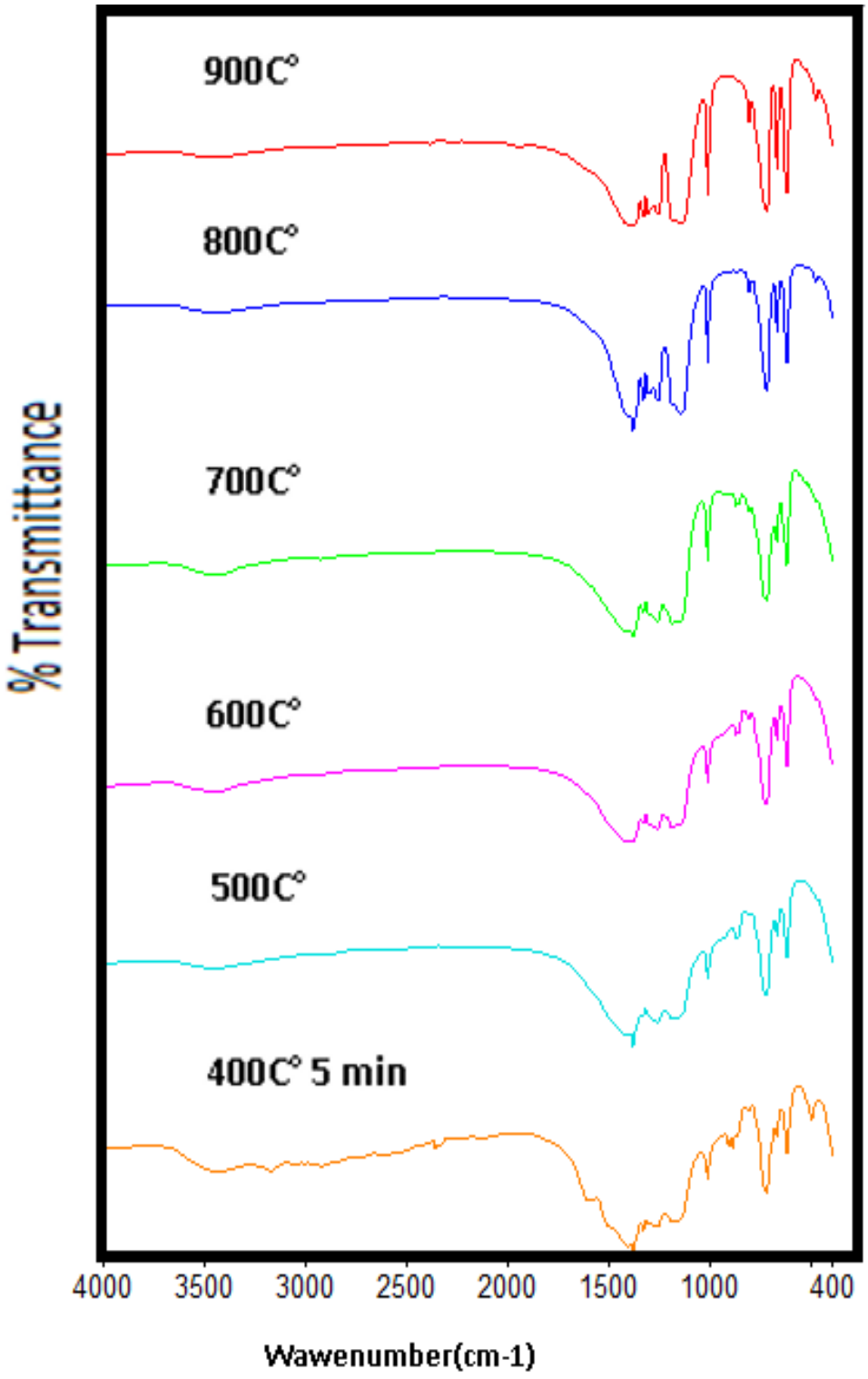

Figure 4.31. FT-IR Spectra of Synthesis 0.005M Eu^{3+} Doped Ca_2 B_2 O_5 (Diff. Temperatures)

In the figure below, it was seen that the FT-IR Spectra of glycine fuel at different concentrations with Eu^{3+} doped at 900°C temperatures. As molarity increases, crystallinity decreases.

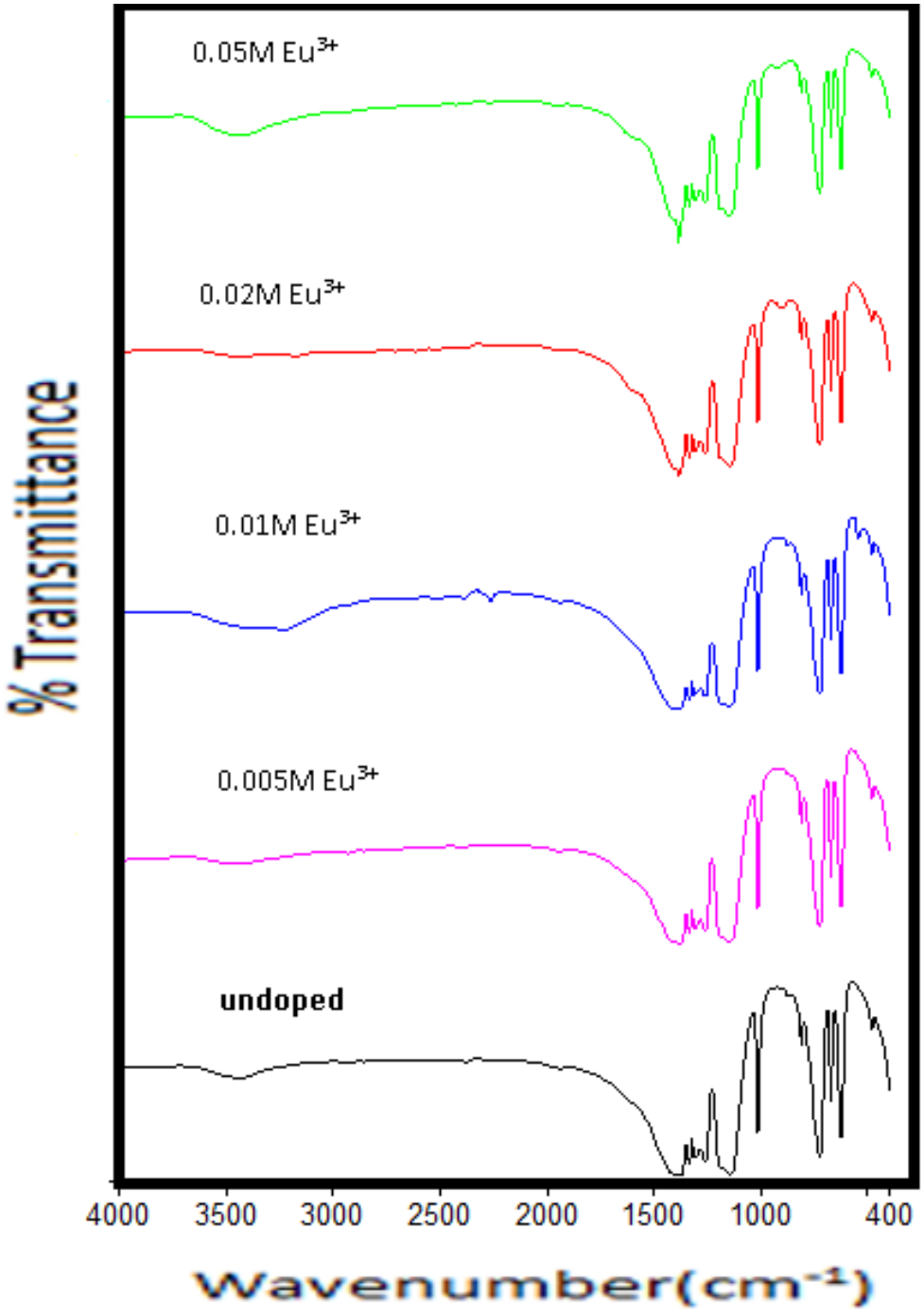

Figure 4.32. FT-IR Spectra of Synthesis Eu^{3+} Doped $Ca_2\ B_2\ O_5$ (Diff. Concentrations)

In the figure below, it was seen the FT-IR Spectra of glycine fuel at different temperatures with Sm^{3+} doped at different temperatures.

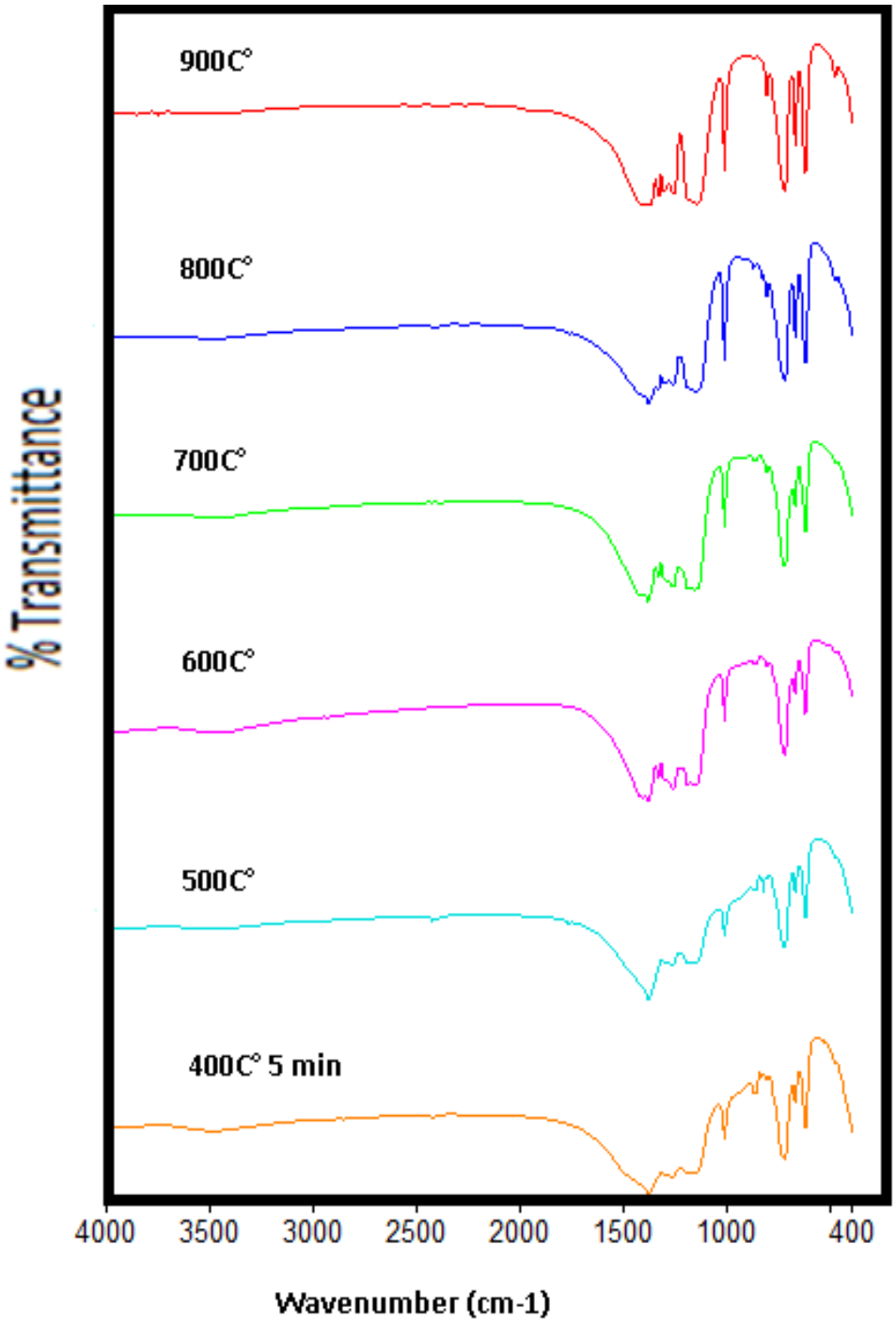

Figure 4.33. FT-IR Spectra of Synthesis 0.005M Sm^{3+} Doped $Ca_2\ B_2\ O_5$ (Diff. Temperatures)

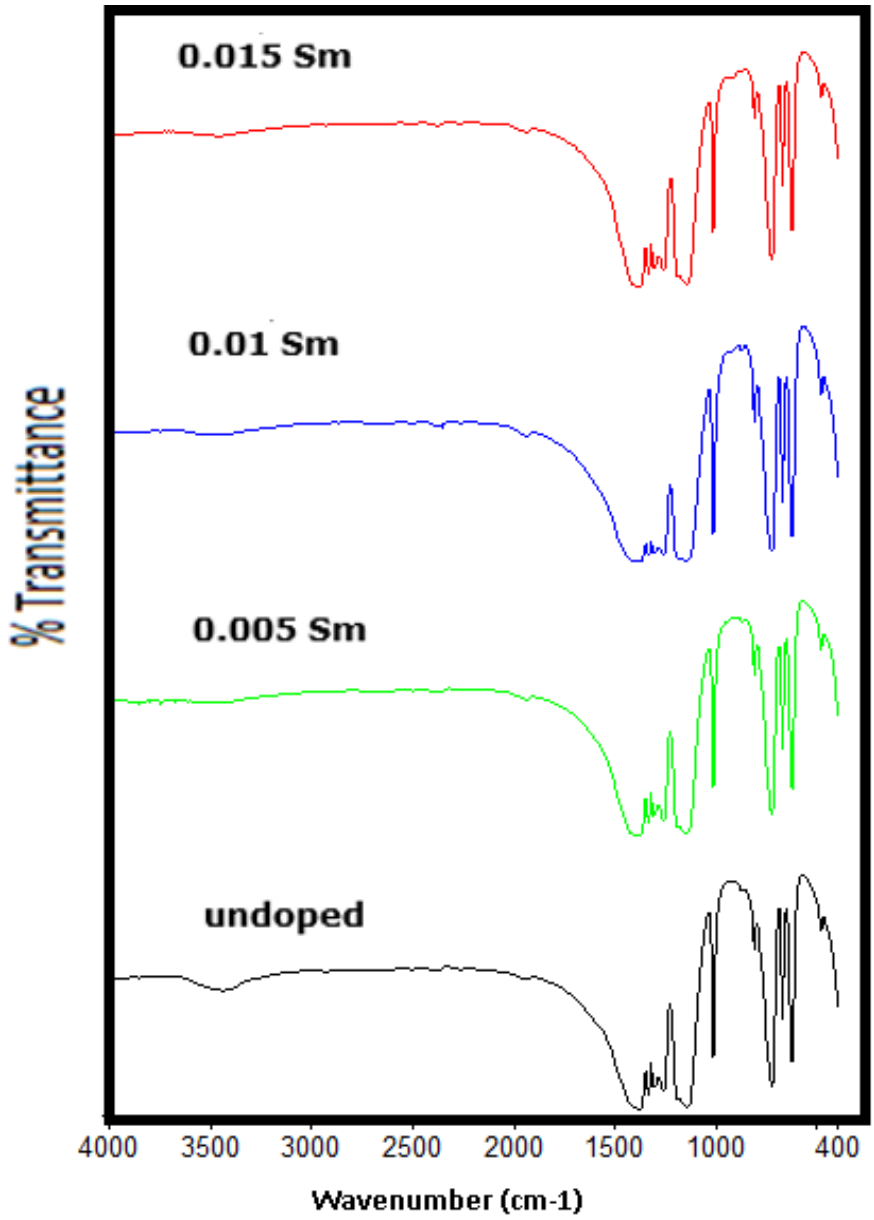

Figure 4.34. FT-IR Spectra of Synthesis Sm^{3+} Doped $Ca_2\ B_2\ O_5$ (Diff. Concentrations)

4.3 X-Ray Diffraction (XRD) Studies

Glycine was employed in the synthesis of calcium pyroborate ($Ca_2\ B_2\ O_5$) along with various Eu^{3+} and Sm^{3+} doped at different concentrations. The compounds were subjected to XRD analysis to examine their structural properties after synthesis and heating.

Initially, undoped calcium borate was synthesized to observe the structures of gly fuel with the presence of different doped elements. These XRD patterns shown the different form of Calcium pyroborate using glycine as fuel. It reported that at 800°C and 900°C the formation of alpha form were observed.

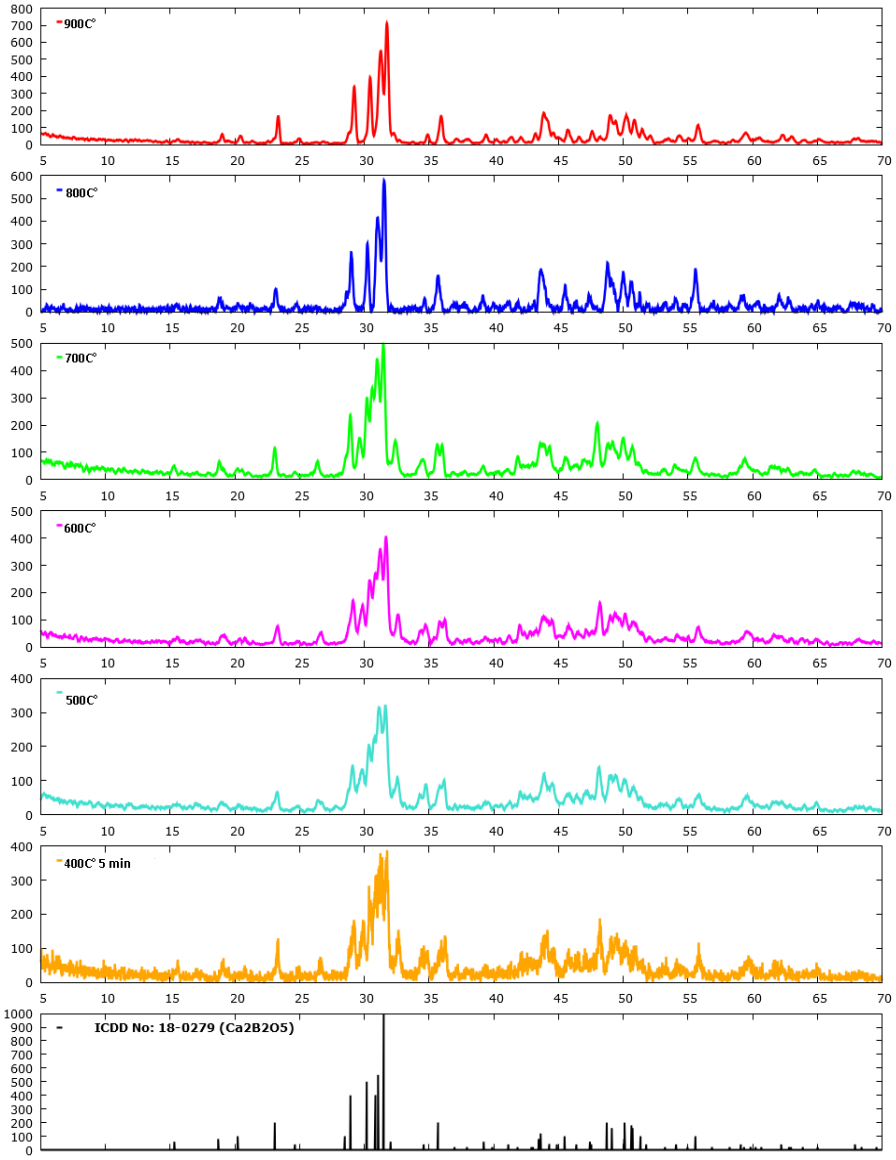

Figure 4.35. $Ca_2\ B_2\ O_5$ with Gly at Different Temperatures

The crystallite size of calcium pyroborate is increase as the temperatures increases. At 900°C the crystallite size was sligthly decrease as the crystallite of $Ca_2\ B_2\ O_5$ increase.

Table 4.1. Crystallite size of the $Ca_2\ B_2\ O_5$ at glycine fuel

Heating Temperatures	Glycine
Synthesis (400°C)	12,7 nm
500°C	17,28 nm
600°C	19,98 nm
700°C	19,96 nm
800°C	27,8 nm
900°C	25,7 nm

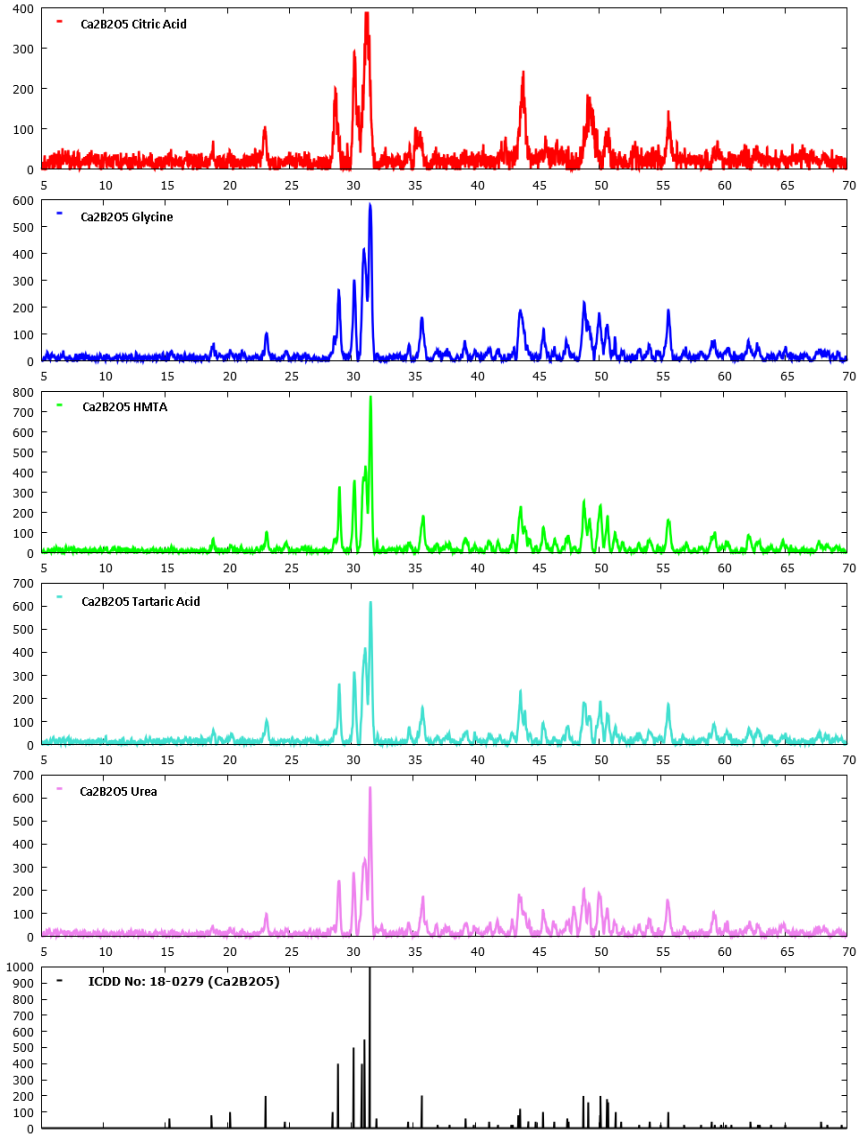

Figure 4.36. $Ca_2\ B_2\ O_5$ with different fuels at 800C°

At 800°C alpha $Ca_2B_2O_5$ are formed by using all the fuels and all the diffraction line are in a good accordance to ICCD Card No 18-0279. The crystallite size are varied between 23-28 nm with the lowest crystallize size belong to the product synthesized by HMTA fuel.

Table 4.2. Crystallite size of the $Ca_2\ B_2\ O_5$ at all fuels

Fuels	Crystallite Size (nm) at 800°C
HMTA	23,04 nm
Citric Acid	24,98 nm
Tartaric Acid	25,46 nm
Glycine	27,8 nm
Urea	28,43 nm

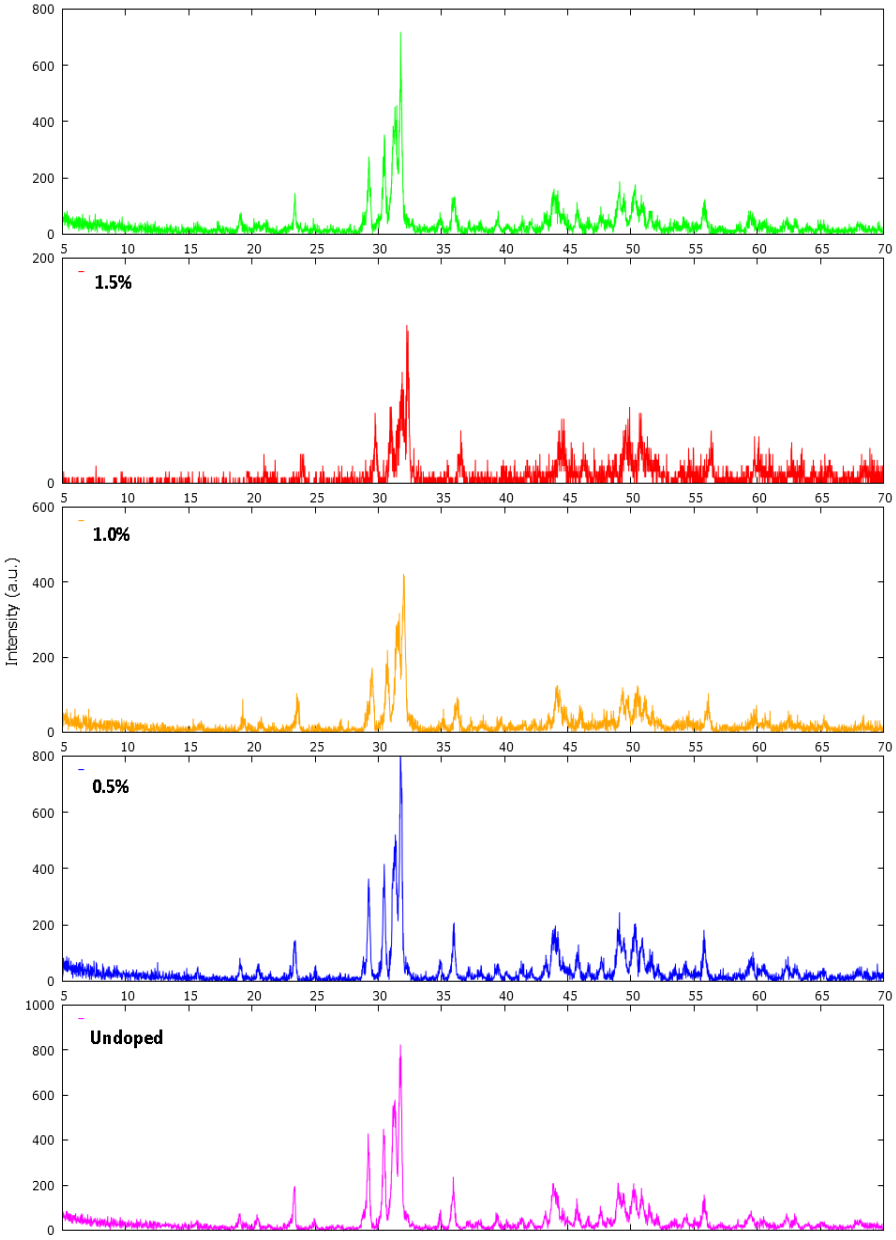

Figure 4.37. Eu^{3+} doped $Ca_2\ B_2\ O_5$ at different concentrations

It is showed that as the molarity increases, the crystallinity of the obtained products decreases. The highest crystallite size observed at the product of 0.05M Eu^{3+} doped $Ca_2B_2O_6$.

Table 4.3. Crystallite size of the Eu^{3+} doped $Ca_2\ B_2\ O_5$ at all concentrations

	0.01M Eu^{3+} Doped $Ca_2\ B_2\ O_5$	**0.02M Eu^{3+} Doped $Ca_2\ B_2\ O_5$**	**0.05M Eu^{3+} Doped $Ca_2\ B_2\ O_5$**	**0.005M Eu^{3+} Doped $Ca_2\ B_2\ O_5$**
900°C	24,68 nm	22,26 nm	26,35 nm	24.81 nm

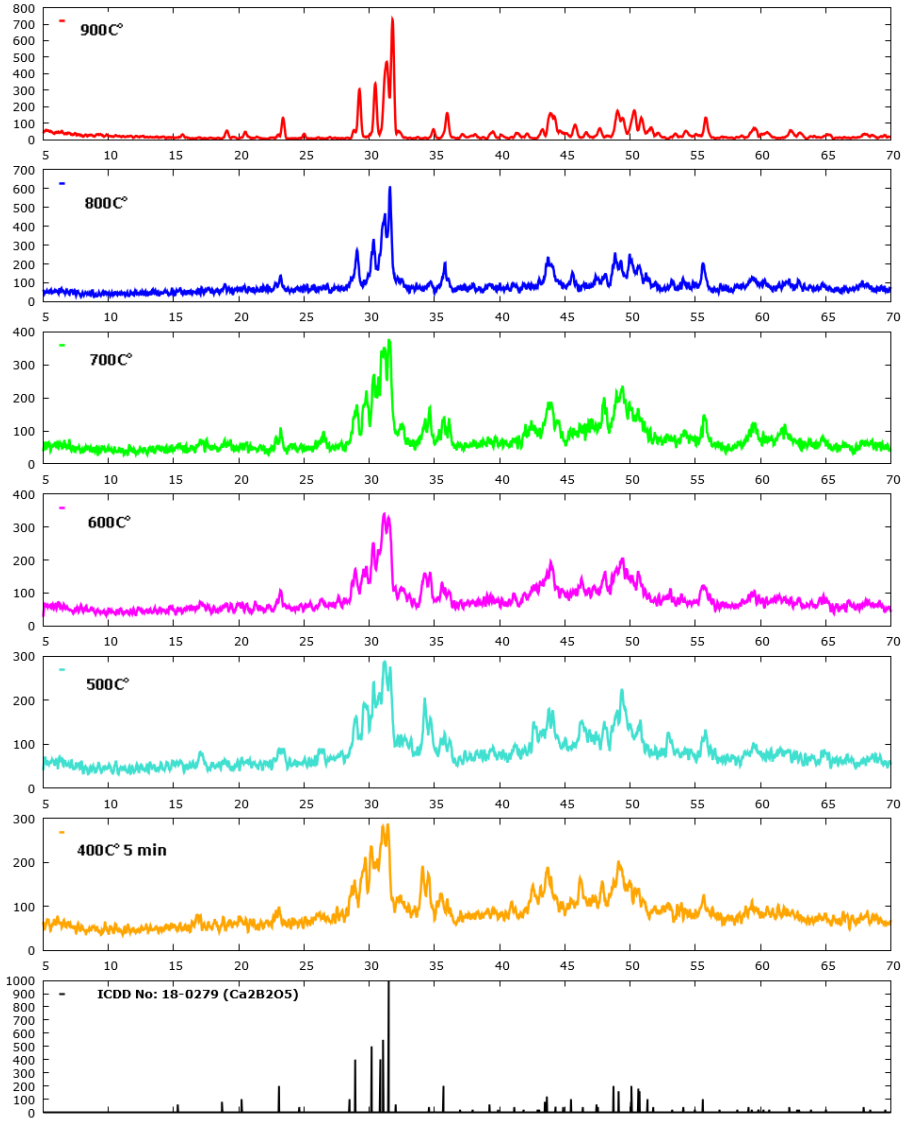

Figure 4.38. Eu^{3+} doped $Ca_2\ B_2\ O_5$ at different temperatures.

The temperature effect on the crystallite size of calcium pyroborate was also determined. As the temperature increases the crystallite size was also increase.

Table 4.4. Crystallite size of the Eu^{3+} doped $Ca_2\ B_2\ O_5$ at all temperatures

	0.005M Eu^{3+} Doped $Ca_2\ B_2\ O_5$
Synthesis	8.27 nm
500°C	16.40 nm
600°C	8.19 nm
700°C	8.09 nm
800°C	19.41 nm
900°C	24.81 nm

Figure 4.39. Sm^{3+} doped $Ca_2\ B_2\ O_5$ at different concentrations (900°C)

At 900°C, the crystallite size of Sm^{3+} doped calcium pyroborates was calculated to be ın the range of 21-27 nm. Its proved the formation of nanosized calcium pyroborate with 0.01M has the highest crystallite size.

Table 4.5. Crystallite size of the Sm^{3+} doped $Ca_2\ B_2\ O_5$ at all concentrations

	0.01M Sm^{3+} Doped $Ca_2\ B_2\ O_5$	**0.015M Sm^{3+} Doped $Ca_2\ B_2\ O_5$**	**0.005M Sm^{3+} Doped $Ca_2\ B_2\ O_5$**
900°C	27.02 nm	21.84 nm	21.09 nm

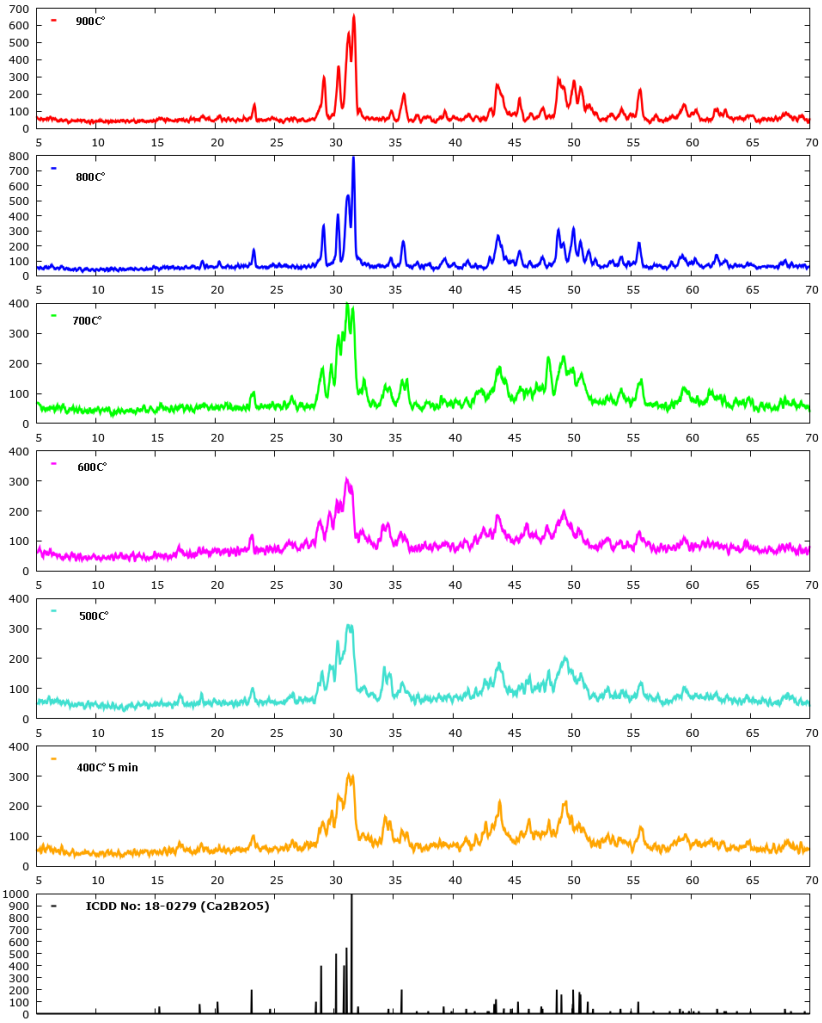

Figure 4.40. Sm^{3+} doped $Ca_2\ B_2\ O_5$ at different temperatures

The temperature effect on the crystallite size of calcium pyroborate was also determined. As the temperature increases the crystallite size was also increase. The highest crystallite size is obtained at 800°C.

Table 4.6. Crystallite size of the Sm^{3+} doped $Ca_2\ B_2\ O_5$ at all temperatures

	0.005M Sm^{3+} Doped $Ca_2\ B_2\ O_5$
Synthesis	7.21 nm
500 °C	10.60 nm
600 °C	7.74 nm
700 °C	4.46 nm
800 °C	24.66 nm
900 °C	21.09 nm

4.4 UV-VIS Studies

The UV-VIS absorbance and reflectance spectra of $Ca_2\ B_2\ O_5$ with different fuels at 800ºC were analyzed and by using their UV-VIS analysis data the optical band gap energy of as-prepared products with each fuel were examine.

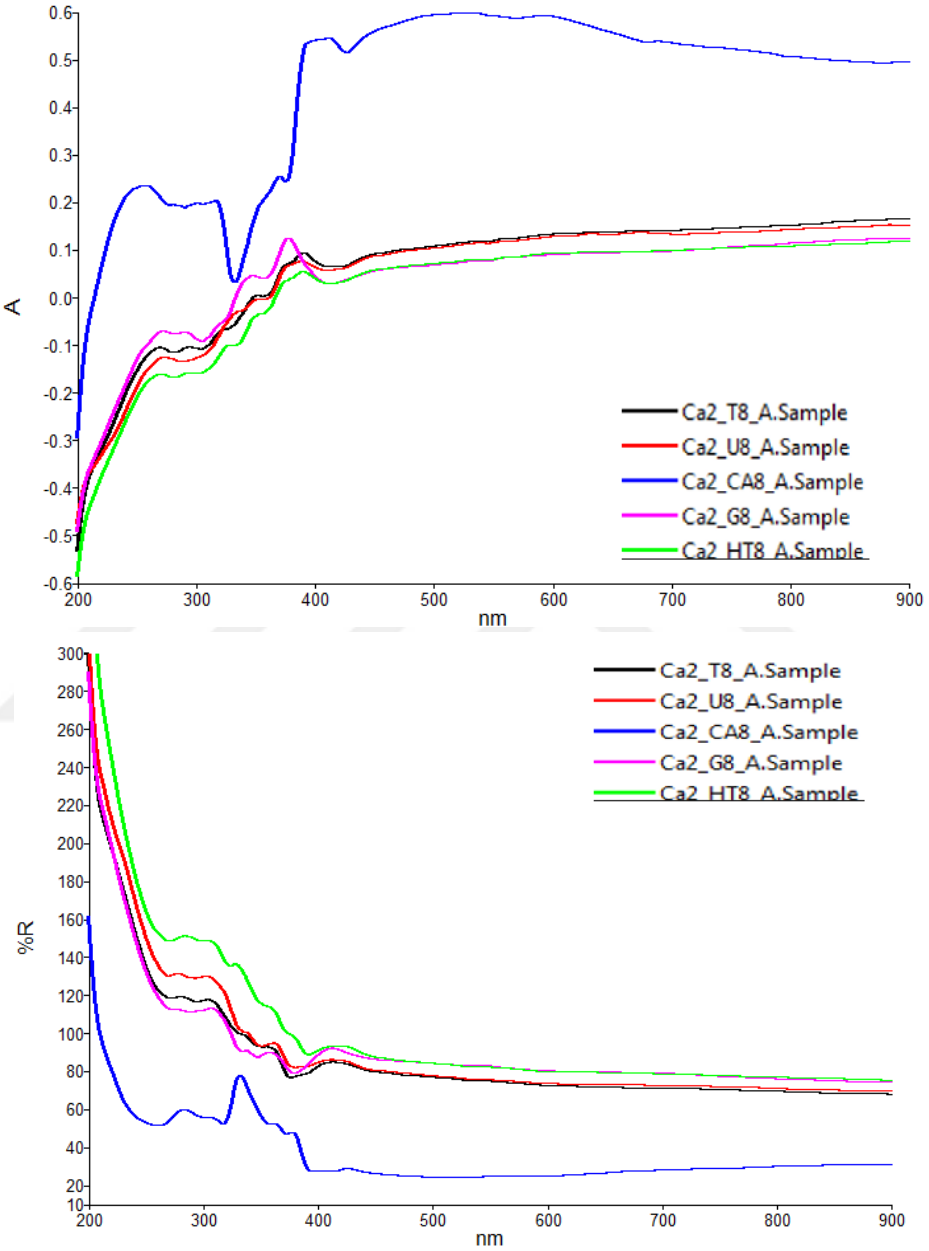

Figure 4.41. UV-VIS absorbance and reflectance spectra of $Ca_2\ B_2\ O_5$ with different fuels at 800°C

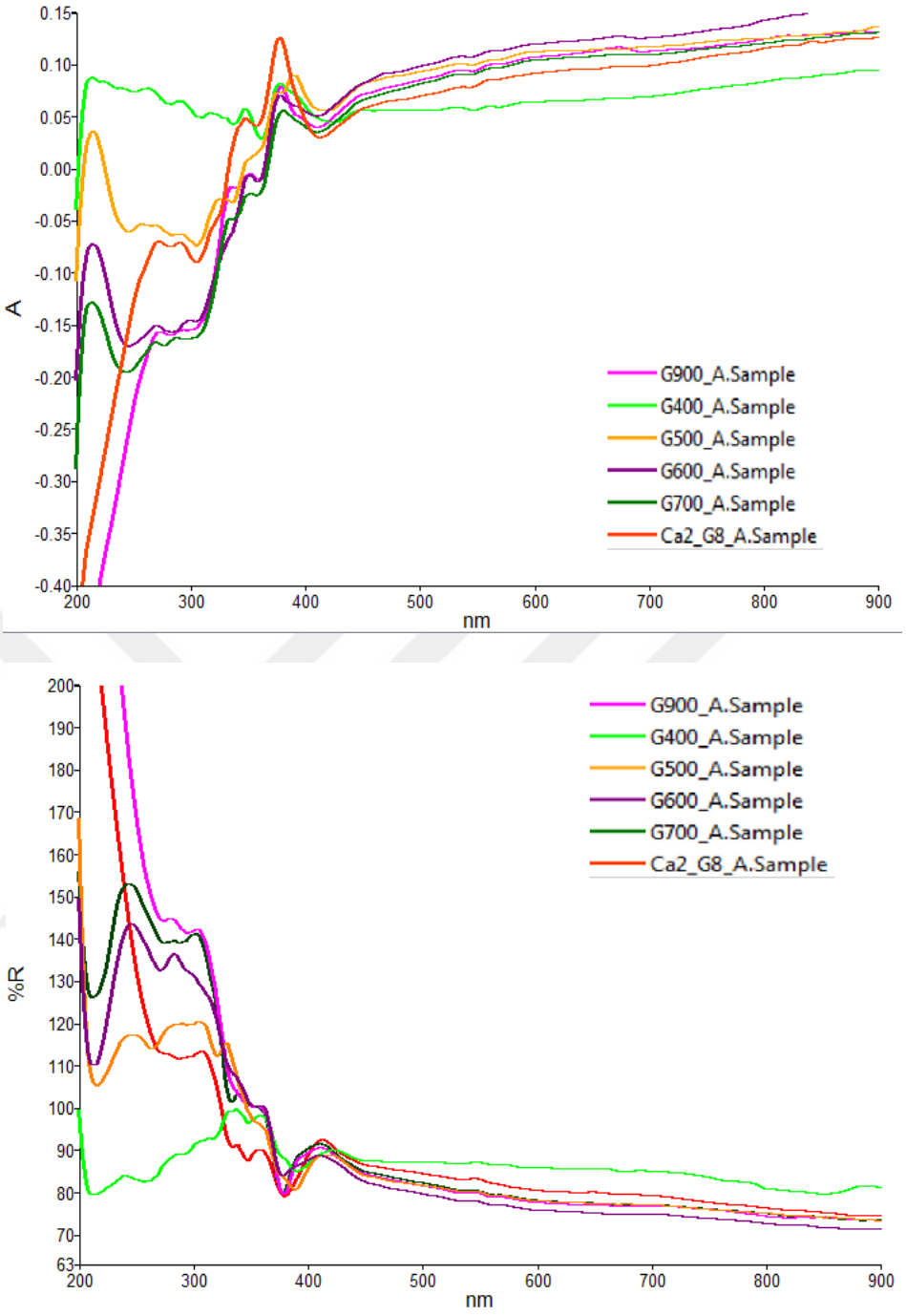

Figure 4.42. UV-VIS absorbance and reflectance spectra of $Ca_2\ B_2\ O_5$ with glycine at different temperatures

In the UV spectra of the products, the bands were only detected at 200-400nm.

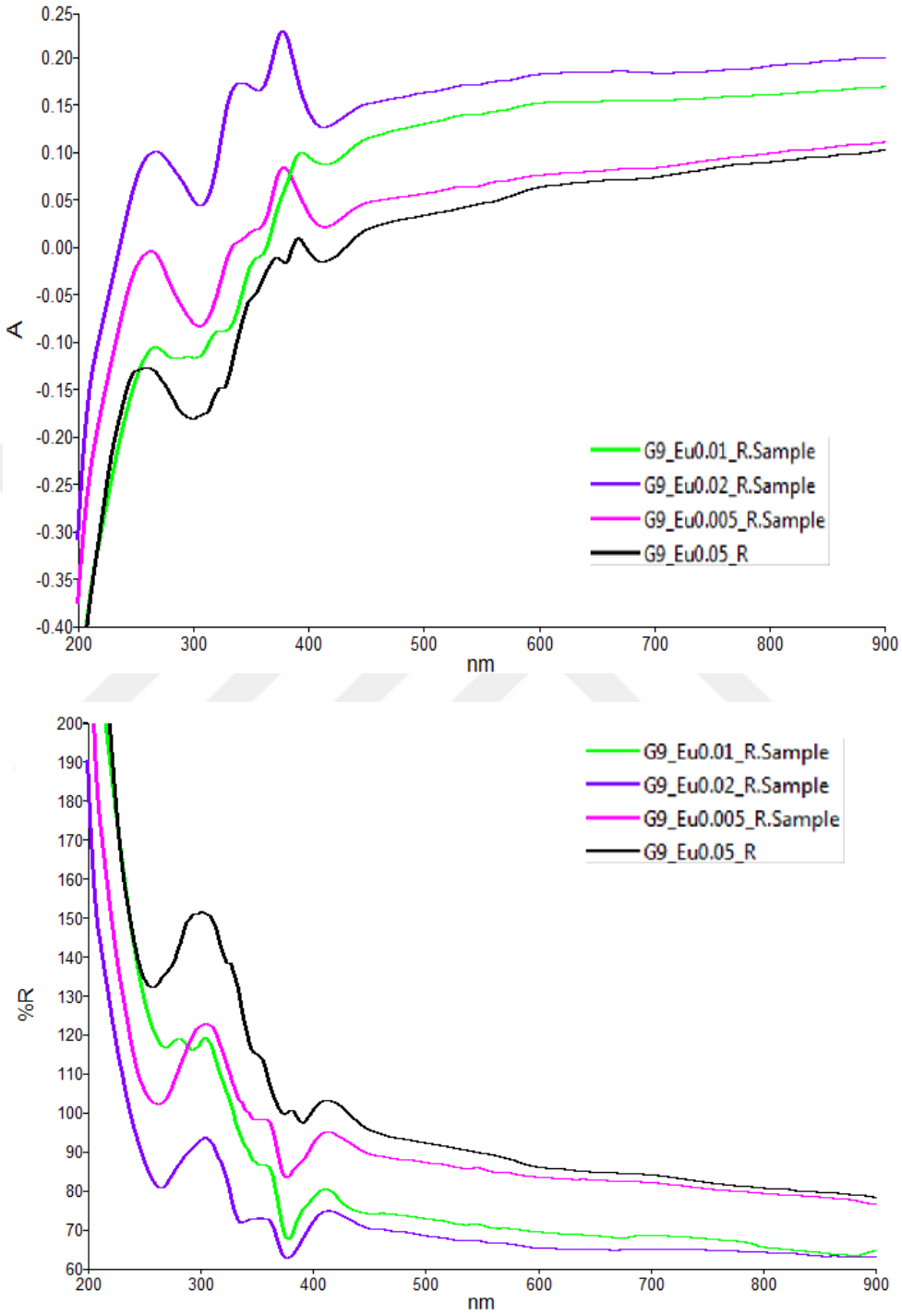

Figure 4.43. UV-VIS absorbance and reflectance spectra of Eu^{3+} doped $Ca_2\ B_2\ O_5$ for different concentrations at 900°C

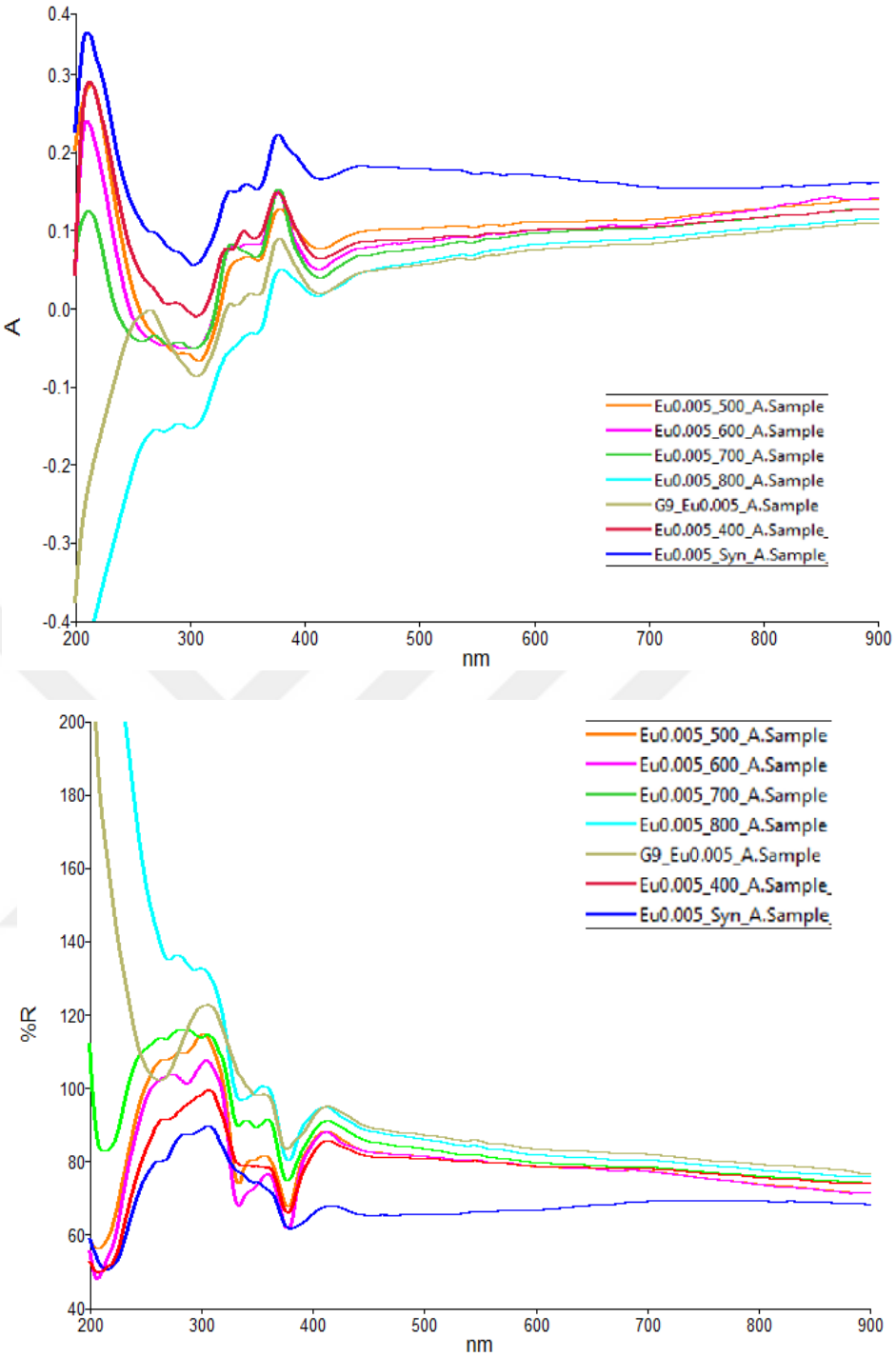

Figure 4.44. UV-VIS absorbance and reflectance spectra of Eu^{3+} doped $Ca_2\ B_2\ O_5$ at different temperatures

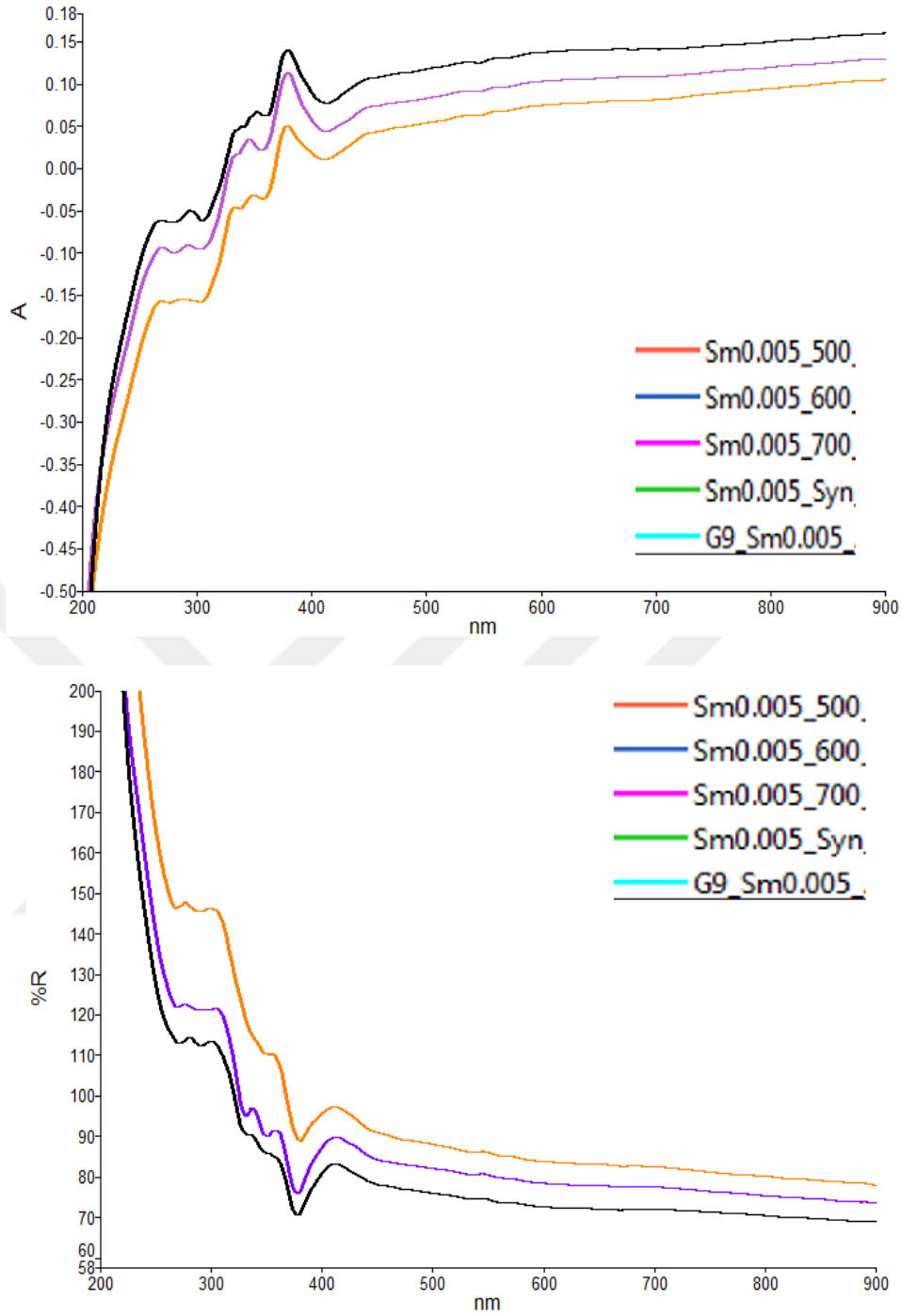

Figure 4.45. UV-VIS absorbance and reflectance spectra of Sm^{3+} doped $Ca_2\ B_2\ O_5$ different concentrations at 900°C

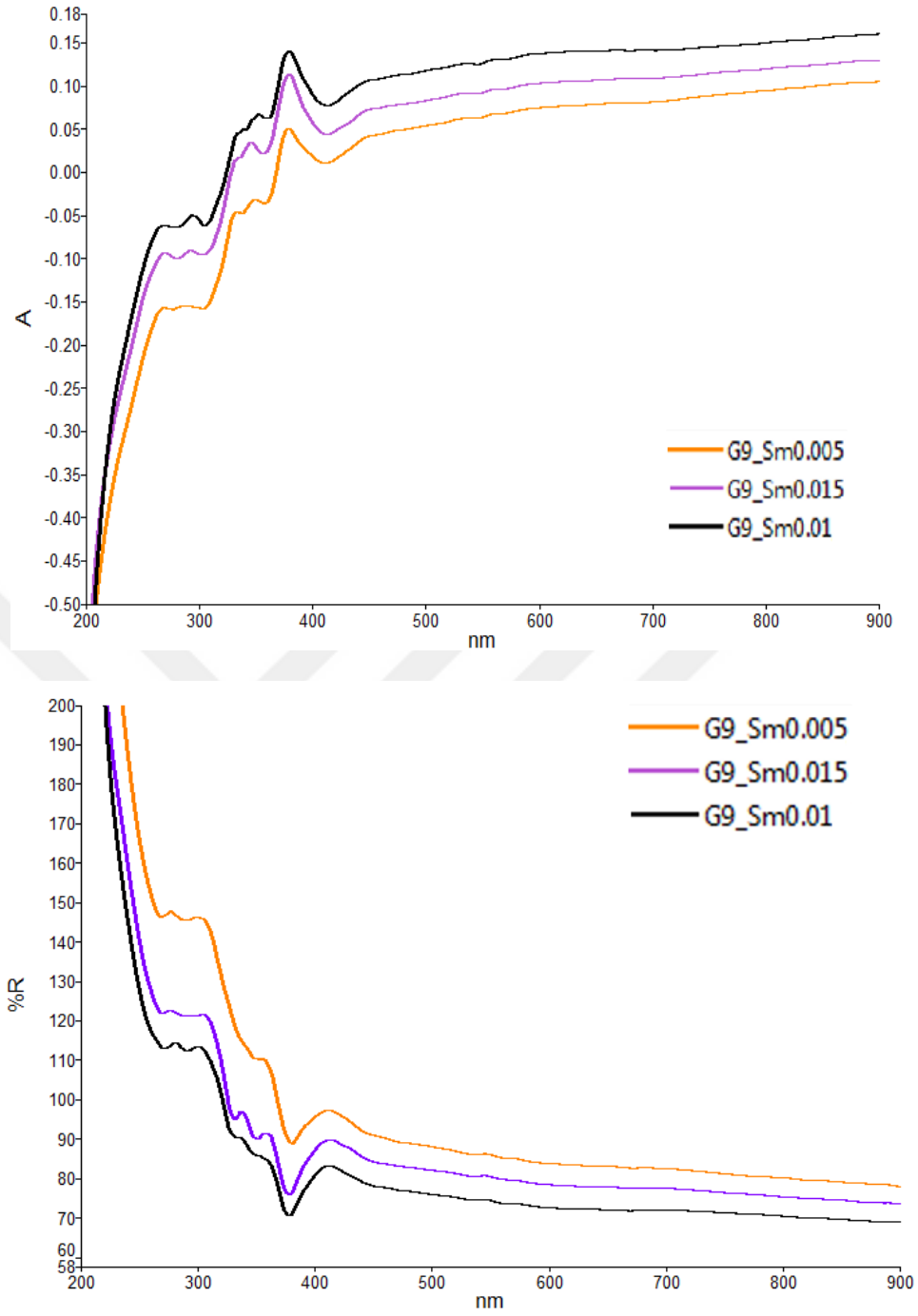

Figure 4.46. UV-VIS absorbance and reflectance spectra of Sm^{3+} doped $Ca_2\ B_2\ O_5$ at different temperatures

When the band gap energy of the products seen in Figure 4.42 was calculated, it has been observed that the band gap energy (Figure 4.47) decreases with the increases of the heating temperatures with glycine fuel.

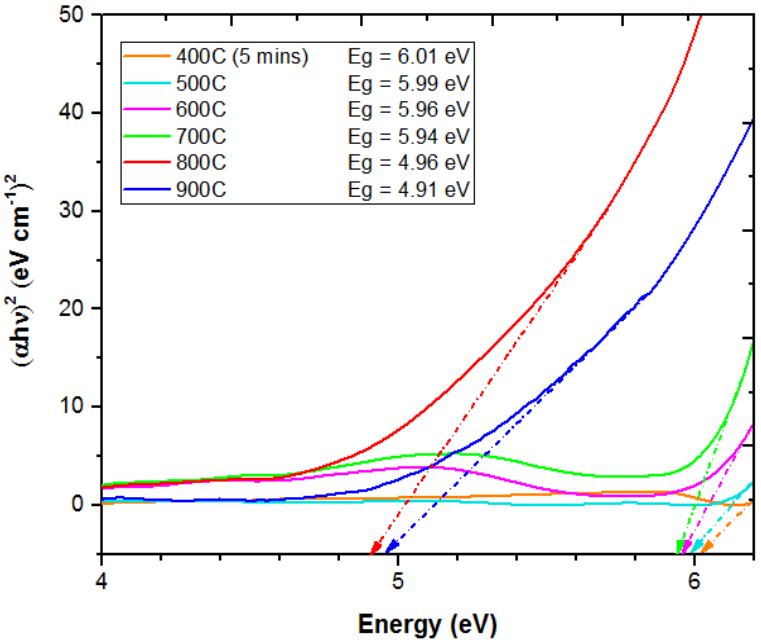

Figure 4.47. Band gap energy of the $Ca_2\ B_2\ O_5$ with glycine at different temperatures

The UV-VIS absorbance and reflectance spectra of $Ca_2\ B_2\ O_5$ with different fuels at 800ºC were analyzed (Figure 4.41) and by using their UV-VIS analysis data the optical band gap energy(Figure 4.48) of as-prepared was varies with different fuels.

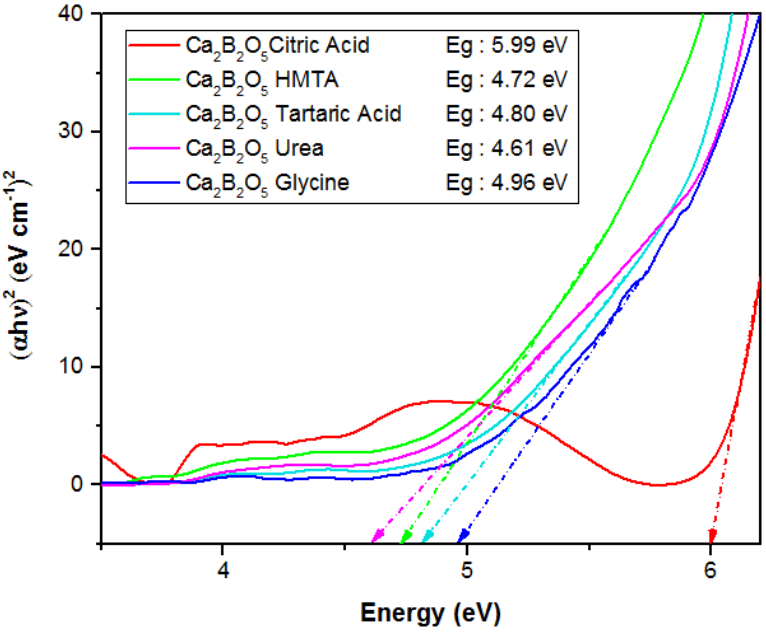

Figure 4.48. Band gap energy of the $Ca_2\ B_2\ O_5$ with different fuels at 800°C

Based on the the literature study the optical band gap energy of calcium pyroborates was reported to be 4.7eV. In this study, the band gap was determined to be 4.64 eV.

As seen in the Figure 4.49, it was observed that the addition of dopant materials increases the band gap energy of the final products.

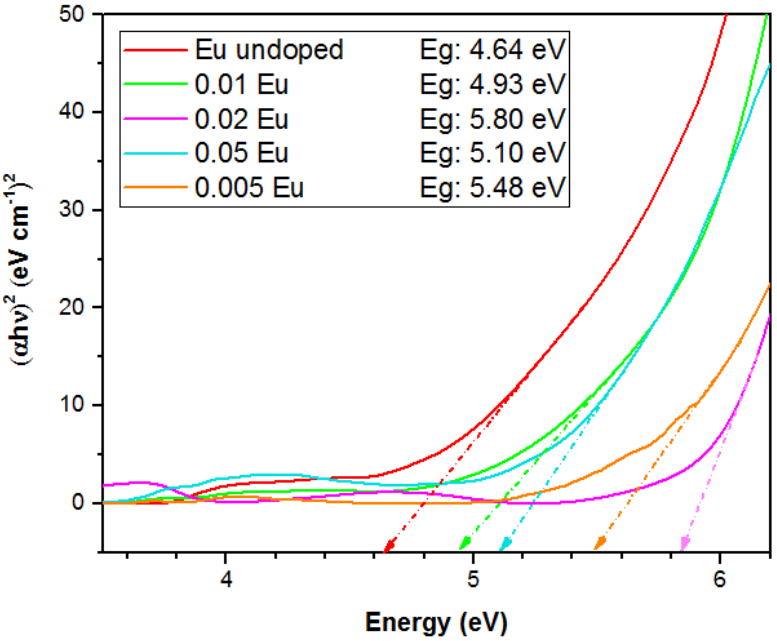

Figure 4.49. Band gap energy of the Eu^{3+} doped $Ca_2\ B_2\ O_5$ all concentrations

The single phase calcium pyroborate was formed between 800-900°C. Therefore, we can say that the highest band gap energy (Figure 4.50) was obtained at 900°C temperatures.

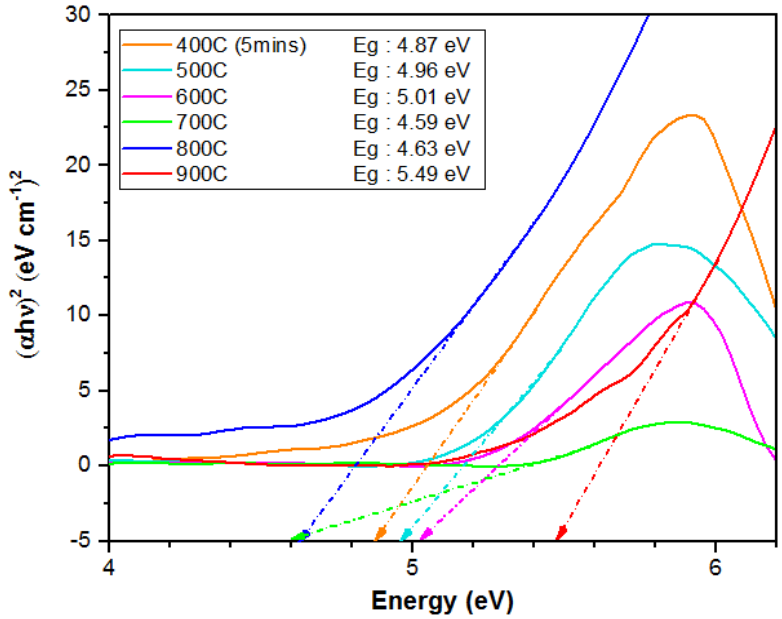

Figure 4.50. Band gap energy of the Eu^{3+} doped $Ca_2\ B_2\ O_5$ at all temperatures

As seen in this section, it was observed that the addition of dopant materials increases the band gap energy (Figure 4.51) of the final products. The highest band gap energy is seen for 0.015M Sm^{3+} .

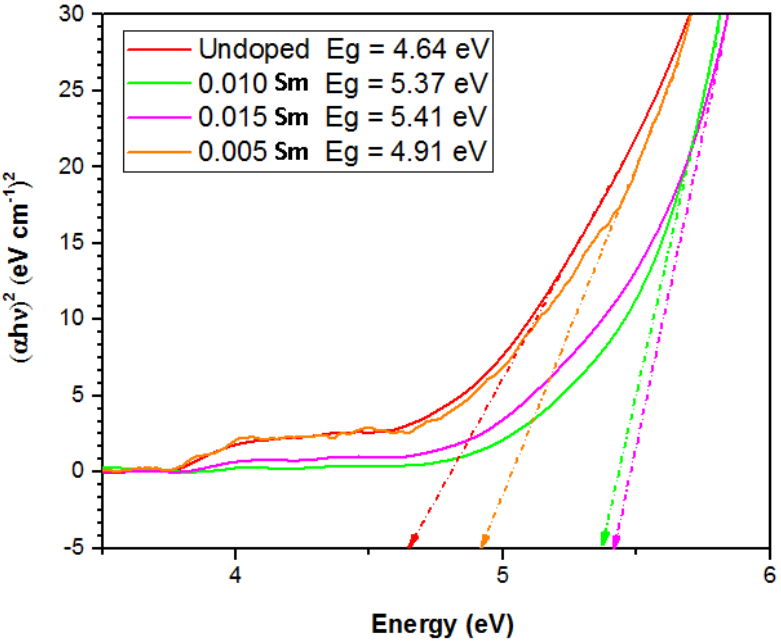

Figure 4.51. Band gap energy of the Sm^{3+} doped $Ca_2 B_2 O_5$ at all concentrations.

In the UV-VIS xpectra, it was observed that there is no peak observed in the visible region and following the XRD analysis the formation of calcium pyroborates was started at 700°C.

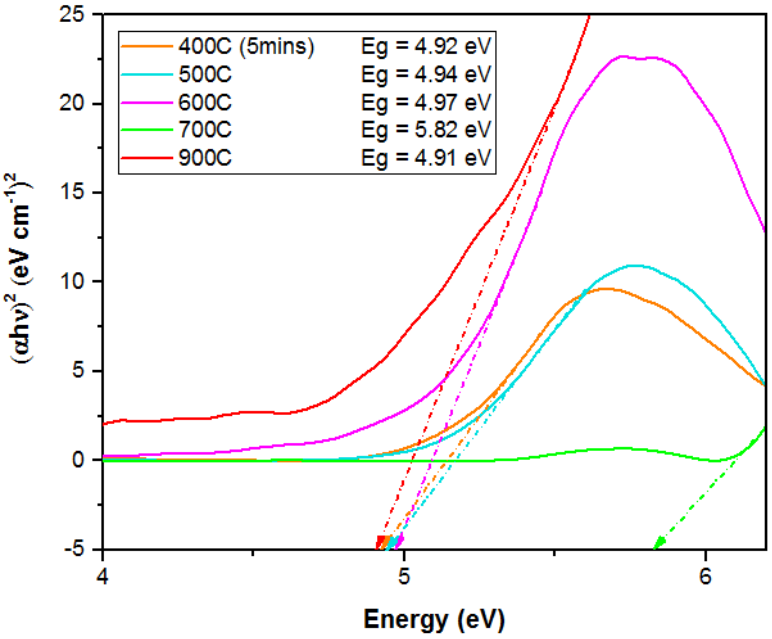

Figure 4.52. Band gap energy of the Sm^{3+} doped $Ca_2 B_2 O_5$ at all temperatures.

5. CONCLUSIONS AND RECOMMENDATIONS

In this present study, nano-crystalline undoped and some lanthanide ion (Eu^{3+} and Sm^{3+}) doped calcium pyroborate ceramic powders were successfully synthesized by a simple, cost effective, and efficient Solution Combustion Synthesis (SCS) method. The single-phase synthesis products were obtained in brief reaction time and low synthesis temperature.

In the analysis of XRD, the formation of α forms of undoped and doped $Ca_2 B_2 O_5$ in monoclinic crystal structure were determined. Single phase calcium pyroborates were started to form at 800 °C and highly crystalline form of monoclinic calcium pyroborates were produced at 900 °C.

During examination of FT-IR spectra, the bands that are belong to characteristic bands of calcium pyroborates were detected. The intense band observed at >1000 cm^{-1} are belonged to the stretching vibration of B-O in BO_3 groups whereas the bands in the range of 600-820 cm^{-1} are contributed to the bending vibration of the B-O-B modes in BO_3 planes. The absences of the peak at around 1500-2000 cm^{-1} also indicated that there is no organic compounds are found in the synthesized products.

The effects of fuels and temperatures on the formation of nanosized calcium pyroborates were well examined. It was found that the crystallite size increased with the increasing temperature and concentration of different dopant materials.

The effect of dopant materials on the optical band gap energy was also determined. For Eu^{3+} and Sm^{3+} doped calcium pyroborates, the band gap energy increased as the dopant's concentrations increased.

6. REFERENCES

Vancouver citation system was used in this thesis.

1. Greenwood NN, Earnshaw A. Chemistry of the elements. 2nd ed. Oxford: Butterworth Heinemann; 1972, 2ed.

2. Sümer G. Boron compounds, II.International Boron Symposium, 23-25 September 2004, Eskişehir, Turkey, 153-164.

3. Demiral Kurtuluş F, Güler H. Synthesis of Some Metal Containing Borate and Boron Phosphate Compounds by Solid-State Methods. Journal of Balikesir University Institute of Natural and Applied Sciences. 2003; 5(1): 141-152

4. Chatterjee, K. K., 2007, Uses of Metals and Metallic Minerals, New Age International Publishers, New Delhi.

5. Kar, Y., Şen, N., Demirbaş, A., 2006. Boron Minerals in Turkey, Their Application Areas and Importance for the Country's Economy. Minerals & Energy, 3-4, 2-10.

6. Boron Element [Internet].[cited 2022 Nov 18]. Available from: http://w3.balikesir.edu.tr/~hguler/bor_kimyasi.htm.

7. Yıldız, T. A., & Durandurdu, M. (2020). Amorphous boron carbide from ab initio simulations. Computational Materials Science, 173, 109397.

8. Balcı, Ö. ve Duman, İ., "Elementer Bor Üretim Proseslerine Genel Bakış". Teknik Yazı, Türk Mühendis ve Mimar Odaları Birliği Metalurji Mühendisleri Odası Dergisi, 156. Sayı, 1-7, 2010.

9. Özkan S. G., Lyday P. A., Physical and chemical treatment of boron ores, SME's Annual Meeting, Denver, Preprint 95-186, 1995.

10. Yılmaz A. Her Derde Deva Hazinemiz Bor. Journal of Science and Technology. 2002; 414: 39-48.

11. Uçar A., Kestelek tesis atıklarından borun kazanılması, Yüksek Lisans Tezi, Anadolu Üniversitesi, Fen Bilimleri Enstitüsü, Eskişehir, 1989.

12. Güyagüler T., Türkiye bor potansiyeli, 4. Endüstriyel Hammaddeler Sempozyumu, İzmir, Sayfa 18-27, 2001

13. Boron Minerals [Internet]. [cited 202 Nov 20]. Available from: https://www.etimaden.gov.tr/bor-mineralleri.

14. www.boren.gov.tr

15. Boron Element [Internet].[cited 2022 Nov 18]. Available from: https://boren.tenmak.gov.tr/tr/calisma-alanlari/bor-elementi.html.

16. National boron research institute Avaible from: http://www.boren.gov.tr/

17. Sokmen N., Büyükakinci B. Y., The Use Of Boron / Boron Compounds In The Text Industry and Their Use In Turkey, Cbu International Innovation Conference Scıence And Educatıon, March 21-23, 2018, Prague, Czech Republic

18. Chatterjee, C. and Sheoran, G. (2007) Vulnerable Groups in India. The Centre for Enquiry into Health and Allied Themes (CEHAT), Mumbai.

19. Kistler, R. B., & Helvaci, C. (1994). Boron and borates. Industrial minerals and rocks, 6, 171-186.

20. Weir CE. Infrared Spectra of the Hydrated Borates. A. Physics and Chemistry. 1966; 70A (2):153-164.

21. Briggs M. Boron Oxides, Boric Acid, and Borates. Kirk-Othmer Encyclopedia of Chemical Technology. 2001; 4:241-294

22. Greenwood, N. N., Earnshaw, A., 1998, Chemistry of The Elements, Butterword Heinemann Pub., Great Bratain.

23. Coulson, C. A., & Dingle, T. W. (1968). The B–O bond lengths in boron–oxygen compounds. Acta Crystallographica Section B: Structural Crystallography and Crystal Chemistry, 24(1), 153-155.

24. (Briggs, 2001)

25. Cheng WD, Zhang H, Zheng FK, Chen JT, Zhang QE, Pandey R (2000) "Electronic Structures and Linear Optics of A2B2O5 (A=Mg,Ca,Sr) Pyroborates" Chemistry of Materials, 12: 3591-3594.

26. Elssfah EM, Elsanousi A, Zhang J, Song HS and Tang C (2007) "Synthesis of magnesium borate nanorods", Mater. Lett. 61, 4358–4361.

27. F.C. Hawthorne, P.C. Burns, J.D. Grice, The crystal chemistry of boron in: boron: mineralogy, petrology and geC°hemistry, Rev. Mineral. 33 (1996) 41–116.

28. R. Bubnova, S. Volkov, B. Albert, S. Filatov, Borates—crystal structures of prospective nonlinear optical materials: high anisotropy of the thermal expansion caused by anharmonic atomic vibrations, Crystals 7 (3) (2017) 93.

29. A.L. Arunachalam, S. Induja, J. Sakthidasan, P.S. Raghavan, Calcium

30. Yukhno, V., Volkov, S., Bubnova, R., Povolotskiy, A., & Ugolkov, V. (2021). High-temperature γ↔ β′↔ α phase transitions in Ca2B2O5: Thermal expansion and crystal structure of α-phase. Solid State Sciences, 121, 106726.

31. Y. Zhu, "Fundamentals and Applications of Boron Chemistry", Elsevier, pp. 1-13 2022.

32. A. Taneri, "Organik ve Anorganik Bor Bileşikleri", Etibank Bülteni, sayı 74, s.20-28, 1985.

33. X. Lu, Z. You, J. Li, Z. Zhu, G. Jia, B. Wu, and C. Tu, "Optical transition properties of the Nd^{3+} ions in Ca3 (BO_3)2", Crystal. Physica Status Solidi (a), vol. 203, no. 3, pp. 551-557, 2006..

34. X. Lu, et al., "Spectroscopy of Ca3(BO_3)2: Dy^{3+} crystal", Journal of Physics and Chemistry of Solids, vol. 66, no. 10, pp. 1801-1805, C°t. 2005.

35. H.S.Huang and H.Z. Liu, "Enhanced photoluminescence property of CaB_2O_4 : Eu^{3+} phosphor prepared by calcining the $Ca_4B_{10}O_{19}\cdot 7H_2O$: Eu^{3+} precursor", Materials Research Bulletin, vol. 49, pp. 88-93, 2014.

36. A. Diaz, D.A. Keszler, "Red, green, and blue Eu^{2+} luminescence in solid-state borates: A structure-property relationship", Materials Research Bulletin", vol. 31, no. 2, Feb. 1996.

37. http://www.etimaden.gov.tr

38. Komiya, H., Kawamura, I., Kawamoto, H., Fujimoto, Y., Koshimizu, M., Okada, G., ... & Asai, K. (2022). Thermoluminescence properties of Ca2B2O5: Dy ceramics for neutron measurement. Japanese journal of applied physics, 61(SB), SB1007.

39. Komiya, H., Kawamura, I., Kawamoto, H., Fujimoto, Y., Koshimizu, M., Kimura, H., ... & Asai, K. (2021). Neutron-induced thermoluminescence properties of Tb^{3+} doped Ca2B2O5 ceramics. Japanese journal of applied physics, 60(9), 092008.

40. Rahaman, M. N., 2003, Ceramic Processesing and Sintering. 2nd edution, CRC press, USA. Chapter 2, 61-92.

41. Yang, L., Wan, Y., Li, Y., Pu, Y., Huang, Y., Chen, C., & Seo, H. J. (2016). Hydrothermal synthesis, characterization, and luminescence of $Ca_2B_2O_5$: RE (RE= Eu^{3+}, Tb^{3+}, Dy^{3+}) nanofibers. Journal of Nanoparticle Research, 18, 1-9.

42. Rao, C. N. R., & Biswas, K. (2015). *Essentials of inorganic materials synthesis*. John Wiley & Sons.

43. Gökdai, D., Metin, G. Ü. R. Ü., & Toğrul, T. (2016). Mekanokimyasal yöntemle bor oksitten elementel bor sentezlenmesi ve karakterizasyonu. Gazi Üniversitesi Mühendislik Mimarlık Fakültesi Dergisi, 31(2).

44. dom.lndb.lv